Final Report 2001-15

Research

The Use of Geosynthetics to Reinforce Low Volume Roads

Minnesota Local Road Research Board

Technical Report Documentation Page

1. Report No.	2.	3. Recipients Accession No.
MN/RC – 2001-15		

4. Title and Subtitle	5. Report Date
THE USE OF GEOSYNTHETICS TO REINFORCE LOW VOLUME ROADS	January 2001 6.
7. Author(s)	8. Performing Organization Report No.
Hans Erickson and Andrew Drescher	
9. Performing Organization Name and Address University of Minnesota Department of Civil Engineering 500 Pillsbury Drive, S.E. Minneapolis, MN 55455-0220	10. Project/Task/Work Unit No. 11. Contract (C) or Grant (G) No. c) 74708
12. Sponsoring Organization Name and Address Minnesota Department of Transportation 395 John Ireland Boulevard Mail Stop 330 St. Paul, Minnesota 55155	13. Type of Report and Period Covered Final Report: 1999-2000 14. Sponsoring Agency Code

15. Supplementary Notes

16. Abstract (Limit: 200 words)

This report presents the results of a study that investigated the reinforcement function of geosynthetics for typical Minnesota low-volume roadways.

Researchers conducted a series of numerical simulations using the finite difference program FLAC. The numerical tests consisted of a static, circular nine kip loading over a variety of typical surfaced and unsurfaced road cross sections that were reinforced with geotextiles and geogrids. Researchers used elastic and elasto-lastic models with frictional interfaces to simulate the layered roadway system.

The results of the study indicate that the addition of a geosynthetic does provide reinforcement to the roadway as long as the geosynthetic is stiffer than the subgrade material. However, for most of the cases studied, the benefit in terms of deflection reduction, was very small. Only for the poorest quality subgrades was the reinforcement benefit substantial.

17. Document Analysis/Descriptors		18. Availability Statement
geosynthetics reinforcement low volume roads	finite difference analysis FLAC numerical simulation	No restrictions. Document available from: National Technical Information Services, Springfield, Virginia 22161

19. Security Class (this report)	20. Security Class (this page)	21. No. of Pages	22. Price
Unclassified	Unclassified	124	

THE USE OF GEOSYNTHETICS TO REINFORCE LOW VOLUME ROADS

Final Report

Prepared by

Hans Erickson and Andrew Drescher

University of Minnesota
Department of Civil Engineering
122 CivE Building
500 Pillsbury Dr. S.E.
Minneapolis, MN 55455-0220

January 2001

Published by

Minnesota Department of Transportation
Office of Research Services
395 John Ireland Boulevard
Mail Stop 330
St. Paul, Minnesota 55155

TABLE OF CONTENTS

Page

CHAPTER 1 - INTRODUCTION 1

CHAPTER 2 – OBJECTIVES AND SCOPE 15

Objectives 15

Scope 16

Mechanistic 16

Material Properties 17

Road Geometry 19

Frictional Interfaces 21

Interface Parameters 27

Analysis Matrix 28

CHAPTER 3 – *FLAC* ANALYSIS 33

FLAC .....

Problem Considered 35

Solution Procedure 36

CHAPTER 4 – RESULTS 41

Percent Normalized Deflection Reduction 41

Percent Normalized $ASAL_{2.5}$ Increase 53

Roadway Cross Sections 62

Stress Distributions 73

CHAPTER 5 – ANALYSIS OF RESULTS 81

Percent Normalized Deflection Reduction 81

Percent Normalized $ASAL_{2.5}$ Increase 85

Stress Distributions 87

CHAPTER 6 – CONCLUSIONS AND RECOMMENDATIONS 89

CONCLUSIONS 89

RECOMMENDATIONS.....91

REFERENCES 93

APPENDIX A A-1

List of Figures

Figure Page

1. Geosynthetic reinforcement functions 2
   a) Lateral restraint
   b) Modified failure surface
   c) Tensioned membrane
2. Geogrids 6
   a) Uniaxial
   b) Biaxial
3. Shear stress at the base of the fill 8
4. Typical cross-section 11
5. Stress-strain behavior of soil under repeated load 13
6. Predicted vs. actual centerline deflections for repeated loadings 13
7. Constitutive models 16
   a) Elastic
   b) Elastic perfectly plastic
8. Typical road cross-sections 19
   a) Unsurfaced
   b) Warm pavement
   c) Cold pavement
9. Road geometry 20
   a) Unsurfaced
   b) Surfaced
10. Vertical displacement vs. friction angle for a frictional interface 23
11. Direct shear analogy 26
   a) Frictional interface
   b) Elastic interface

12. Vertical deflection vs. relative grid stiffness for a cohesive and non-cohesive interface 27
13. Test matrix flow chart 29
(a) <150 HCADT and 150-300 HCADT
(b) 300-600 HCADT and >1100 HCADT
(c) Underdesigned
14. *FLAC* calculation cycle 34
15. Axisymmetric problem 35
16. Typical *FLAC* mesh used in the analysis 37
17. Velocity profile for gravitational stress field with large interface shear stiffness 38
18. Normalized deflection reduction vs. subgrade modulus 43
a) Unsurfaced, underdesigned structure
b) Unsurfaced, <150 HCADT structure
c) Unsurfaced, 150-300 HCADT structure
d) Unsurfaced, 300-600 HCADT structure
19. Normalized deflection reduction vs. subgrade modulus 47
a) Warm pavement, <150 HCADT structure
b) Warm pavement, 150-300 HCADT structure
c) Warm pavement, 300-600 HCADT structure
20. Normalized deflection reduction vs. subgrade modulus 50
a) Cold pavement, <150 HCADT structure
b) Cold pavement, 150-300 HCADT structure
c) Cold pavement, 300-600 HCADT structure
21. Benkelman beam apparatus 54
22. Normalized $ASAL_{2.5}$ increase vs. subgrade modulus 56
a) Warm pavement, <150 HCADT structure
b) Warm pavement, 150-300 HCADT structure
c) Warm pavement, 300-600 HCADT structure

23. Normalized $ASAL_{2.5}$ increase vs. subgrade modulus 59
a) Cold pavement, <150 HCADT structure
b) Cold pavement, 150-300 HCADT structure
c) Cold pavement, 300-600 HCADT structure
24. Road cross-sections and deflections for underdesigned, unsurfaced 63
25. Road cross-sections and deflections for <150 HCADT structure, unsurfaced 64
26. Road cross-sections and deflections for 150-300 HCADT structure, unsurfaced 65
27. Road cross-sections and deflections for 300-600 HCADT structure, unsurfaced 66
28. Road cross-sections and deflections for <150 HCADT structure, surfaced, cold 67
29. Road cross-sections and deflections for 150-300 HCADT structure, surfaced, cold 68
30. Road cross-sections and deflections for 300-600 HCADT structure, surfaced, cold 69
31. Road cross-sections and deflections for <150 HCADT structure, surfaced, warm 70
32. Road cross-sections and deflections for 150-300 HCADT structure, surfaced, warm 71
33. Road cross-sections and deflections for 300-600 HCADT structure, surfaced, warm 72
34. Position of horizontal stress distributions 74
35. Horizontal stress vs. depth 75
a) Underdesigned, unsurfaced, soft subgrade, 6.3”
b) Underdesigned, unsurfaced, soft subgrade, 10”
c) Underdesigned, unsurfaced, soft subgrade, 15.6”
36. Horizontal stress vs. depth 78
a) Underdesigned, unsurfaced, medium subgrade, 6.3”
b) Underdesigned, unsurfaced, medium subgrade, 10”
c) Underdesigned, unsurfaced, medium subgrade, 15.6”

List of Tables

Table		Page
1.	Range of strength and Young's modulus for geotextiles	3
2.	Range of strength and Young's modulus for geogrids	4
3.	Subgrade and base material properties	17
4.	HMA material properties	18
5.	Geosynthetic material properties	18
6.	Frictional interface properties	28
7.	Representative maximum mobilized friction angle at the interface	82
8.	Percent normalized deflection reduction – unsurfaced cases	83
9.	Percent normalized deflection reduction – 40^{o} C pavement	84
10.	Percent normalized deflection reduction – -20^{o} C pavement	84
11.	Percent normalized $ASAL_{2.5}$ increase – 40^{o} C pavement	86
12	Percent normalized $ASAL_{2.5}$ increase – -20^{o} C pavement	86

EXECUTIVE SUMMARY

The use of geosynthetics is widespread in the field of civil engineering. One particular application that has seen a great deal of use has been as a separating layer between the aggregate base layer and subgrade of low volume roadways. Since geosynthetics may be very stiff, they may provide an additional benefit of reinforcement to the roadway. For this study, only the reinforcement functions of geosynthetics were investigated. Long term separation and increased bearing capacity during construction were not considered.

The research described herein was originated to investigate the reinforcement function of geosynthetics for typical Minnesota low-volume roadways. To this end, a series of numerical experiments were conducted using the finite difference program *FLAC* (1993). The tests consisted of a static, circular, 9 kip loading over a variety of typical surfaced and unsurfaced road cross sections that were reinforced with geotextiles and geogrids. The results are shown in terms of percent normalized deflection reduction and percent normalized accumulated standard axle load to a serviceability level of 2.5 ($ASAL_{2.5}$) increase. Additionally, the effect of a geosynthetic reinforcement layer on the horizontal stress distribution is illustrated.

The results of the study indicate that the addition of a geosynthetic does provide reinforcement to the roadway as long as the geosynthetic is stiffer than the subgrade material. However, for most of the cases studied, the benefit in terms of deflection reduction, was very small. Only for the poorest quality subgrades was the reinforcement benefit substantial.

CHAPTER 1
INTRODUCTION

The use of geosynthetics in geotechnical construction projects has gained tremendous popularity over the past 30 years. Ranging from the reinforcement and separation functions in roadway construction, to the filtration functions in earthen dams, geosynthetic applications are as varied as the types of geosynthetics available on today's market. Of special interest to civil engineers is the use of geosynthetics to reinforce roadways. Sometimes it is necessary to construct a road on very poor quality soil, and the intended use of the road does not merit the expense of constructing a high quality road. Examples of such roads are service or access logging roads, and low volume rural roads. The use of geosynthetics in large-scale civil construction projects has not only saved both time and money, but also made the resulting structures safer.

Typical applications for geosynthetics in civil engineering projects include reinforcement, separation, and filtration and drainage. Figures 1(a)-(c) illustrates the three reinforcement mechanisms geosynthetics can provide for roadways: lateral restraint, modified failure surface, and tensioned membrane. Figure 1(a) illustrates how interlocking and friction between the geosynthetic and the soil provides a lateral restraint for the aggregate base layer. Under repeated loads, the aggregate base layer tends to spread laterally; however, if the geosynthetic is placed at a depth of high lateral strain, the shear stress in the soil can be transferred to tensile stress in the geosynthetic. If the geosynthetic used is stiff, it will act to restrain the lateral spreading and result in a stiffer road.

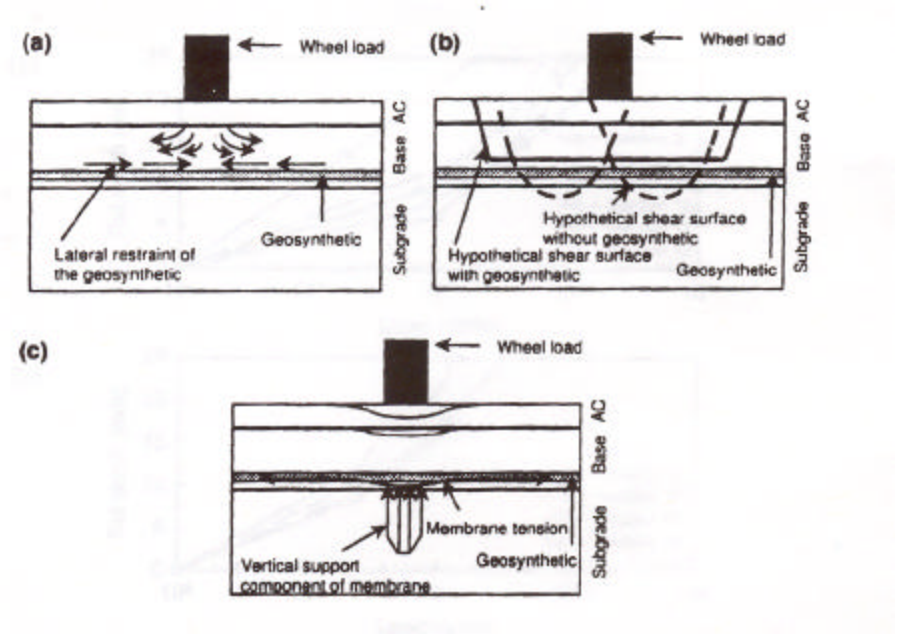

Fig. 1. Geosynthetic reinforcement functions (a) Lateral restraint, (b) Modified failure surface, and (c) Tensioned membrane (Perkins and Ismeik, 1997)

Second, Fig. 1(b) depicts how geosynthetics can increase the bearing capacity of a soil. If placed at a depth where they will interfere with the failure surface, geosynthetics can increase the bearing capacity of a soil. Finally, Fig.1(c) illustrates the tensioned membrane effect. As the repeated wheel loading produces rutting in the road, the geosynthetic is deformed and stretched. Similar to a trampoline, the geosynthetic is able to provide an upward elastic resistance to this deformation and aid in supporting the wheel load.

The separation function is typically utilized in road construction where the subgrade condition is poor. A geosynthetic will act as a barrier preventing the roadway's base material from being pushed into the weaker subgrade material, resulting in a smaller amount of base material required for the construction of the road. Geosynthetics may also aid in the construction of filters and drains. For instance, a drain may be constructed of a coarse-grained soil layer placed between two fine-grained layers. Geosynthetics placed between the coarse and fine-

grained layers would allow the water to freely pass into the coarse grained material while holding the fine-grained material out.

Geosynthetics may be divided into two distinct categories: geotextiles and geogrids. Geotextiles are typically made from petroleum products such as polypropylene, polyester, and polyethylene; however, they may also be made from fiberglass. Geotextiles may be further divided by the manner in which they were manufactured. For instance, woven geotextiles are made by weaving individual filaments together to create an interlocking structure. Conversely, nonwoven geotextiles are manufactured by bonding together randomly oriented short fibers or filaments to form a planar structure. For nonwoven geotextiles, the bonding process may be chemical, thermal, or mechanical. Chemical bonds utilized some sort of glue to hold the fibers together. Thermal bonding is achieved by melting the fibers together, and needle punching creates mechanical bonds. Due to the many different materials geotextiles may be created from, and the different creation processes, the range of material properties of geotextiles is very large. Table 1 shows a typical range of elastic moduli for geotextiles.

Table 1. Range of strength and Young's modulus for geotextiles

Manufacturer/ Name	Strength @ 5% Strain (KN/m)	E (MPa) assuming t = 0.00254 m
USA Spantex/ Spantex 5710	400	3150
TC Mirafi Filterweave 401	5.3	42

Geogrids are also made from petroleum products such as polypropylene and polyethylene, and are woven or bonded together to create a planar surface. One type of geogrid is constructed by punching out sections of polypropylene or polyethylene sheets. These punched out sections, or openings, are called apertures, and act to allow interlocking of the material above and below the geogrid. Geogrids are typically used as reinforcing elements. Table 2 shows a typical range of elastic moduli for geogrids.

Table 2. Range of strength and Young's modulus for geogrids

Manufacturer/ Name	Strength @ 5% Strain (KN/m)	E (MPa) assuming t = 0.00254 m
Maccaferri Gabions Inc./ Paralink 1250s	537	4230
Strata Systems Inc./ Stratagrid 100	4.4	35

Geogrids may be further divided into two categories: uniaxial geogrids, and biaxial geogrids. Figure 2 shows an example of each type of grid. Uniaxial geogrids are stretched in one direction to create long molecular chains of high strength in that direction. Similarly, biaxial geogrids are stretched in both directions. The stretching process results in a geogrid with a larger ultimate tensile strength and elastic modulus.

Over the past 20 years, significant experimental work has been done to understand how geosynthetics will work in various roadway systems, and how to optimize those systems. The reader is directed to the paper by Perkins and Ismeik (1997) for a synthesis of the major

laboratory experimental projects that have been conducted. Although not a complete summary of all the work that has been done, the paper does give a representative idea of the type and scope of laboratory work.

An example of laboratory test is the program currently being conducted by the Corps of Engineers Cold Regions Research and Engineering Laboratory (CRREL). The test program investigates the effect of geosynthetics used as base course reinforcement subject to a simulated 20-year traffic loading. Additional parameters to be investigated will be the influence of freeze/thaw cycles, variable moisture conditions, hot-mix asphalt (HMA) thickness, base thickness, and subgrade strength. The results of the tests will be quantified in terms of a Traffic Benefit Ratio (TBR) and a Base Course Reduction (BCR) ratio. The TBR is the ratio of the number of load cycles to reach a defined failure state for a reinforced section to the number of cycles to reach the same failure state for an unreinforced section. The BCR is the ratio of the percent reduction in base thickness for a reinforced section to an unreinforced section with the same base and pavement properties (Geosynthetic Manufacturer Association, 2000).

In addition to laboratory work, several researchers have used numerical methods to analyze the effect of geosynthetics in roadways. Again, Perkins and Ismeik (1997) provide an overview of many of the major numerical analysis that have been conducted.

For unsurfaced roads, Barksdale et al. (1982) conducted a finite element study on plane strain and axisymmetric geotextile reinforced soils. The authors were able to compare their finite element results to a series of physical model tests, which they also conducted. The finite element program was able to account for the inability of the granular material to sustain tension, and the inability of the geotextile element to sustain compression or bending. A nonlinear load-deflection curve was used in the analysis for the geotextile element.

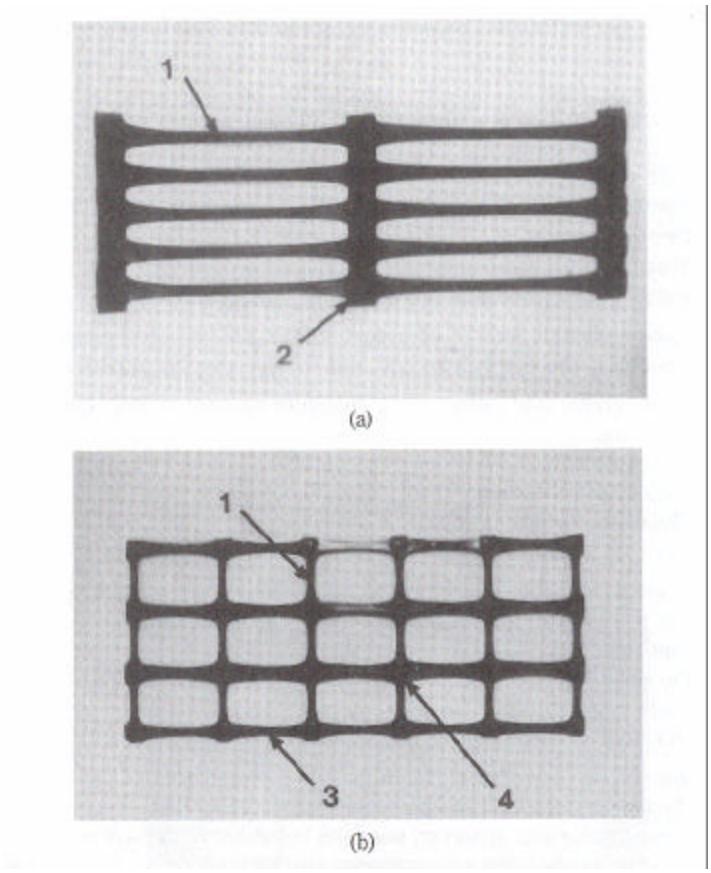

Fig. 2. Geogrids (a) Uniaxial; (b) Biaxial (Das, 1999)

Additionally, special elements were used to capture the frictional behavior of the interface, where the shear stress at the interface was limited by a Mohr-Coulomb failure criterion. The frictional interface parameters were taken from laboratory direct shear tests. The main limitations are that the analysis disregarded the gravitational stress field, and cyclic loads were applied at the same location. The results of the study indicate that the road sections with a geotextile will experience less rutting, and be able to withstand a larger number of loading cycles than a similar unreinforced road section. Both the laboratory tests and the numerical work indicate that the presence of the geotextile changes the stress field. It was observed that the

vertical and radial stresses under the loaded area were reduced, while the vertical compressive stress outside the loaded area was increased. These stress alterations were attributed to the membrane effect and an increased subgrade modulus resulting from the lateral restraint provided by the geotextile. The conclusion was that the stress field modification resulting from the geotextile was the principal reason for the observed greater rutting resistance.

Burd and Brocklehurst (1990) performed a finite element study to investigate the reinforcement mechanisms of geosynthetics in unpaved roads. They performed a plane strain analysis with a static loading and quantified the effect of reinforcement stiffness on deflections. It was assumed that no slip occurred at the soil-geosynthetic interface. An elastic perfectly plastic frictionless material model was used for the clay subgrade layer, an elastic perfectly plastic frictional model with non-associative flow rule was used for the base, and the reinforcement was modeled as an elastic material that could not sustain compression. The results indicated that the stiffness of the reinforcement had a marginal effect on the resulting deflection; however, it had a substantial effect on the magnitude of the shear stress acting at the soil-geosynthetic interface. A plot of the calculated shear stress acting vs. distance from the load centerline is shown in Fig. 3, where run A corresponds to the lowest stiffness geosynthetic and run E corresponds to the highest stiffness geosynthetic.

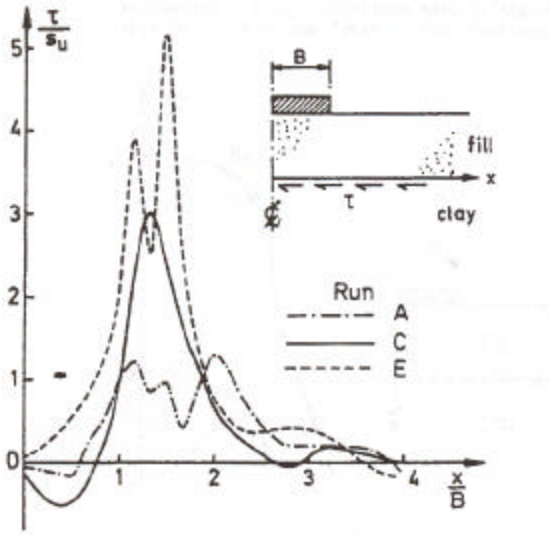

Fig. 3. Shear stress at the base of the fill (Burd and Brocklehurst, 1990)

It is clear that the value of geosynthetic stiffness has a large effect on the shear stress at the interface, with the high stiffness geosynthetic creating the highest shear stress. The authors suggested that this result was the effect of the geosynthetic providing lateral restraint on the base material. Further, the conclusion was made that little benefit is to be gained by using an excessively stiff geosynthetic for small deflections under static loading as large shear stresses are developed at the soil-base interface.

Similar numerical studies have been performed on surfaced roads. The main difference between geosynthetics use in unpaved and paved roads is that the membrane reinforcement effect generally does not develop in the paved case. In order for the membrane effect to be generated, large deflections in the geosynthetic are required. However, for paved roads, large deflections are not acceptable. Therefore, if the geosynthetic is not pretensioned during construction, the membrane effect cannot be relied upon to provide any reinforcement.

One such study was done by Dondi (1994) who performed a three dimensional static finite element study of a reinforced paved road using the commercially available program *ABAQUS*. Differing material models were used for each layer of the road's cross-section. An elastic material model was used for both the HMA material and the geosynthetic. The base material was assumed to be an elastic perfectly plastic, cohesive, non-associative material with the Drucker-Prager failure criterion. The subgrade was assumed to be an elastic perfectly plastic, cohesive Cam-Clay type material. Additionally, the frictional behavior of the geosynthetic-soil interface was assumed to follow a Mohr-Coulomb elastoplastic model.

The results of the analysis show that the use of geosynthetics in paved roads is beneficial. For instance, under Italian design loading (130 kN axle load), a 20% reduction in vertical deflection was calculated for a geosynthetic modulus of 1200 kN/m, and a 15% reduction for a modulus of 600 kN/m. Additionally, it was found that the shear stresses in the subgrade were reduced for the reinforced sections.

The fatigue behavior of the paved roads was also estimated using the method outlined by Giannini and Camomilla (1978). The percentage increase in fatigue live was given by the following equation

$$\Delta N = \left[\left(\frac{e_u}{e_r} \right)^{4.27} - 1 \right] * 100 \qquad (1.1)$$

where e_u is the maximum volumetric strain in the HMA layer for the unreinforced case, and e_r is the maximum volumetric strain in the HMA layer for the reinforced case. The fatigue life for reinforced roads was estimated to be more than 2 times higher than for unreinforced roads.

Experimental work by Carrol, Walls, and Haas (1987) has also demonstrated this large increase in fatigue life.

Giannini and Camomilla concluded that the addition of geosynthetics to paved roads is beneficial even though deflections large enough to develop the membrane effect are not present. It was determined that the presence of geosynthetics at the bottom of the base layer decreases the shear stress in the subgrade, and increase the fatigue life of the road.

Another example of a finite element study on a geosynthetic reinforced flexible pavement is that conducted by Wathugala et al. (1996). The authors chose to analyze the effect of differing material models for the soil and HMA. Both elastic and elasto-plastic material models were used. The geosynthetic was assumed to be elastic for all cases studied. Additionally, the effect of geosynthetic modulus was studied. The problem was idealized as axisymmetric, and the program ABAQUS was used to perform the analysis.

In contrast to the work of other researchers, the road cross section had a more complicated geometry. Previously studied road cross sections consisted of only four layers: HMA, aggregate base, geosynthetic, and subgrade; however, for this study, 6 layers were used, and were meant to represent a full scale experimental test road section being built by the Louisiana Transportation Research Center. The cross section used in the study is shown in Fig. 4.

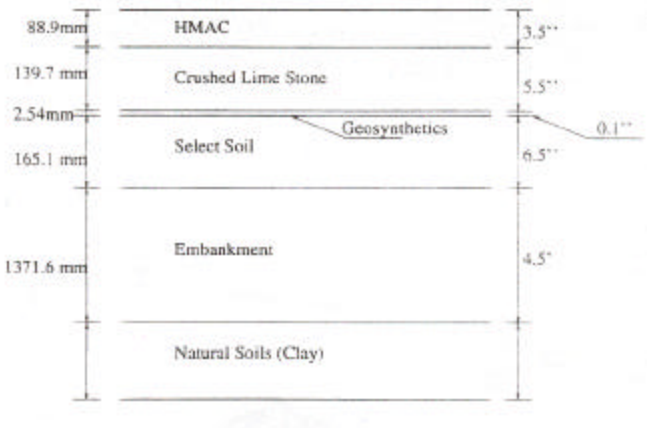

Fig. 4. Typical cross-section (Wathugala et al., 1996)

For the analysis with elasto-plastic material models, different models were used for different soil layers. For instance, the crushed limestone base and the HMA layers were assumed to follow a cohesionless Drucker-Prager material model. The select soil, embankment, and clay were assumed to follow a Hierarchical Single Surface (HiSS) model. The HiSS model used for the soil in the study could account for the nonlinear stress-strain behavior, the lack of tensile strength, the variation of compressive strength with confining pressure, the shear dilation that depends on confining pressure, and the plastic strain upon unloading. Further, the HiSS model was extended for the cohesive clay material to account for nonlinear behavior for overconsolidated soil. A von Mises model was used for the geosynthetic, and no attempt was made to model the interface behavior.

The results of the numerical analyses indicate that the use of geosynthetics in paved roads is beneficial. The results of the elasto-plastic analysis indicate that the presence of geosynthetics reduces the deflections upon application of the load as compared to the unreinforced case. Additionally, the deflection is dependent on the stiffness of the geosynthetic, with stiffer

geosynthetic reinforcement producing smaller deflections. Similarly, the plastic deflections remaining after removal of the load are smaller when the stiffer geosynthetic is used. In other words, a stiffer geosynthetic will produce a smaller deflection.

The results of the purely elastic analyses were found not to accurately represent the behavior of the road. This conclusion was drawn from the result that the elastic solutions predicted a tensile stress at the bottom of the base layer. Since the base material was meant to represent a purely granular crushed limestone material which cannot sustain tension, this result is clearly in error. Additionally, the elastic analysis could not capture the plastic displacements remaining after the load was removed. For these reasons an elasto-plastic analysis should be conducted.

Additional numerical research has gone into predicting the behavior of reinforced pavements subject to repeated loadings. One such computation was performed by Davies and Bridle (1990). The researchers used a finite difference approximation for the equilibrium equations for an axisymmetric problem, with the centerline displacement as the model output.

In order to correctly model a material's response to repeated loading, an appropriate constitutive model must be used that will capture the variable stiffness with load cycle. Experimental work has shown that when a soil is loaded such that some plastic deformations take place, the soil will exhibit a greater stiffness upon unloading. When the soil is reloaded to the same stress level, more permanent deformations are observed. Fig. 5 illustrates this behavior.

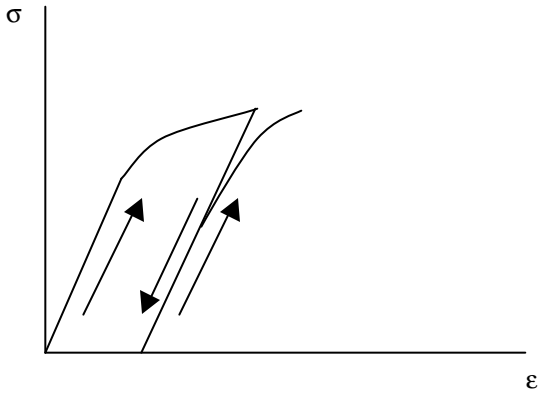

Fig. 5. Stress-strain behavior of soil under repeated load

The authors were able to capture this behavior by “fine tuning” the parameters of their material model such that an identical value of permanent deflection was given from both the laboratory experiment and the numerical analysis. An additional analysis was then performed considering a different geometry and the results compared to an identical laboratory test. The results of this test may be seen in Fig. 6, where it is evident that the numerical model can adequately predict the behavior of the real system.

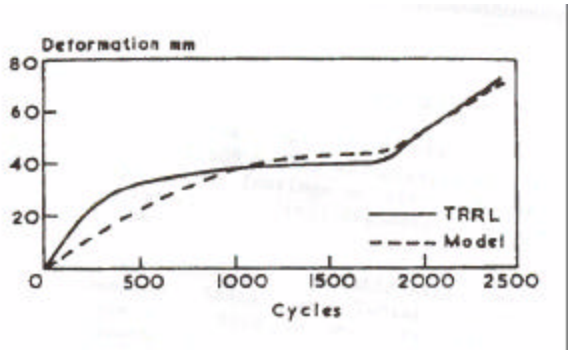

Fig. 6. Predicted vs. actual centerline deflections for repeated loadings
(Davies and Bridle, 1990)

The results of the experiment indicate that the repeated load behavior of a geosynthetic reinforced flexible pavement can be adequately analyzed. However, the amount of information required to correctly model the soil makes the method too complicated for normal design use.

CHAPTER 2
OBJECTIVES AND SCOPE

2.1 Objectives

The main objective of the project was to determine the effect of reinforcement on deflections of Minnesota's typical low volume roads subject to the specific single wheel load of 40 kN (9000 lbs.). The research and results described in Chapter 1 addressed the general effects of geosynthetic reinforcement on roadway behavior. Conversely, this study focuses on actual road designs constructed in Minnesota. In an attempt to understand the behavior of geosynthetics in typical Minnesota low volume roadways, a series of numerical experiments using the commercially available finite difference program *FLAC* was conducted. It should be noted that the objectives of this research relate to the reinforcement functions of the geosynthetics; specifically their ability to reduce deflections under static loads. The benefits of geosynthetic use relating to separation and filtration are not considered in this study.

In order to ensure the behavior of geosynthetic reinforced low-volume Minnesota roads was captured, an analysis matrix was developed encompassing a range of typical designs. The analysis matrix is comprised of three basic sections. First, the mechanistic models, or constitutive models used for the materials to be represented. Second, the range of material properties used for various subgrades, geosynthetics, and hot-mix asphalt (HMA). Finally, the individual road geometries, which were determined from the Minnesota State Aid Design Manual.

2.2 Scope

2.2.1 Mechanistic Models

The mechanistic models used are illustrated in Fig. 7, and were chosen such that they best represented the mechanical behavior of the material. An elastic perfectly plastic, frictional model with a tension "cut-off" was chosen to represent the aggregate base material, such that the negligible tensile strength could be represented. The subgrades were represented as elastic perfectly plastic, frictional, cohesive, non-associative materials with a Mohr-Coulomb failure criterion, and the HMA and geosynthetics were represented as elastic materials.

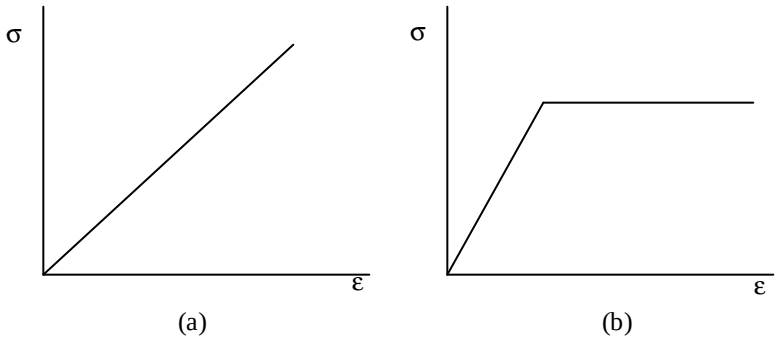

Fig. 7. Constitutive models (a) Elastic, (b) Elastic perfectly plastic

Since the analysis consists of static loading, no consideration is given to altering the constitutive models for any material under repeated loading.

2.2.2 Material Properties

Four different soil subgrades were represented, and one type of aggregate base material (Table 3). The subgrades were chosen to be representative of soils found in Minnesota that may require some form of geosynthetic application, and ranged in American Association of State and Highway Transportation Officials (AASHTO) soil class from A-2-4 to A-7-6. The Young's moduli (E) of the subgrade soils ranged from 15 MPa for the soft subgrade to 100 MPa for the stiff subgrade. Additionally, the friction angle (ϕ) was assumed to vary from 15^o for the soft subgrade to 30^o for the stiff subgrade. The value of Poisson's ratio (ν) was held constant at 0.4, the dilation angle (ψ) was held at 0^o, the cohesion (c) was held at 7.47 kPa, and the tensile strength (S_t) was assumed to be 0.

The aggregate base material was to be representative of a Minnesota Department of Transportation (Mn/DOT) Class 5, with an elastic modulus of E = 150 MPa. The value of Poisson's ratio was $\nu = 0.35$, the friction angle $\phi = 30^o$, the dilation angle $\psi = 0^o$, and no cohesion or tension strength.

Table 3. Subgrade and base material properties

	E(MPa)	n	f	j	**c (kPa)**	**S_t**
soft	15	0.4	15^o	0^o	7.47	0
medium-soft	30	0.4	20^o	0^o	7.47	0
medium	50	0.4	25^o	0^o	7.47	0
stiff	100	0.4	30^o	0^o	7.47	0
Base	150	0.35	30^o	0^o	0	0

For the HMA, two cases were studied to represent the differing mechanical behavior of the material due to temperature effects (Table 4). Two temperatures were chosen to be representative of the extreme temperatures experienced in Minnesota. At the coldest temperature, -20^0 C, the stiffness was E = 10 GPa and the Poisson's ratio ν = 0.3. At the warmest temperature, $+40^0$ C, the stiffness was E = 1 GPa and the Poisson's ratio ν = 0.3.

Table 4. HMA material properties

	E(GPa)	n
Warm ($+40^0$ C)	1	0.3
Cold (-20^0 C)	10	0.3

The geosynthetic properties were chosen to encompass the full range of geosynthetics available in today's market, and were taken from the Geotechnical Fabrics Report Specifier's Guide 1999 (Table 5). In total, six geosynthetics were chosen, three

Table 5. Geosynthetic material properties

Geotextile	**Strength @ 5% Strain (kN/m)**	**E(MPa) assuming t=0.00254m**
Stiff	400	3150
Medium	200	1575
Soft	5.3	42

Geogrid	**Strength @ 5% Strain (kN/m)**	**E(MPa) assuming t=0.00254m**
Stiff	537	4230
Medium	250	1970
Soft	4.4	35

representing geotextiles and three representing geogrids. The geosynthetics were further divided based on the relative values of their Young's moduli, where two were stiff, two medium, and two soft. The geosynthetic's Young's moduli were taken from published reference as determined from the wide width tensile properties as outlined in the American Society for Testing and Materials (ASTM) standard D4595. The Young's moduli of the geotextiles ranged from E = 42 MPa for the softest to E = 3150 MPa for the stiffest. The Young's moduli of the geogrids ranged from E = 35 MPa for the softest to E = 4230 MPa for the stiffest. In order to model the possible slip between the geosynthetic and the soil a frictional interface was used.

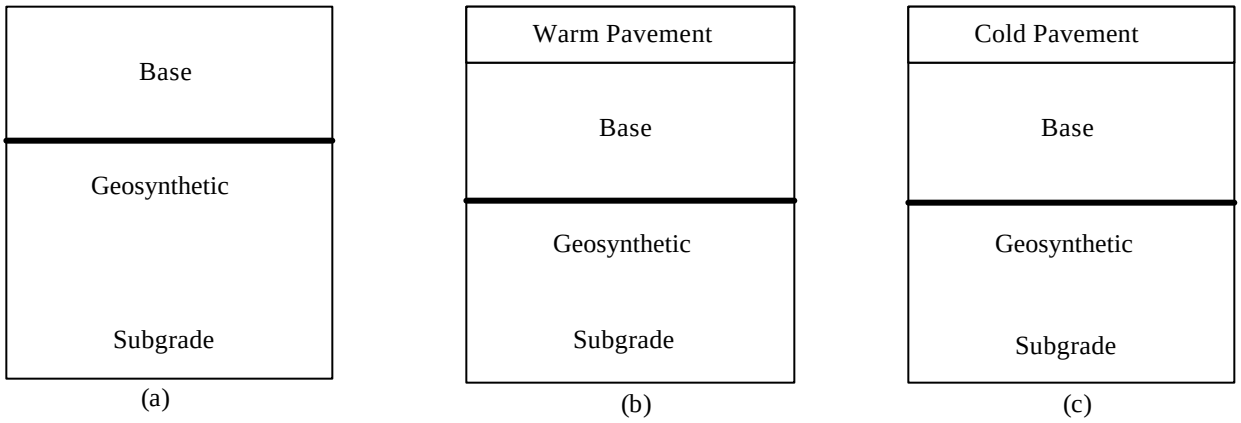

Fig. 9. Typical road cross-sections (a) Unsurfaced, (b) Warm pavement, (c) Cold pavement

2.2.3 Road Geometry

Differing geometries for the road cross-sections were used depending on the combination of HMA (warm or cold), geosynthetic, subgrade, and loading desired (Table 6a,b). The geometries were determined from the MnDOT state aid manual, and the thickness of the geosynthetic was held constant at 0.00254 m (0.1inch). Typical road geometries are shown in Fig. 9.

In regard to the loading, a static, single wheel load of 40 kN (9000 lbs.) was chosen as representative of "in-field" conditions. The loading was distributed uniformly as a normal stress over a 150mm (5.91 in) radius on the model boundary. The three cases studied are based on designs for three volumes of 40 kN axle load trucks. Additionally, a fourth case was studied involving an "underdesigned" unsurfaced road. This case was meant to represent a situation where no roadway design was involved prior to construction, and an insufficient amount of base material was used.

Table 6. Road geometry (a) Unsurfaced

	Soil	cm of base (inches)
underdesigned	soft	25.4 (10)
	medium-soft	20.3 (8)
	medium	15.2 (6)
	stiff	----
<150 HCADT	soft	53.3 (21)
	medium-soft	48.3 (19)
	medium	45.7 (18)
	stiff	27.9 (11)
150-300 HCADT	soft	63.5 (25)
	medium-soft	58.4 (23)
	medium	53.3 (21)
	stiff	----
300-600 HCADT	soft	73.7 (29)
	medium-soft	68.6 (27)
	medium	63.5 (25)
	stiff	40.6 (16)
>1100 HCADT	soft	96.5 (38)
	medium-soft	----
	medium	83.8 (33)
	stiff	53.3 (21)

Table 6. Road geometry (b) Surfaced

Surfaced	Soil	cm Class 5 (inches)	cm HMA (inches)
<150 HCADT	soft	38.1 (15)	7.6 (3)
	medium-soft	33 (13)	7.6 (3)
	medium	30.5 (12)	7.6 (3)
	stiff	12.7 (5)	7.6 (3)
150-300 HCADT	soft	45.7 (18)	8.9 (3.5)
	medium-soft	40.6 (16)	8.9 (3.5)
	medium	35.6 (14)	8.9 (3.5)
	stiff	---	8.9 (3.5)
300-600 HCADT	soft	53.3 (21)	10.2 (4)
	medium-soft	48.3 (19)	10.2 (4)
	medium	43.2 (17)	10.2 (4)
	stiff	20.3 (8)	10.2 (4)
>1100 HCADT	soft	71.1 (28)	12.7 (5)
	medium-soft	---	12.7 (5)
	medium	58.4 (23)	12.7 (5)
	stiff	27.9 (11)	12.7 (5)

2.2.4 Frictional Interfaces

In *FLAC*, two types of interface elements are available: elastic and elastic perfectly plastic. In order to correctly model the possible slip of the geosynthetic/subgrade and geosynthetic/base interfaces, a numerical experiment was conducted to determine which interface element to use. The numerical computation was done using materials, loading, and a road cross-section that were not representative of actual cases, as the intent was to isolate the interface such that only the effect of altering the interface parameters could be studied. To corroborate the *FLAC* results, a Windows based version of the program WESLEA (1989), which was developed to analyze layered elastic media, was used.

The input parameters necessary for the elastic interface elements are normal and shear stiffness. This type of interface element is one that is meant to represent an interface along which no slip or separation can take place, but allows elastic deformations according to the given stiffness. Such an interface is said to be "glued". The *FLAC* manual recommends values for the interface normal and shear stiffness such that minimal elastic deformations take place within the interface, while keeping computation times manageable. The recommend values are

$$k_n = 10k_s = \max\left(\frac{K + \frac{4}{3}G}{\Delta z_{min}} \right) \qquad (2.1)$$

where k_n is the normal stiffness, k_s is the shear stiffness, K is the bulk modulus of the surrounding material, G is the shear modulus of the surrounding material, and Δz_{min} is the smallest thickness of any element adjacent to the interface element.

The input parameters for the elastic perfectly plastic interface also include the normal and shear stiffness; however, a value of interface friction angle, cohesion, and tensile strength are also required. This type of interface element is meant to represent an interface along which slip or separation can take place if the Mohr-Coulomb failure criterion is breached. Such an interface is said to be "frictional".

Figure 10 indicates the test results for the frictional interface. The upper and lower bounds corresponding to the full slip and fully bonded cases as determined by both a *FLAC* and WESLEA analyses are shown. The plot indicates that the frictional interface will give the correct response for varying interface friction angles. In other words, decreasing the interface

friction angle increases deflection in a stable manner. Figure 10 also shows that the deflections determined using the frictional interface are bounded by the fully bonded and full slip cases, and vary in a stable fashion between the upper and lower limits.

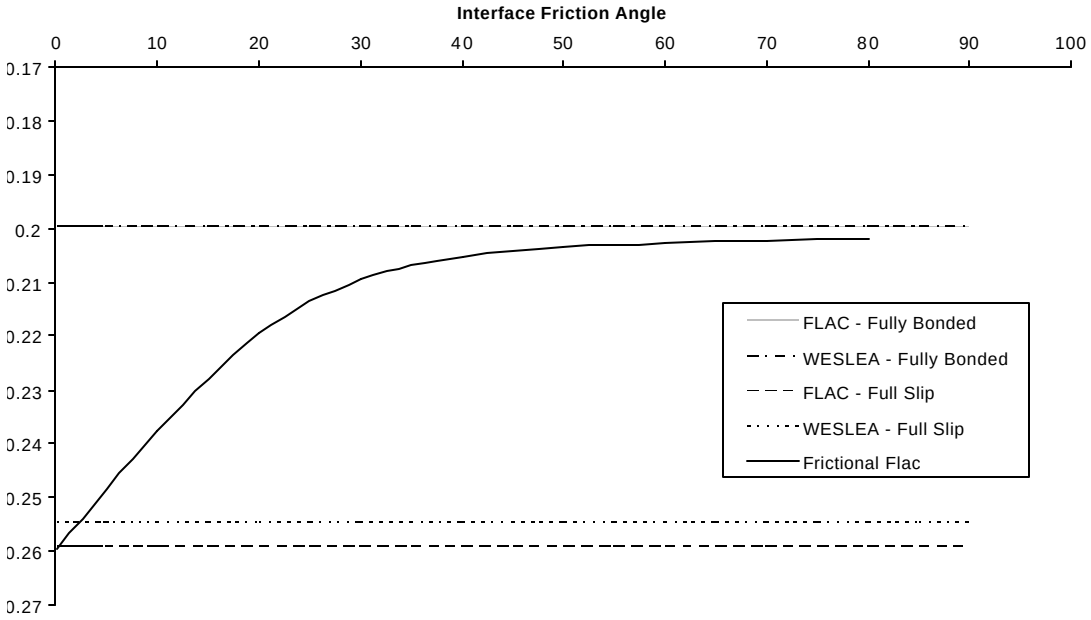

Fig. 10. Vertical deflection vs. friction angle for a frictional interface

In addition to stable behavior between the two deflection bounds, the frictional interface also accurately captures the interface strength dependence on normal stress. Initially, a glued interface was used to model the slipping nature of the geosynthetic-base and geosynthetic-subgrade interface. The glued interface is one for which the interface element may be thought of as a set of elastic springs, each with an elastic stiffness in the normal and shear directions (Fig. 11 (a)). If the analogy of a direct shear test is used in which the gap between the two halves of

the shear box is the interface element, useful insight to the response of the system can be gained. For instance, if the interface is modeled in the glued fashion, the response is independent of the value of the applied normal force. Additionally, no limit exists for the magnitude of force that the springs may carry. The only variable that effects the system response is the value of the elastic spring constants. On the other hand, if a frictional model is used, the intuitive physical response of the system is captured. For instance, the maximum value of shear force the interface can sustain is dependent on the value of the normal force (Fig. 11(b)). Also once the limiting value of shear force has been reached, slip can take place.

As an example, subject the shear box to shear and normal forces T_1 and N_1 (Fig. 11 (a), (b)). In order for the glued interface to give the proper displacement, the value of interface shear stiffness, k_1 must have been correctly chosen. If the normal force is increased to the value N_2, the frictional model results in a larger value of shear force, T_2, at the same value of displacement. In order for the glued model to predict a larger resulting shear force, a different value of stiffness, k_2, would have to be chosen.

The final advantage of the frictional interface model is the presence of experimental data for the value of interface friction angle. Several laboratory tests have been conducted, and values of interface friction angle reported for various interface conditions in the literature. For example, based on direct shear tests using geotextiles attached to one half of the shear box, Saxena and Budiman (1985) report interface friction angles of between 0.84 ϕ_{base} to ϕ_{base} for the geotextile-base interface, and between $0.58\phi_{base}$ to 0.72 ϕ_{base} for the geotextile-subgrade interface. Similar results are published by Martin, Koerner, and Whitty (1984), and Bearden and Labuz (1998). Fewer results have been published for the interface properties of geogrid

interfaces, which are usually assumed equal to the surrounding material's friction angle since the open apertures of the geogrid allow particle interlock.

An extensive literature review done by Bearden and Labuz (1998) concluded that the frictional resistance of the geogrid-base interface is approximately equal to the frictional resistance of the base alone. Additionally, the Federal Highway Administration (FHWA) manual found on a CD-ROM provided by the Minnesota Local Road Research Board (1998) states that the interface friction angle approaches that of the soil itself.

An additional interface parameter that is an option in the numeric model is the value of interface cohesion. An extensive literature review yielded little information on the topic, so a numeric test was done to determine if interface cohesion would be important for the purpose of this study. Two values of interface cohesion were investigated: one where the geosynthetic-subgrade interface cohesion was equal to that of the subgrade, and one where the interface cohesion was set equal to zero. Only cohesion on the geosynthetic-subgrade interface was investigated, as the base material was assumed cohesionless. Fig. 12 illustrates the results for the unsurfaced, <150 HCADT, soft subgrade, geogrid reinforced condition. Clearly, the value of interface cohesion has little effect on deflection, as the maximum difference between the two curves is 0.15 %. For the remainder of the study, interface cohesion was not included.

Based on the stable dependence on friction angle of the interface between the full slip and fully bonded conditions, the ability to model a slipping condition, and the availability of experimentally determined values of interface friction angle, the frictional model was chosen as the interface condition for the geosynthetic.

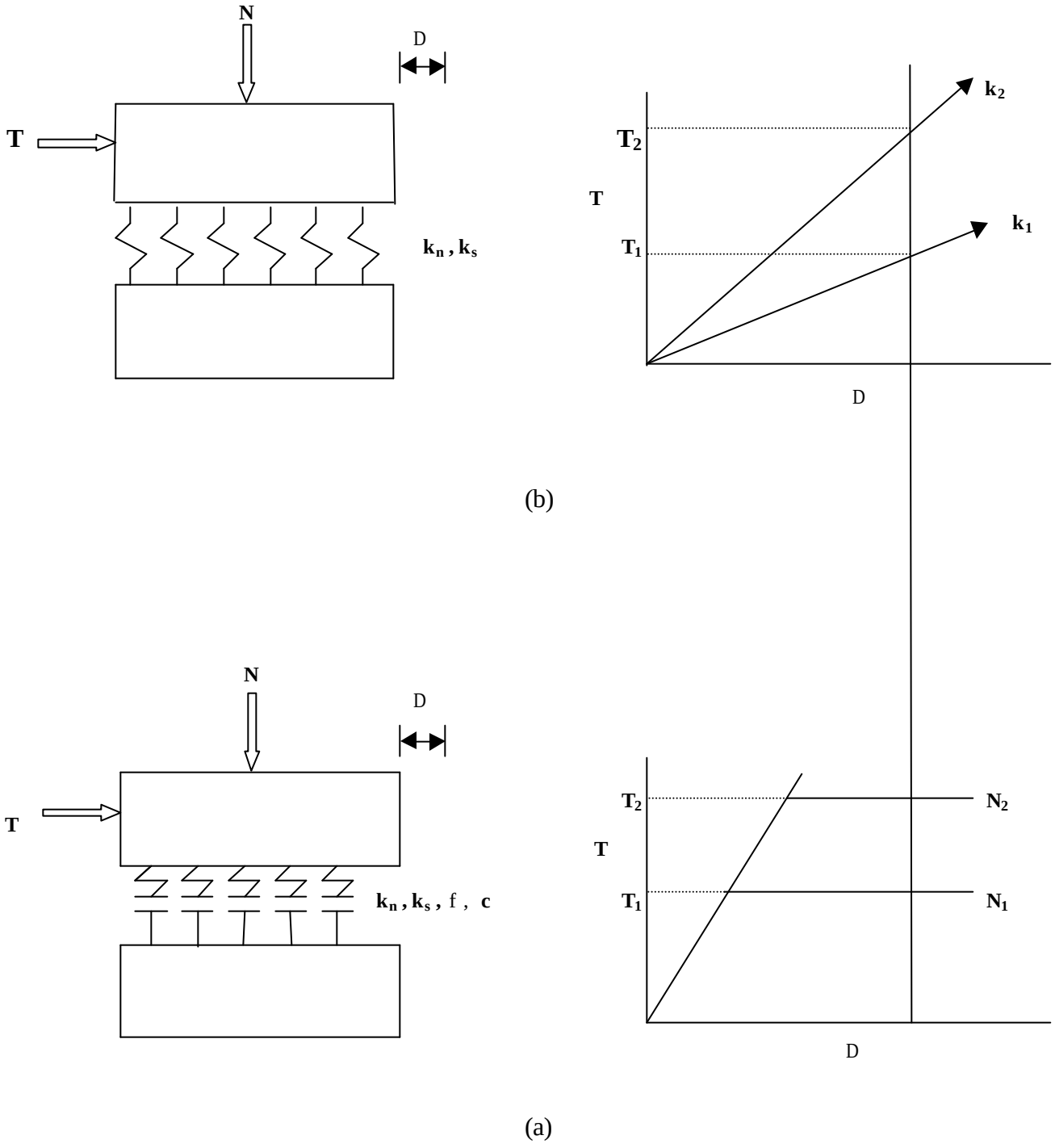

Fig. 11. Direct shear analogy (a) Frictional interface (b) Elastic interface

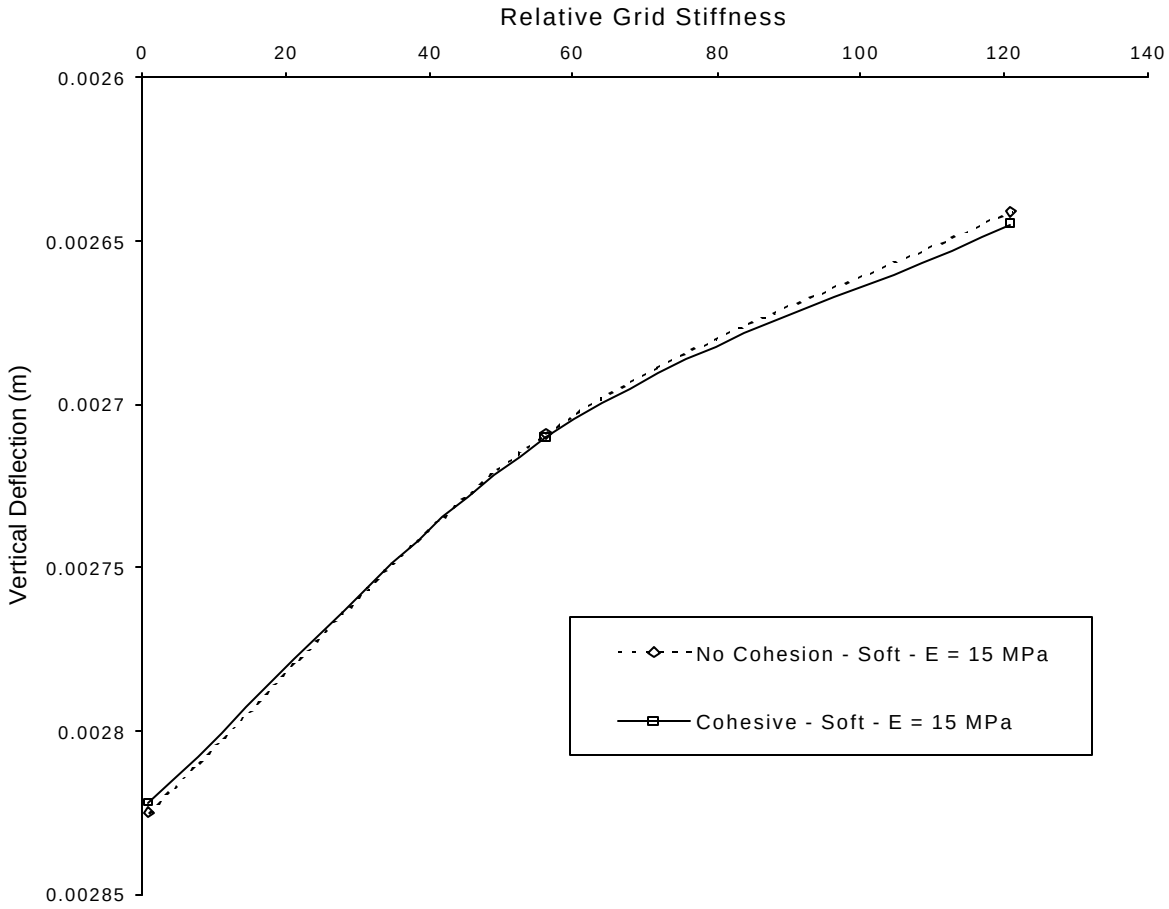

Fig. 12. Vertical deflection vs. relative grid stiffness for a cohesive and non-cohesive interface

2.2.5. Interface Parameters

The values of interface friction angle adopted for this study are based on the experimental tests quoted in section 2.2.4, and are outlined in Table 6.

Table 6. Frictional interface properties

	$\phi_{base/geosynthetic}$	$\phi_{subgrade/geosynthetic}$	c	K_n (MPa/m)	K_s (MPa/m)
Geogrid	ϕ_{base}	$\phi_{subgrade}$	0	$7.4*10^8$	$7.4*10^7$
Geotextile	$0.9*\phi_{base}$	$\phi_{subgrade}$	0	$7.4*10^8$	$7.4*10^7$

Additionally, the values of normal and shear stiffness are determined from equation (2.1). Since the geometry and material properties vary from case to case, the interface normal and shear stiffness were held constant such that any additional elastic deflections resulting from the interface are eliminated by the normalization process. For the surfaced cases considered, an additional interface exists between the pavement and the base material. This interface was assumed fully bonded, and no interface elements were used.

2.2.6 Analysis Matrix

The analysis matrix flow chart is shown in Fig. 13 (a)-(c) and represents all cases analyzed for this study. It should be noted that the data from certain cases are omitted from the results section of this report. For instance, a stiff subgrade is not considered for the road geometry that is designed assuming 150-300 HCADT. This was done as preliminary results indicated that the addition of geosynthetic reinforcement had little effect on reducing deflections when a very stiff subgrade was used. For comparison, all analyses are repeated assuming an unreinforced case. In total, the analysis matrix contains over 320 cases.

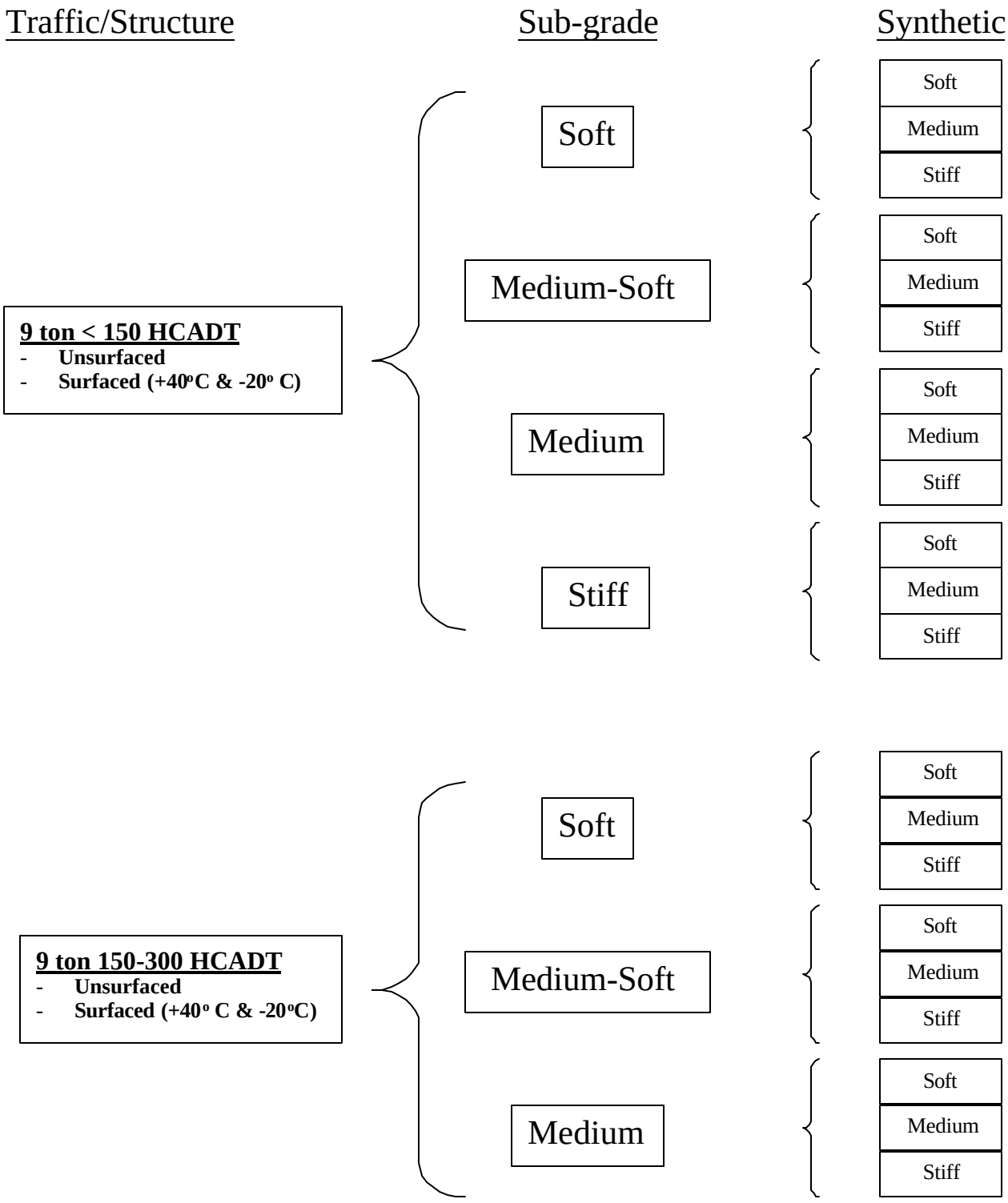

Fig. 13. Test matrix flow chart (a) <150 HCADT and 150-300 HCADT

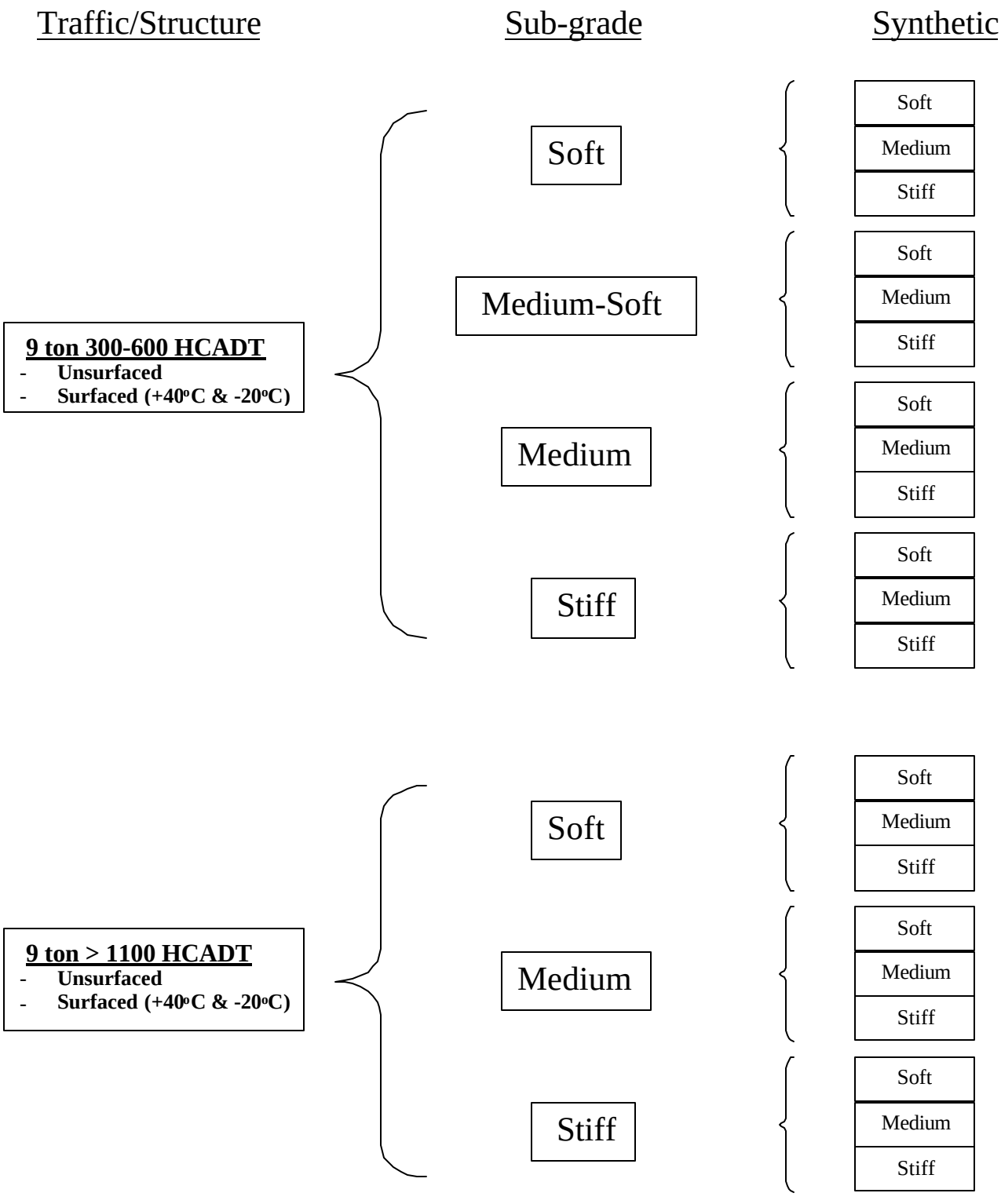

Fig. 13. Test matrix flow chart (b) 300-600 HCADT and >1100 HCADT

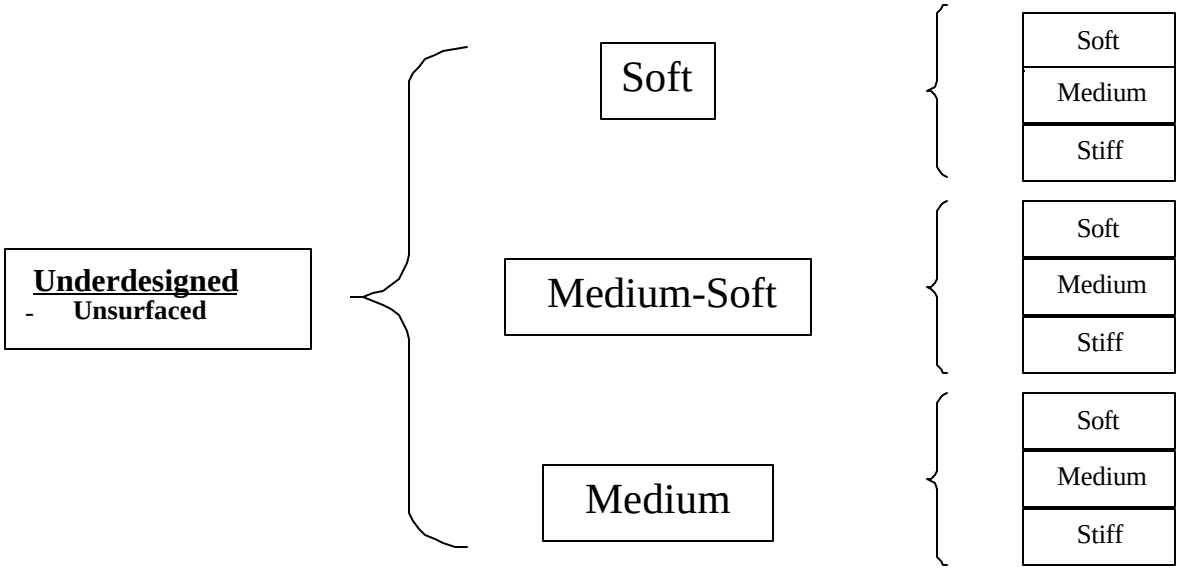

Fig. 13. Test matrix flow chart (c) Unsurfaced

CHAPTER 3
FLAC ANALYSIS

In order to perform the analysis on the cases outline in the analysis matrix, the commercially available finite difference program *FLAC* was used. *FLAC* stands for Fast Lagrangian Analysis of Continua and is widely used by engineers to study geotechnical problems. For this study, two versions of *FLAC* were used to perform the analysis; the single precision version 3.4 and the double precision version 4.0. Two versions were used to expedite the analysis.

3.1.1 *FLAC*

FLAC uses an explicit finite difference formulation to find solutions to the dynamic equations of motion for the specific problem to be analyzed. Either two-dimensional plane strain or axisymmetric problems may be analyzed with the versions used in this study. The user is required to create an input file that contains the specified problem geometry and boundary conditions, the constitutive model and material properties appropriate to the materials being modeled, and the desired loading. *FLAC* will then calculate the response of the system. The general calculation procedure used by *FLAC* is outlined in Fig. 14. An example of a typical input file is provided in the appendix.

The first step in the process is to derive new velocities and displacements from the applied or inertial stresses and forces via the dynamic equations of motion. From the velocities, strain rates are calculated. The selected constitutive law is then used to calculate stresses and forces from the strains. This process is repeated until force equilibrium is reached.

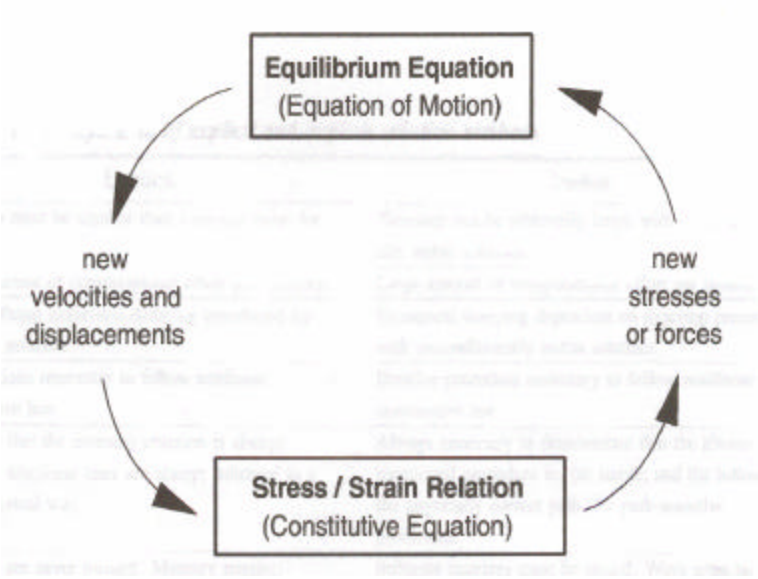

Fig. 14. *FLAC* calculation cycle (*FLAC* Manual, 1995)

An important characteristic of the explicit scheme used by *FLAC* is that one calculation step represents one time around the loop, so the calculation time-step is an important parameter affecting the rate of deformation and computer time required to reach equilibrium. Within the calculation cycle, grid variables are "frozen", and new variables are calculated from the known values of the previous step. In other words, when new stresses are calculated from the velocities, the effect of these new stresses on future velocities are not seen until the next time step. Intuitively, this seems incorrect, as a change in stress for one element should induce a change in velocity in its neighbor. However, if the time-step is chosen small enough such that information cannot physically pass from one element to its neighbor, the assumption that changes in stress do not immediately produce a change in velocity is valid. Therefore, the length of the time-step used by *FLAC* is dependent on the size of the grid elements, and the physical properties of the

material being modeled. The time-step is determined automatically as part of the solution procedure, and is typically quite small.

3.1.2 Problem Considered

The problem to be modeled for this study consists of a circular wheel load on a layered medium as shown in Fig. 15. The layers constitute a variety of materials with different constitutive models and material properties. Since the problem is axisymmetric about the center axis of the uniform pressure, the axisymmetric function in *FLAC* was used. In *FLAC*, axisymmetric problems are solved using "pie shaped" elements, with the r,z plane subdivided into a planar grid as shown in Fig. 16.

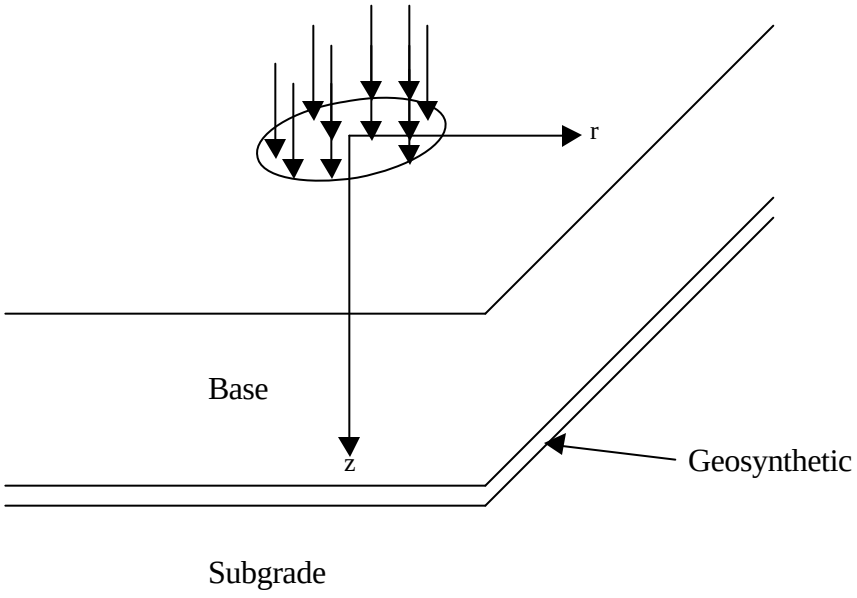

Fig. 15. Axisymmetric problem

3.1.3 Solution Procedure

In order for *FLAC* to perform an analysis, an input data file containing *FLAC* commands must be created. The input file must contain information regarding the size and geometry of the system being modeled, the constitutive law and material properties, the type and location of the loading, and the type and location of the output information desired. The grid used for the analysis is shown in Fig. 16. In order to minimize the calculation time while ensuring sufficient accuracy, a graded mesh was developed. The benefits of the graded mesh are that a large number of small elements are present at the area of large deformation near the edge of the load, a large change in element aspect ratio is not present at the soil-geosynthetic interface, and a small number of elements are present near the model edges where little is happening.

The number of elements used in the grid was held constant at 1960, and the number of elements used for the geosynthetic was held at 160, 4 vertically and 40 horizontally. Otherwise, the number of elements in each layer was adjusted for the given geometry such that the change in element size between layers was not too extreme. The constitutive law for each layer was chosen to best represent the behavior of the material being modeled, and the output parameters were chosen such that the maximum vertical deflection under the center of the given load could be determined.

The simulated wheel loading was applied as a normal stress acting over a 0.15 m radius as shown in Fig. 16. This stress corresponds to a 40 kN (9000 lbs.) single wheel load. The load was applied as one portion and not increased in steps. The maximum number of calculation cycles required to reach equilibrium was roughly 500000, which took about 4 hours on a 400 MHz machine.

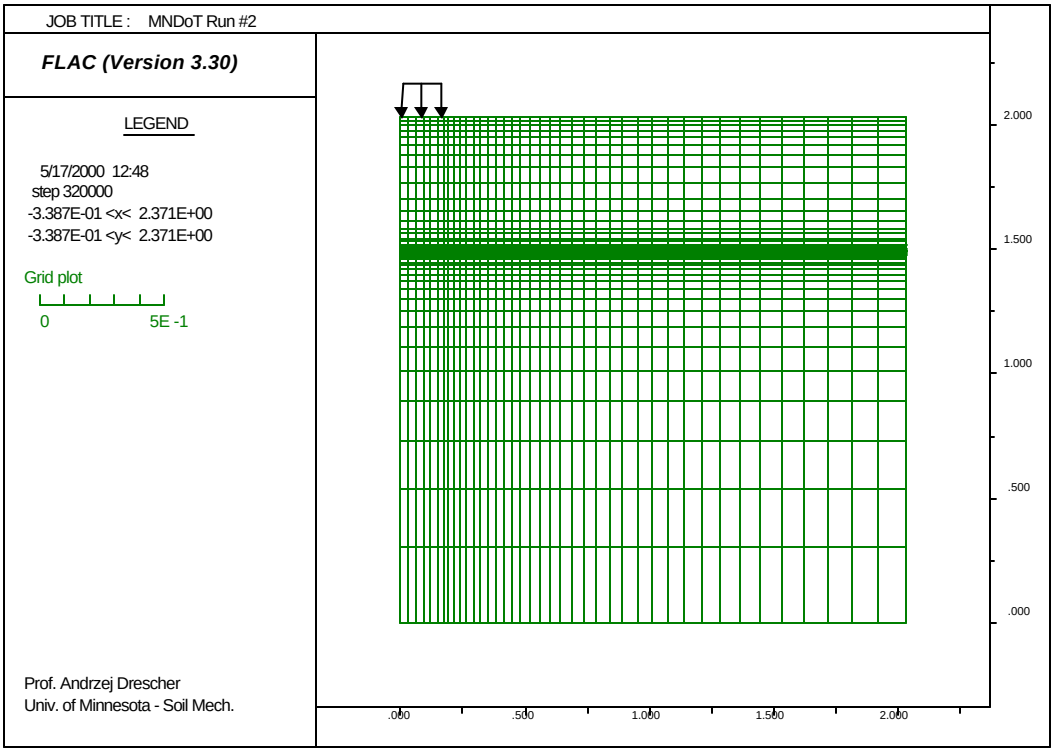

Fig. 16. Typical *FLAC* mesh used in the analysis

For the solution procedure used by *FLAC*, caution must be exercised when establishing the gravity stress distribution for an artificially created layered system. For example, in actual road construction soils are excavated to a prescribed depth and then back-filled with suitable soils and base materials. When this system is modeled, however, a different sequence of events takes place. First, the geometry of the model is specified and the boundary conditions set. Next, the constitutive law is assigned and the material properties input. Then, gravity is turned on and the system allowed to reach equilibrium. For the layered cross sections of differing Poisson's

ratio considered in this study, great difficulty was encountered in achieving predictable behavior under gravity loads. Fig. 17 demonstrates the unexpected behavior exhibited by the model under the influence of gravity alone.

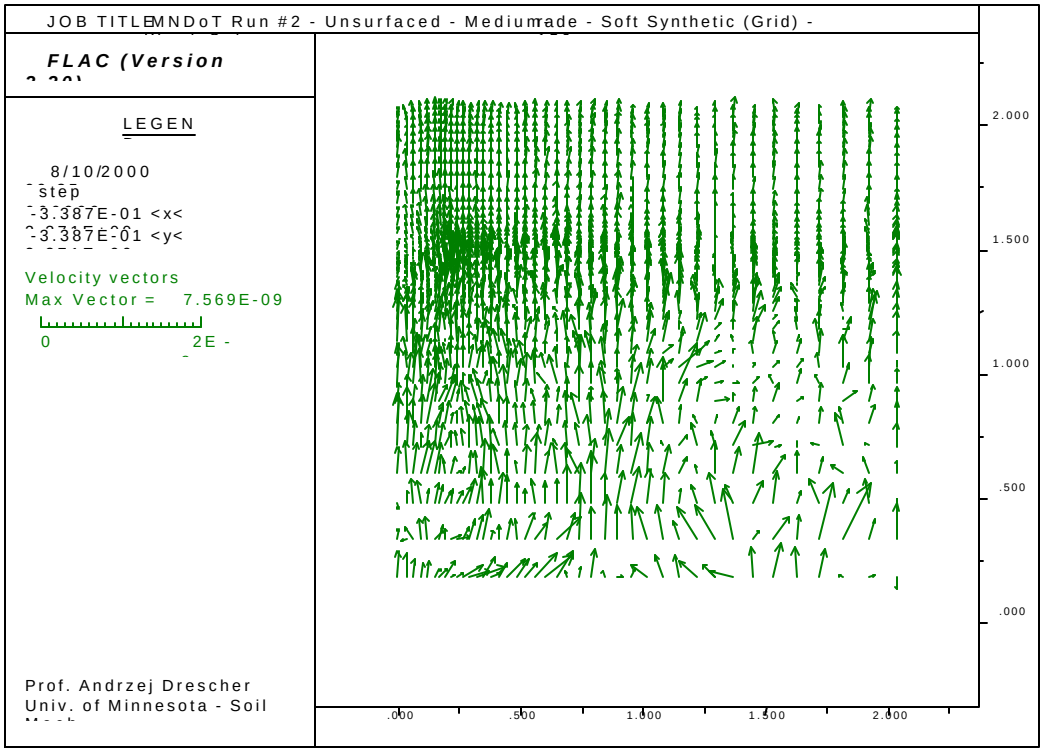

Fig. 17. Velocity profile for gravitational stress field with large interface shear stiffness

As may clearly be seen in the figure, the velocity distribution is clearly incorrect with nearly all of the velocity vectors pointing upward.

Significant testing was done in order to determine the cause of this behavior. The results of these tests indicated that incompatible horizontal displacements at the interfaces due to the layered soil were causing the strange behavior. In other words, at the geosynthetic layer, three

materials were coming together and each had a different value of Poisson's ratio. Since these three layers were connected together with very stiff interface elements, the layers were unable to deform as they would in a natural setting (i.e. the interface was controlling the horizontal behavior of the materials near the geosynthetic layer). The result of this incompatible horizontal displacement is the upward velocity profile shown in Fig. 17.

In order to alleviate this upward behavior, due to incompatible horizontal displacements at the interfaces, the following modeling sequence was selected. Upon generating the grid and specifying material properties, unrestricted slip at the interfaces was allowed. This was accomplished by assigning a very small value of the interface shear stiffness, k_s. Alternatively, the value of interface friction angle could have been chosen as zero. Next, the gravity was turned on, and the model cycled until static equilibrium was reached. Once the gravitational stress field was established, the value k_s was increased to that given in Table 6 and the model cycled with the surface stress applied.

CHAPTER 4
RESULTS

The results of the study are indicated in terms of percent normalized reduction in surface deflection at the center of the loaded area, and percent normalized increase in serviceability life. Additionally, horizontal stress distributions at three locations on the roadway cross-section have been created. In order to display these results, two series of plots have been created. The first series illustrates the percent normalized deflection reduction, and the second series the percent normalized increase in $ASAL_{2.5}$'s. For both series, the results are plotted against the subgrade's elastic modulus. The intent is to indicate how much and in what fashion a proposed roadway will benefit from the additional stiffness a reinforcing layer can provide. Additionally, the deflection results have been summarized in a series of road cross sections that qualitatively give a sense of the thickness of the layers and the resulting deflections. The addition of the geosynthetic reinforcing layer also affects the stress field in the soil. Since it is difficult to quantify this effect, a representative set of plots shows qualitatively how the stress field is altered.

4.1 Percent Normalized Deflection Reduction

The first series of plots illustrates percent normalized deflection reduction vs. subgrade elastic modulus. In order to determine the percent normalized deflection reduction, a second series of numerical tests was run on unreinforced road sections, and the resulting deflection determined. The percent normalized deflection reduction, $\overline{\Delta}$, could then be determined from the following equation:

$$\overline{\Delta} = (1 - \Delta_{syn}/\Delta_{no\ syn})*100 \qquad (4.1)$$

where Δ_{syn} represents the deflection under the center of the wheel load for the reinforced case, and $\Delta_{no\ syn}$ represents the corresponding deflection for the unreinforced case. The data were plotted in this fashion so that the deflection reduction in terms of percentage over the unreinforced case could be easily observed.

On each plot two different types of geosynthetic reinforcement are shown, geotextile and geogrid. Curves using the circular data points represent the geotextile reinforced results, while curves using the triangular data points represent the geogrid reinforced results. Three different stiffnesses of geogrid and geotextile are used resulting in six curves on each plot. The legend indicates the individual stiffness of each geogrid and geotextile used as well as the assumed thickness of the reinforcing layer.

In order to give a sense of how the amount of base structure influences the geosynthetic reinforcement, each set of plots for a given road type has the same scale on the vertical axis. In other words, all of the plots for unsurfaced roads have the same vertical axis, all of the plots for the HMA surfaced roads (-20^o C) have the same vertical axis, and all of the plots for the HMA surfaced roads (40^o C) have the same vertical axis.

The plots of percent normalized deflection reduction vs. subgrade modulus are given in Figs. 18 (a)-(d), Figs. 19 (a)-(c), and Figs. 20 (a)-(c).

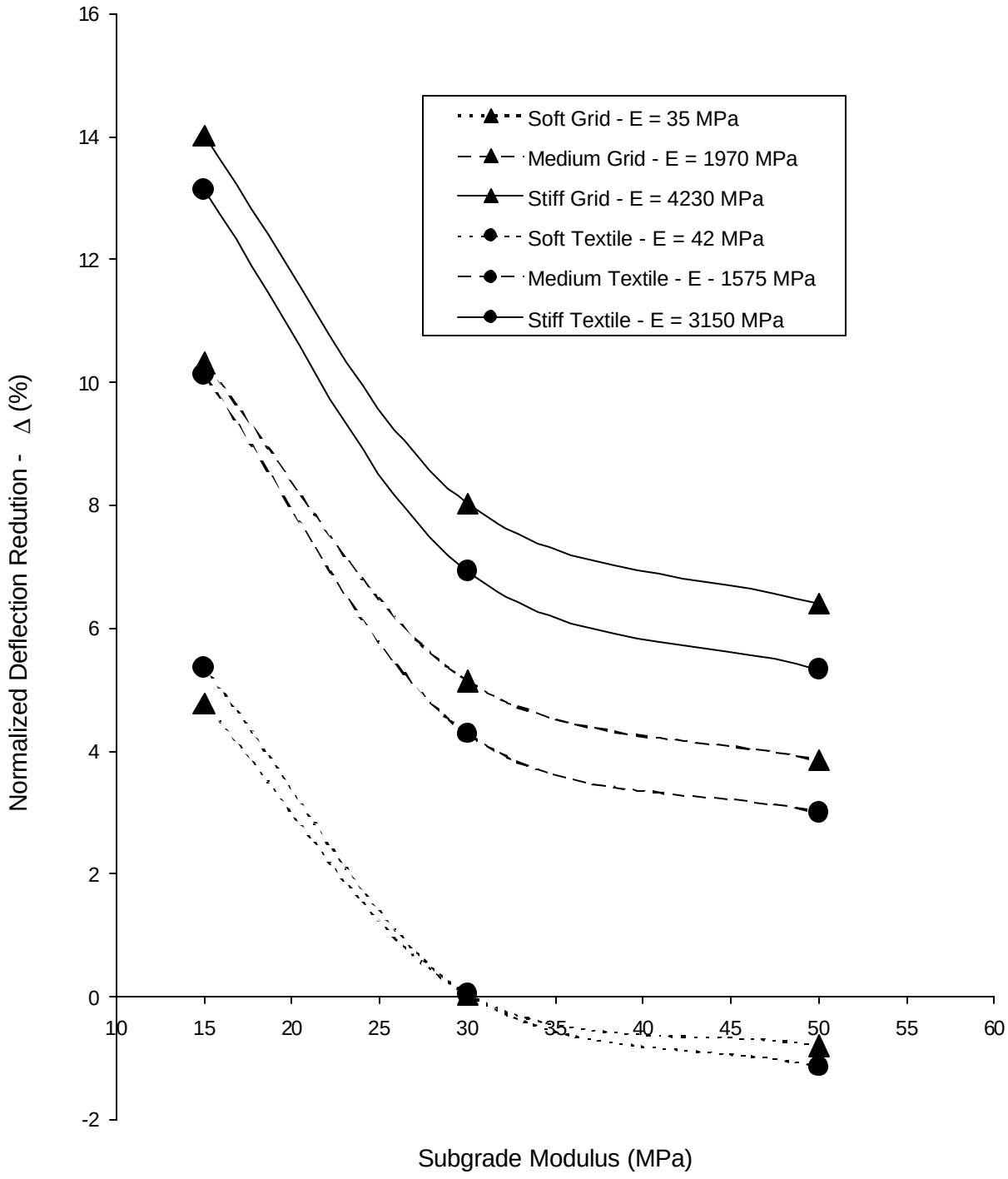

Fig. 18. Normalized deflection reduction vs. subgrade modulus –
(a) Unsurfaced, underdesigned structure

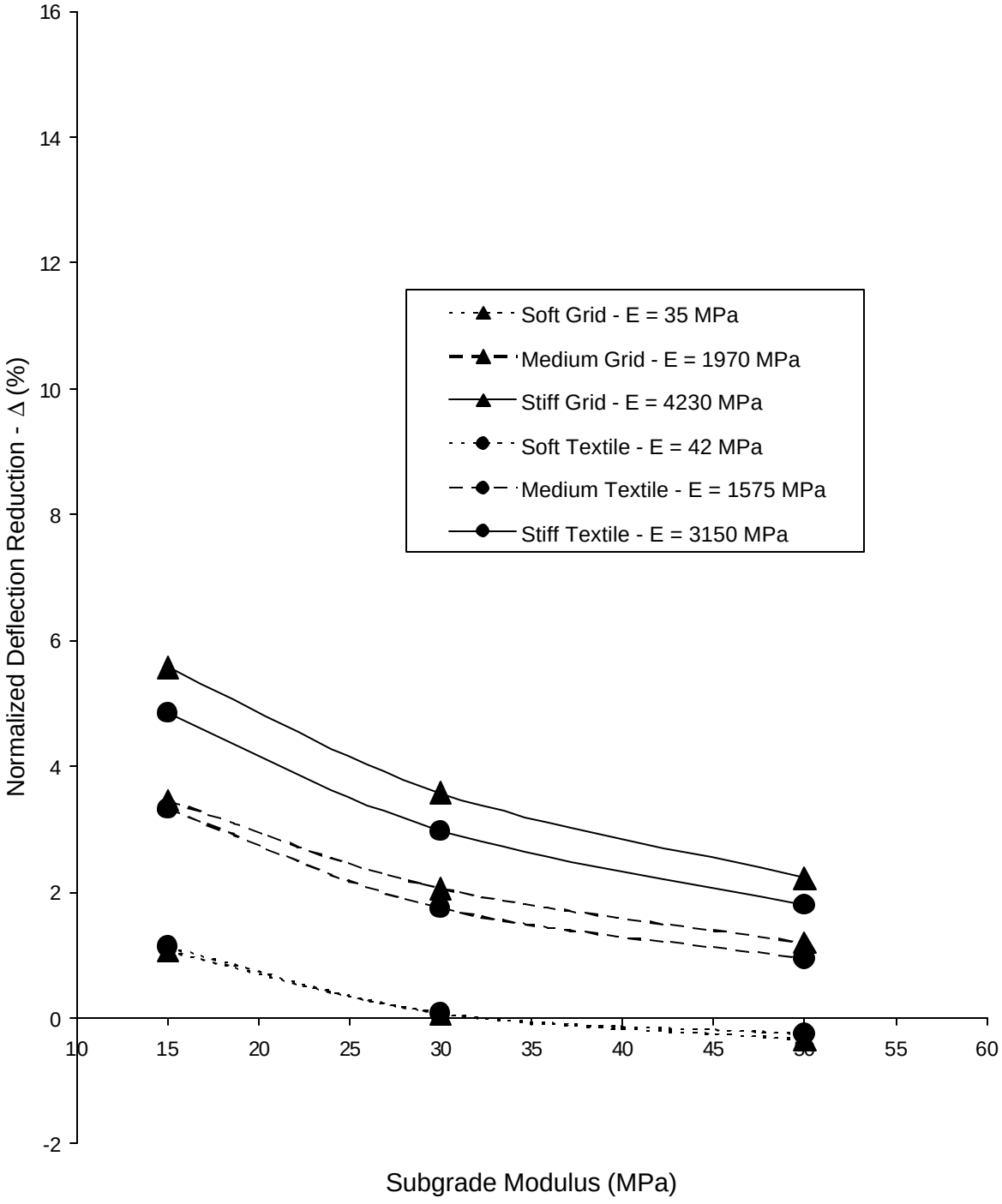

Fig. 18. Normalized deflection reduction vs. subgrade modulus –
(b) Unsurfaced, < 150 HCADT structure

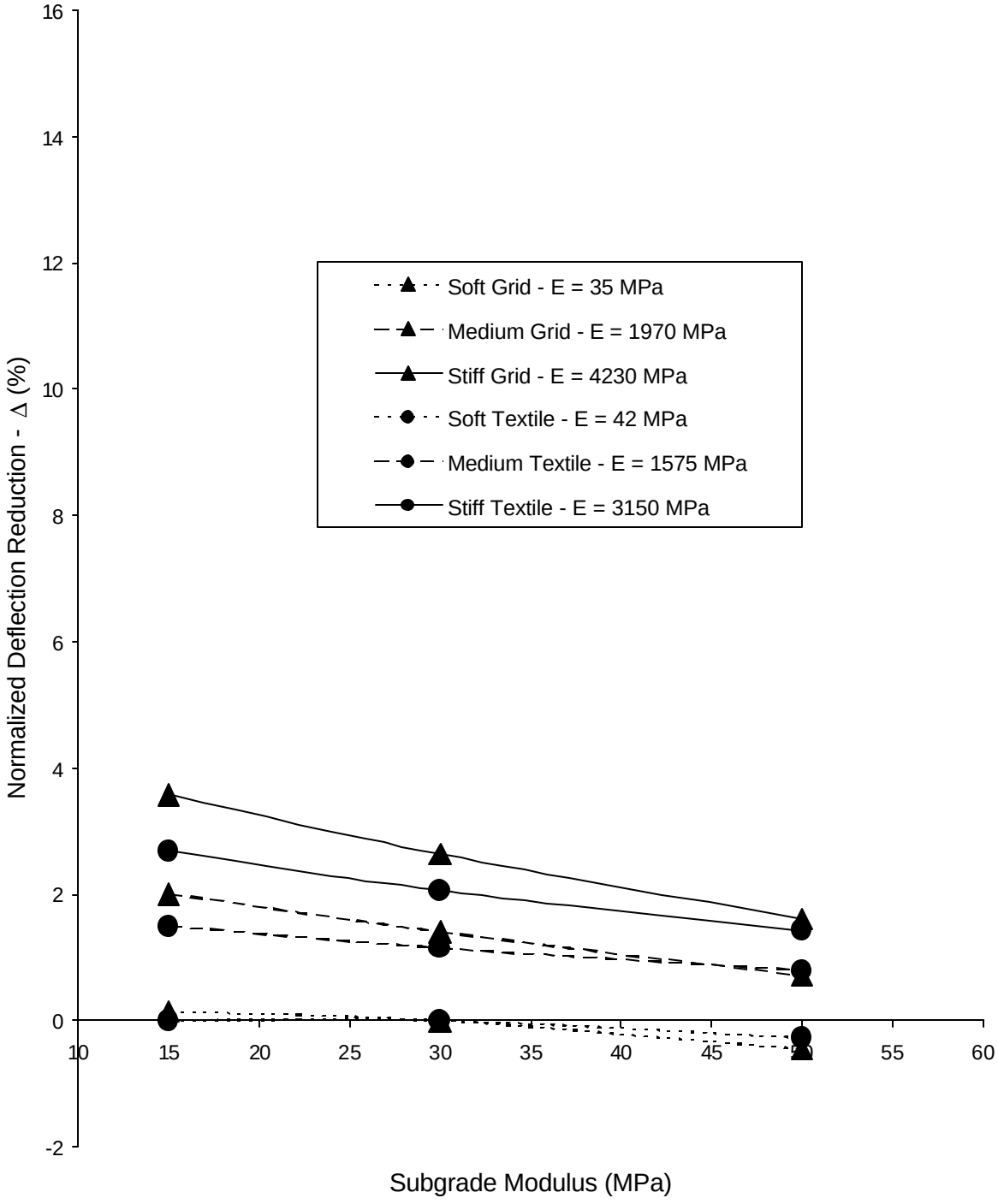

Fig 18. Normalized deflection reduction vs. subgrade modulus –
(c) Unsurfaced, 150-300 HCADT structure

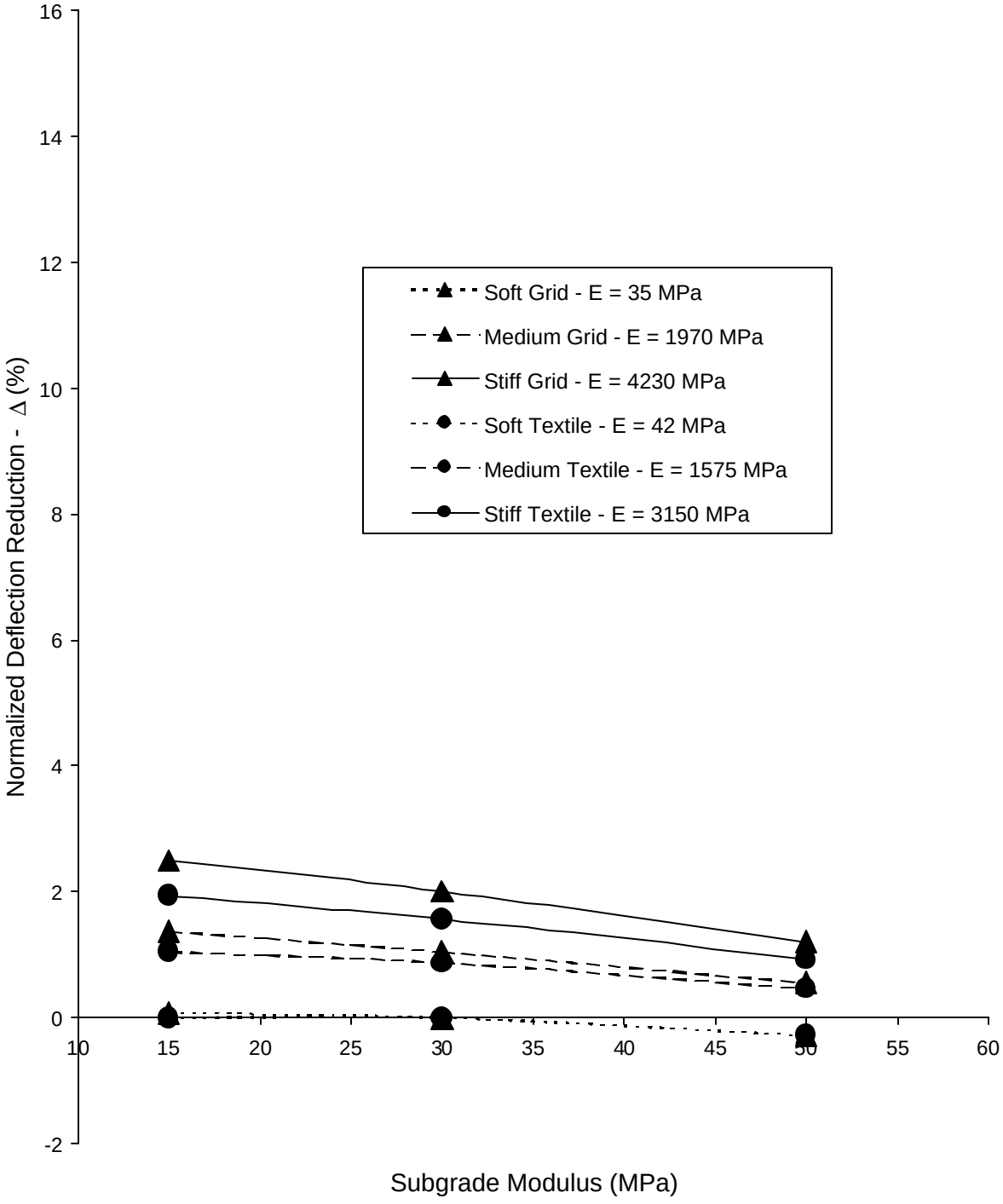

Fig. 18. Normalized deflection reduction vs. subgrade modulus –
(d) Unsurfaced, 300-600 HCADT structure

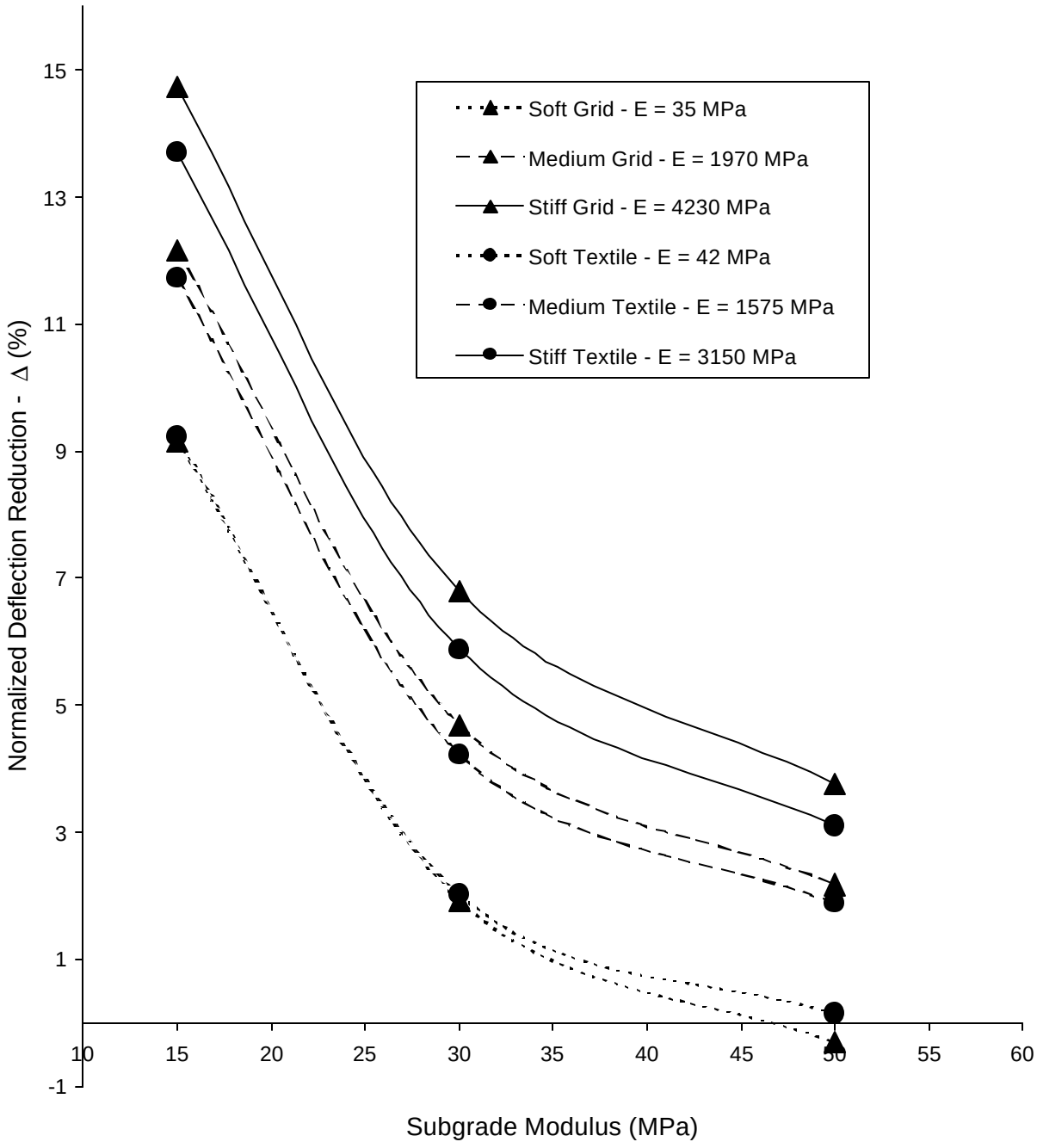

Fig. 19. Normalized deflection reduction vs. subgrade modulus –
(a) 40^{o} C pavement, <150 HCADT structure

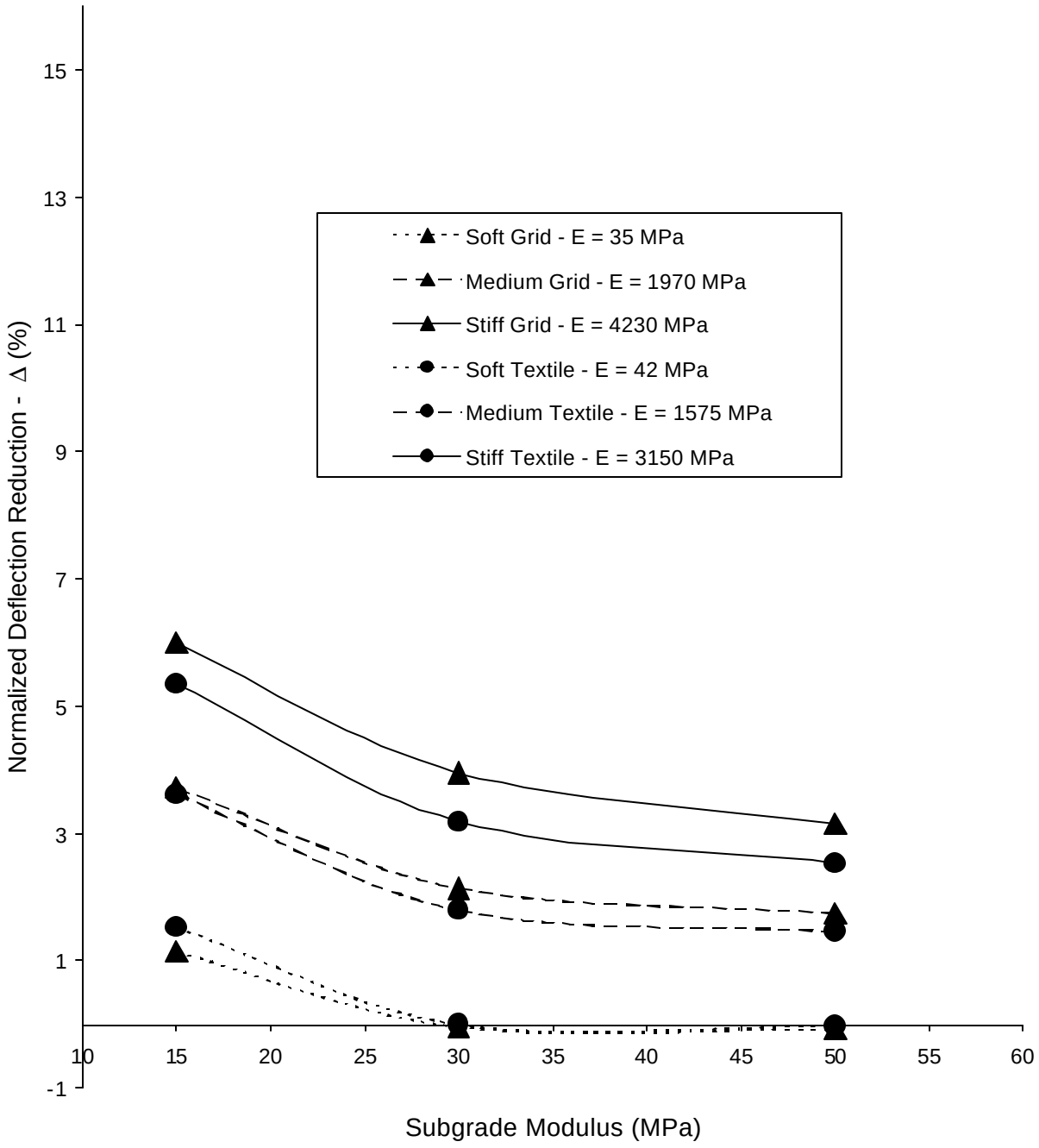

Fig. 19. Normalized deflection reduction vs. subgrade modulus –
(b) 40^{o} C pavement, 150-300 HCADT structure

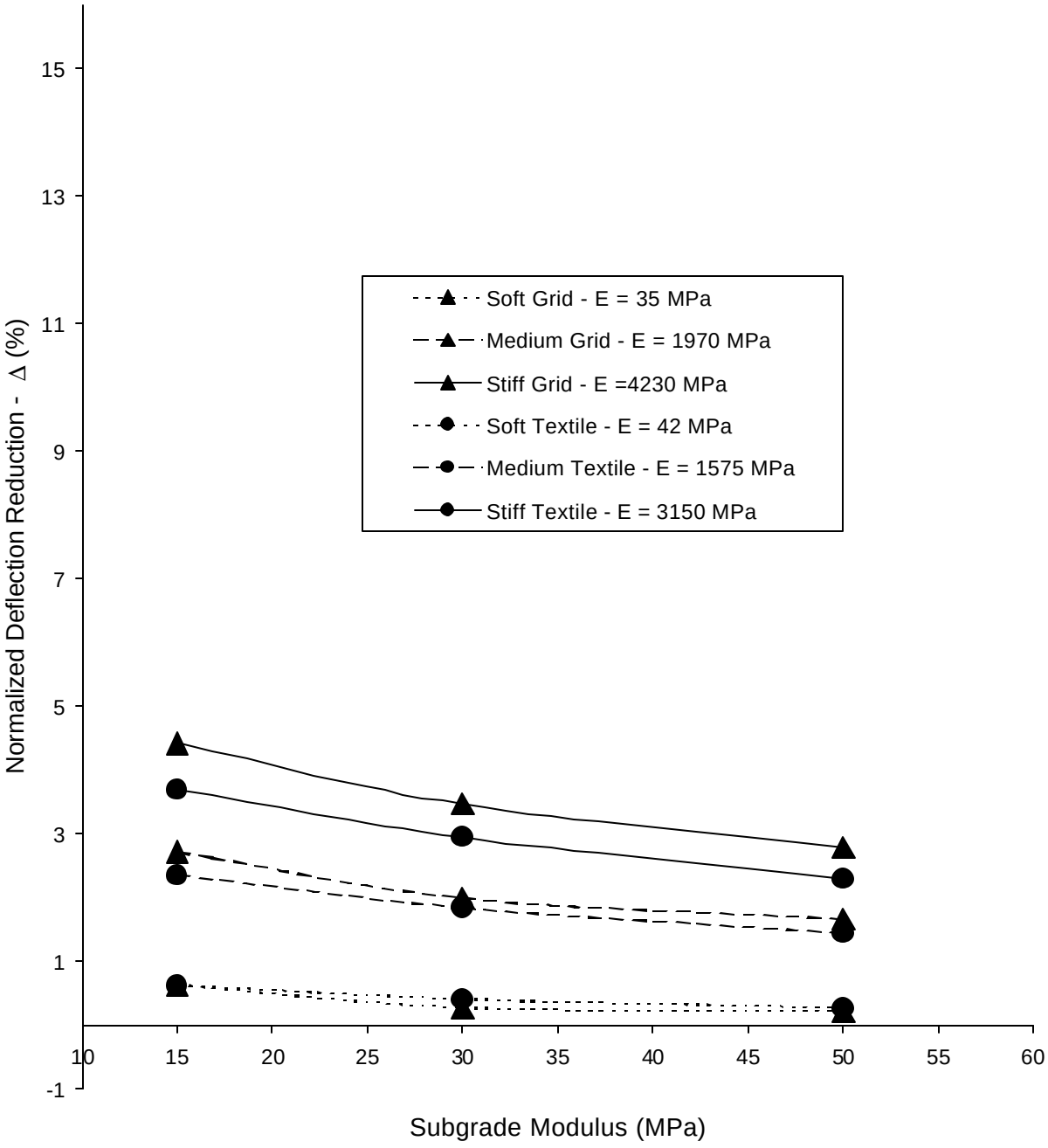

Fig. 19. Normalized deflection reduction vs. subgrade modulus –
(c) 40^{o} C pavement, 300-600 HCADT structure

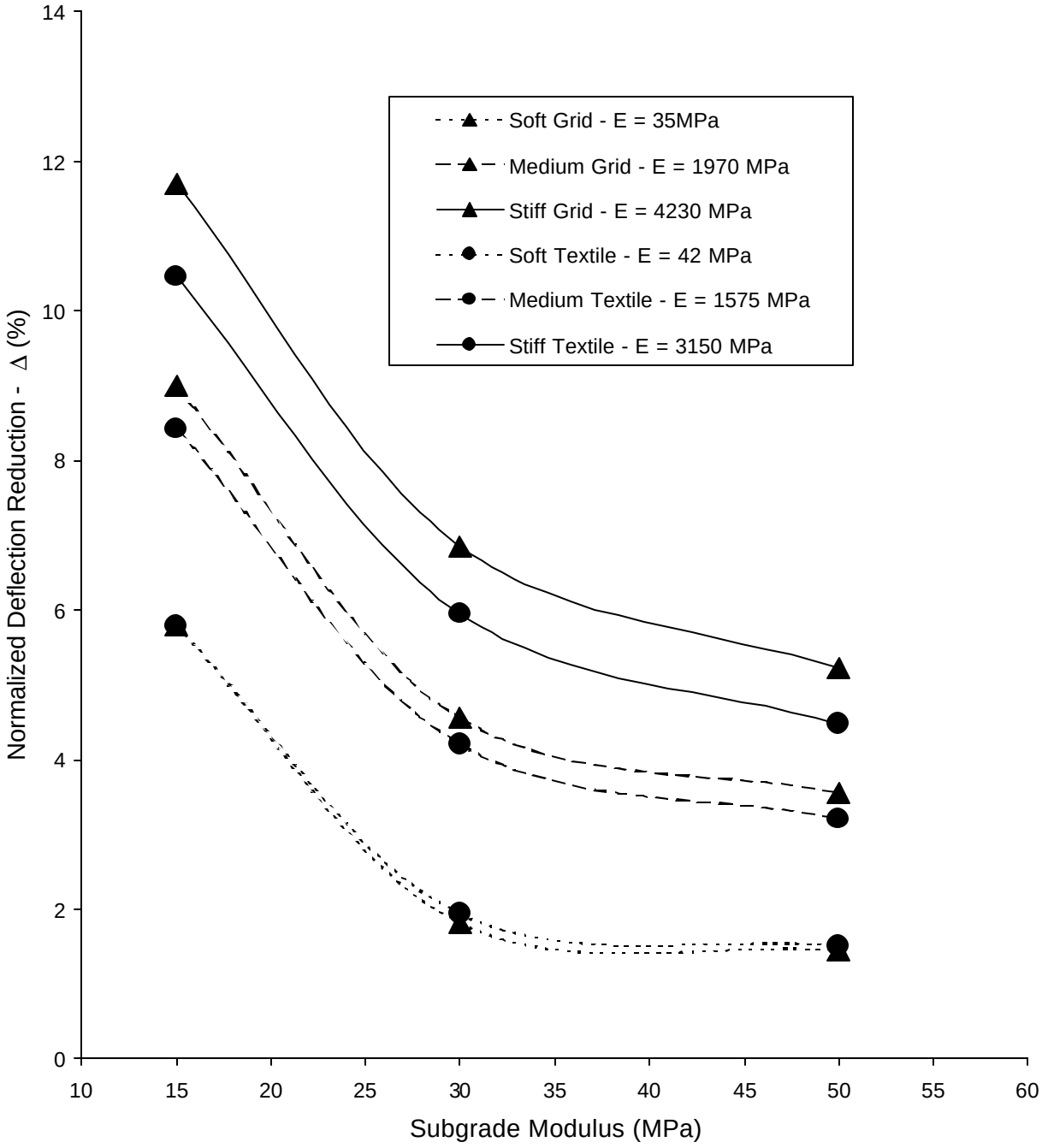

Fig. 20. Normalized deflection reduction vs. subgrade modulus –
(a) -20^{o} C pavement, <150 HCADT structure

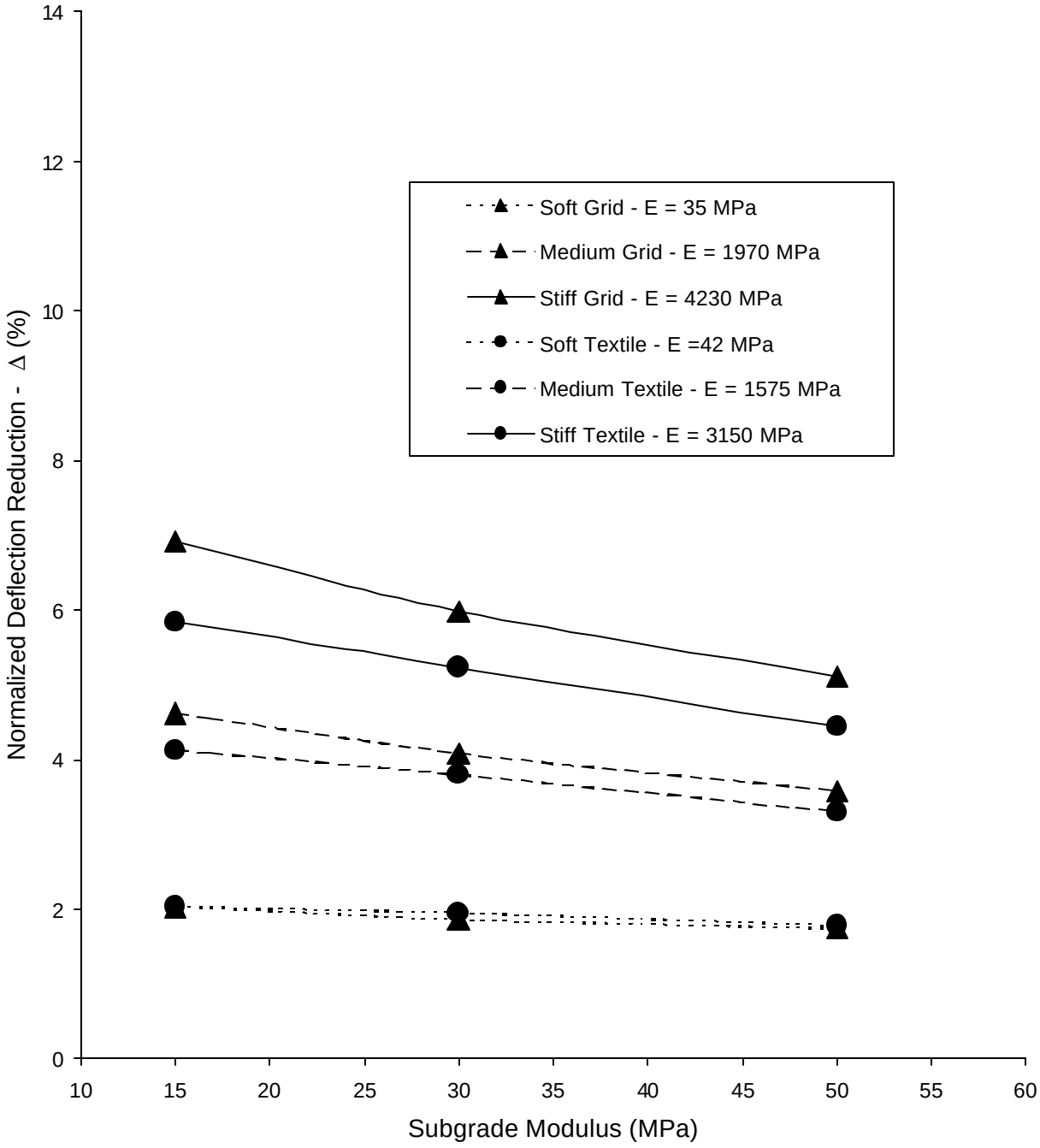

Fig. 20. Normalized deflection reduction vs. subgrade modulus –
(b) -20^{o} C pavement, 150-300 HCADT structure

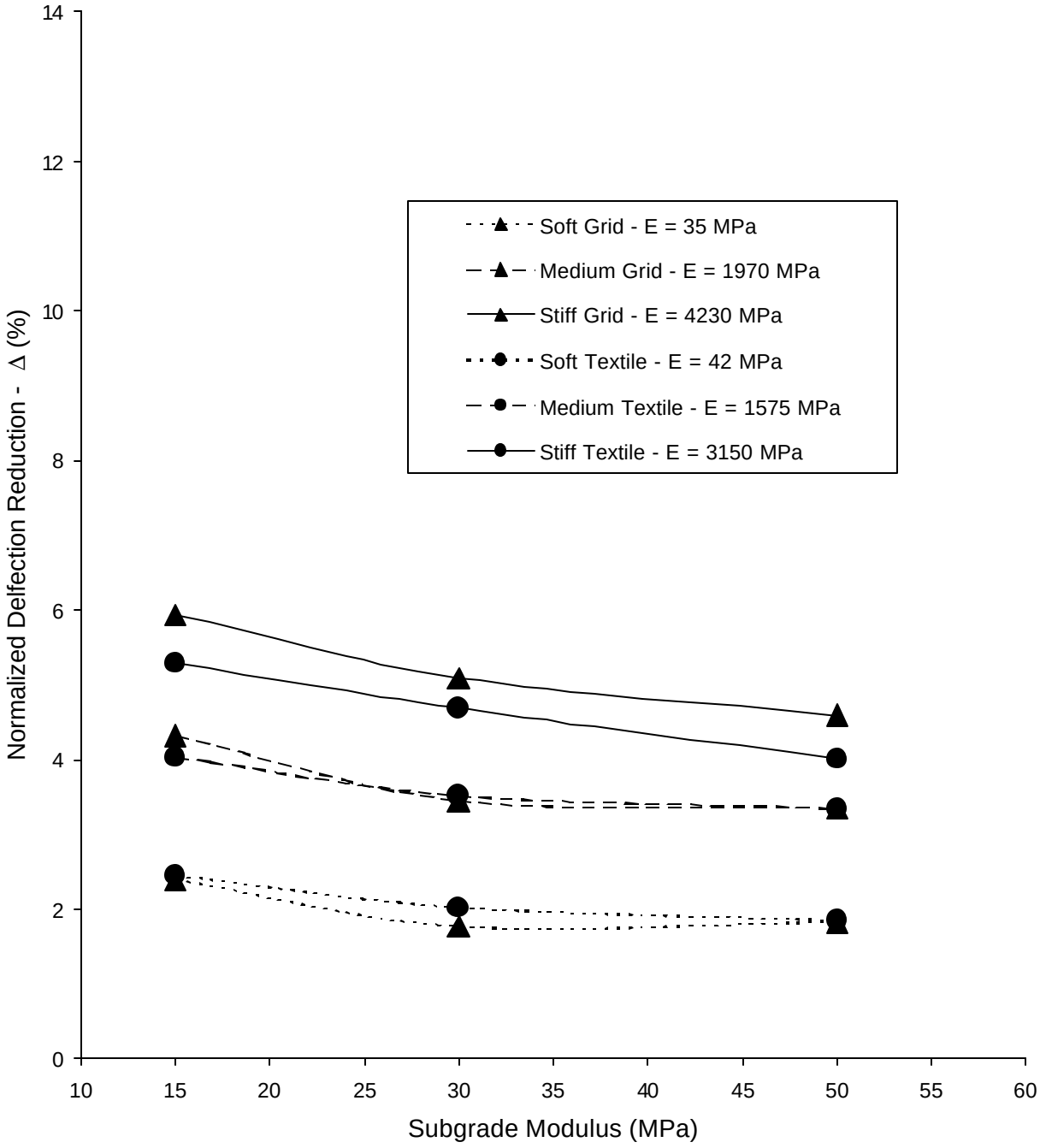

Fig. 20. Normalized deflection reduction vs. subgrade modulus –
(c) -20^{o} C pavement, 300-600 HCADT structure

4.2 Percent Normalized $ASAL_{2.5}$ Increase

In addition to displaying the benefits of geosynthetics by a percent reduction in deflection, a flexible pavement design equation relating deflection to number of $ASAL_{2.5}$'s was used to illustrate how geosynthetics can reduce pavement fatigue. As a guideline for the state's design engineers, Mn/DOT has adopted a flexible pavement fatigue equation from The AASHO Road Test, Report No. 5. The equation relates a Benkelman Beam deflection to the accumulated number of standard axle loads that result in a serviceability of 2.5 ($ASAL_{2.5}$). The equation used to determine the number of $ASAL_{2.5}$'s to failure based on deflection is as follows

$$\log(ASAL_{2.5}) = 11.06 - 3.25\log(d_s) \qquad (4.2)$$

where d_s is the Benkelman Beam deflection in thousandths of an inch.

The Benkelman Beam apparatus is shown in Fig. 21, and consists of a lever arm that is attached to an adjustable base frame. Measurements are made for the Benkelman Beam test by placing the beam probe between the dual wheels of an 18-kip axle load truck, and zeroing the gage reading deflection. The truck is then moved away and the upward movement of the pavement recorded by the dial gage. Care must be taken when running the Benkelman Beam test as the load frame must be placed outside of the deflected area under the influence of the wheel load, or the test results will be erroneous.

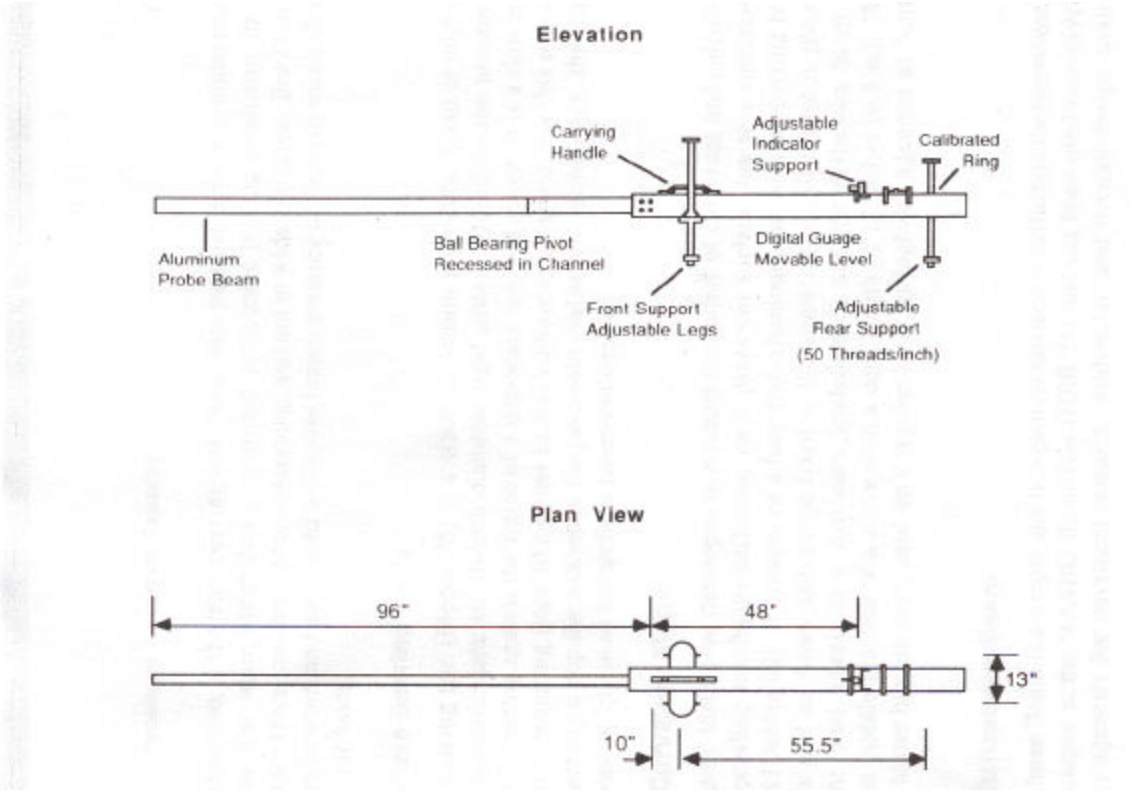

Fig. 21. Benkelman beam apparatus (Haas, Hudson, and Zaneiwski, 1994)

As Eq. (4.2) makes use of deflections measured in the Benkelman Beam test at mid-distance between the two loaded areas (tires), its use to analyze the results of the present computations may seem inappropriate. However, since the $ASAL_{2.5}$'s are normalized relative to the unreinforced case, it is believed that the ratio is valid, even though the deflections are not derived from the Benkelman Beam test. In other words, for a given base thickness, geosynthetic, subgrade, and pavement, the $ASAL_{2.5}$ ratio should be identical regardless of whether the deflections are from a Benkelman Beam test or from the numerical simulation as the system remains elastic for both.

Similar to the percent normalized deflection reduction plots, the normalized $ASAL_{2.5}$ increase plots all have identical scales on the vertical axis for a given road type. To determine

the percent normalized $\overline{ASAL}_{2.5}$ increase relative to the unreinforced case, the following equation was used

$$\overline{ASAL}_{2.5} = (1 - ASAL_{2.5\ no\ syn}/ASAL_{2.5\ syn})*100 \qquad (4.3)$$

where $ASAL_{2.5\ no\ syn}$ is the equivalent number of standard axle loads given by equation (4.2) for a deflection based on an unreinforced road, and $ASAL_{2.5\ syn}$ is the equivalent number of standard axle loads given by equation (4.2) for a deflection based on a road reinforced with a geosynthetic. The test results are presented in this fashion in order to show the percent increase in serviceability life the addition of a geosynthetic reinforcement layer can provide a given flexible pavement.

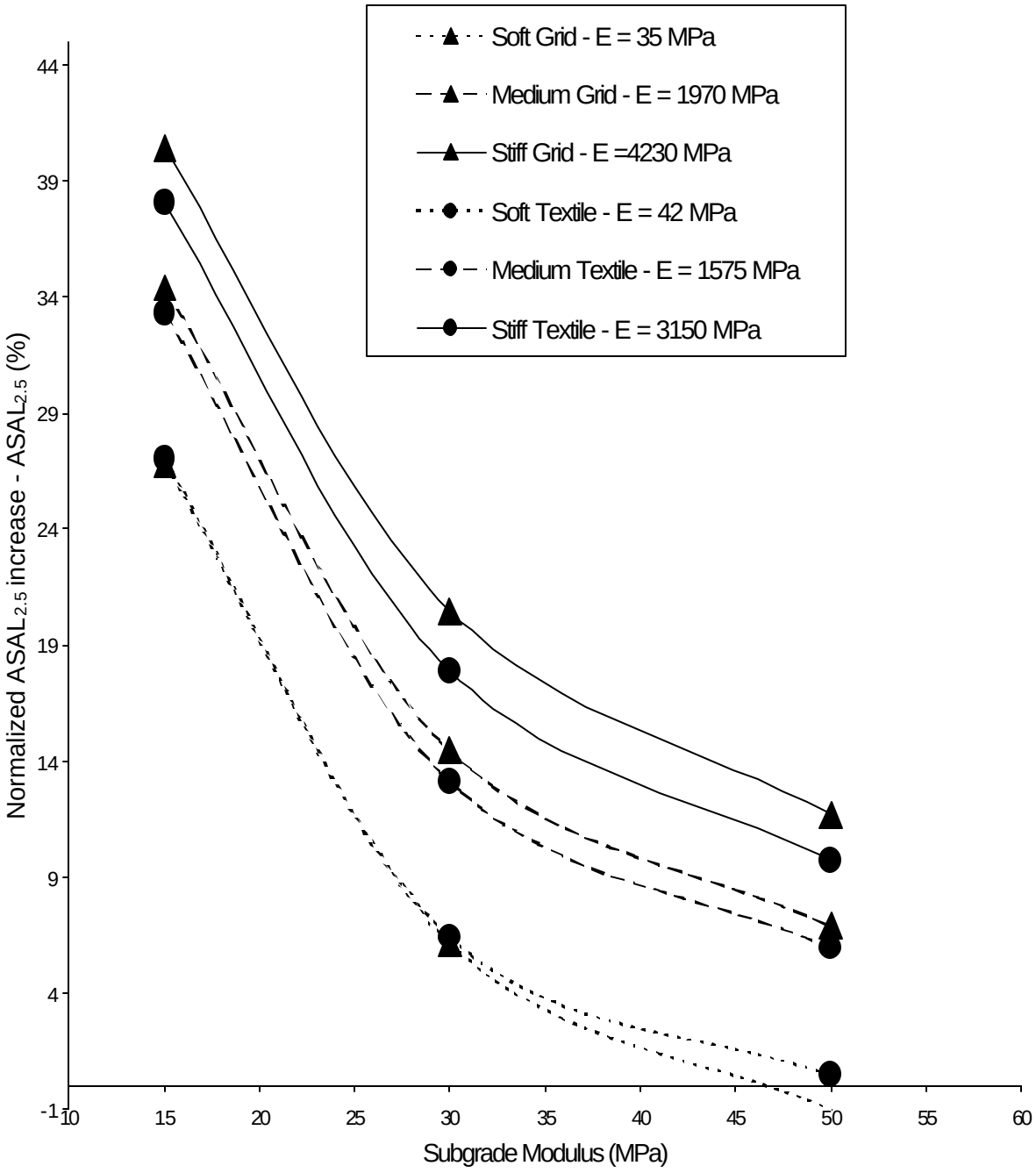

Fig. 22. Normalized $ASAL_{2.5}$ increase vs. subgrade modulus –
(a) 40^{o} C pavement, <150 HCADT structure

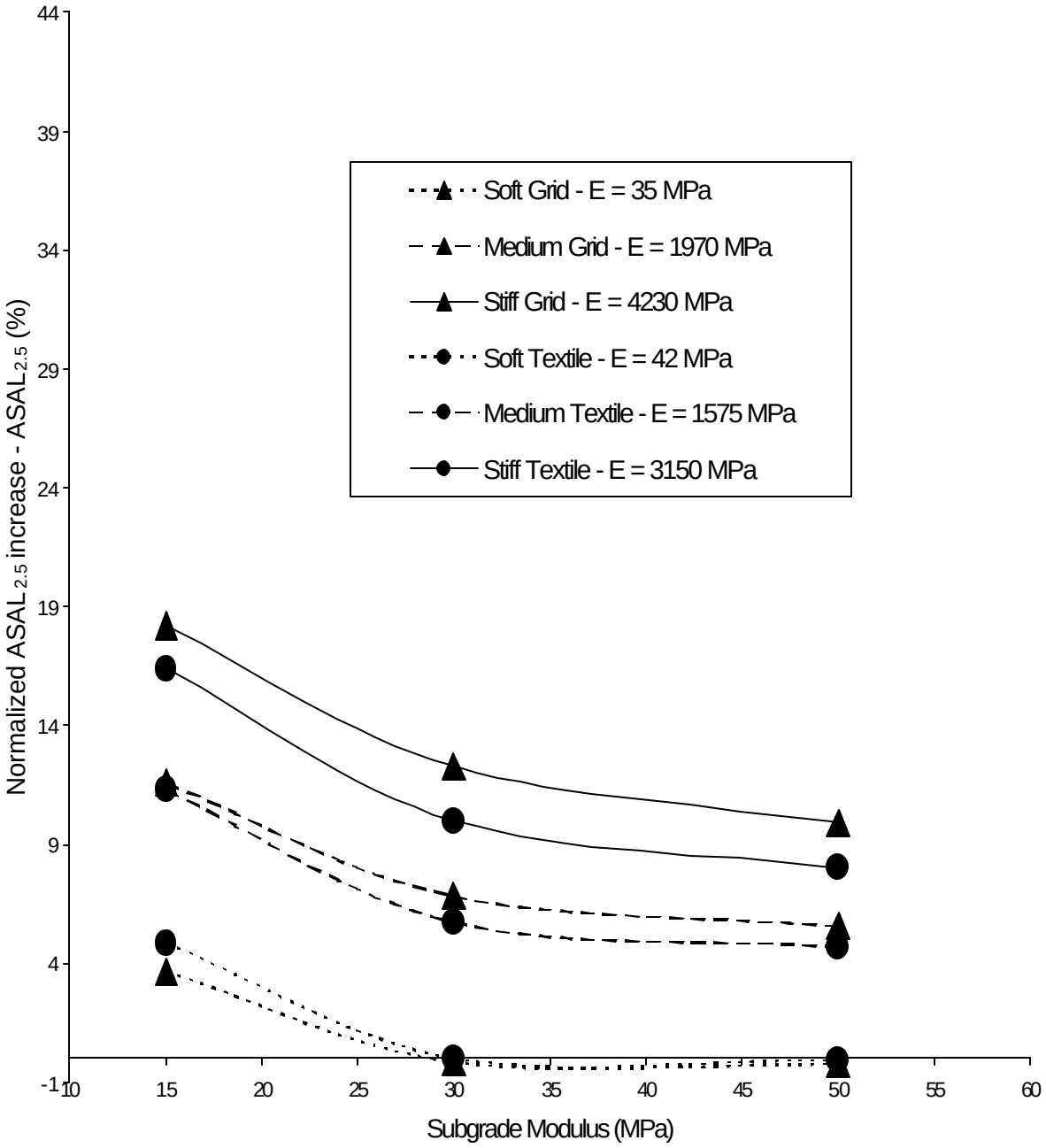

Fig. 22. Normalized $ASAL_{2.5}$ increase vs. subgrade modulus –
(b) 40^{o} C pavement, 150-300 HCADT structure

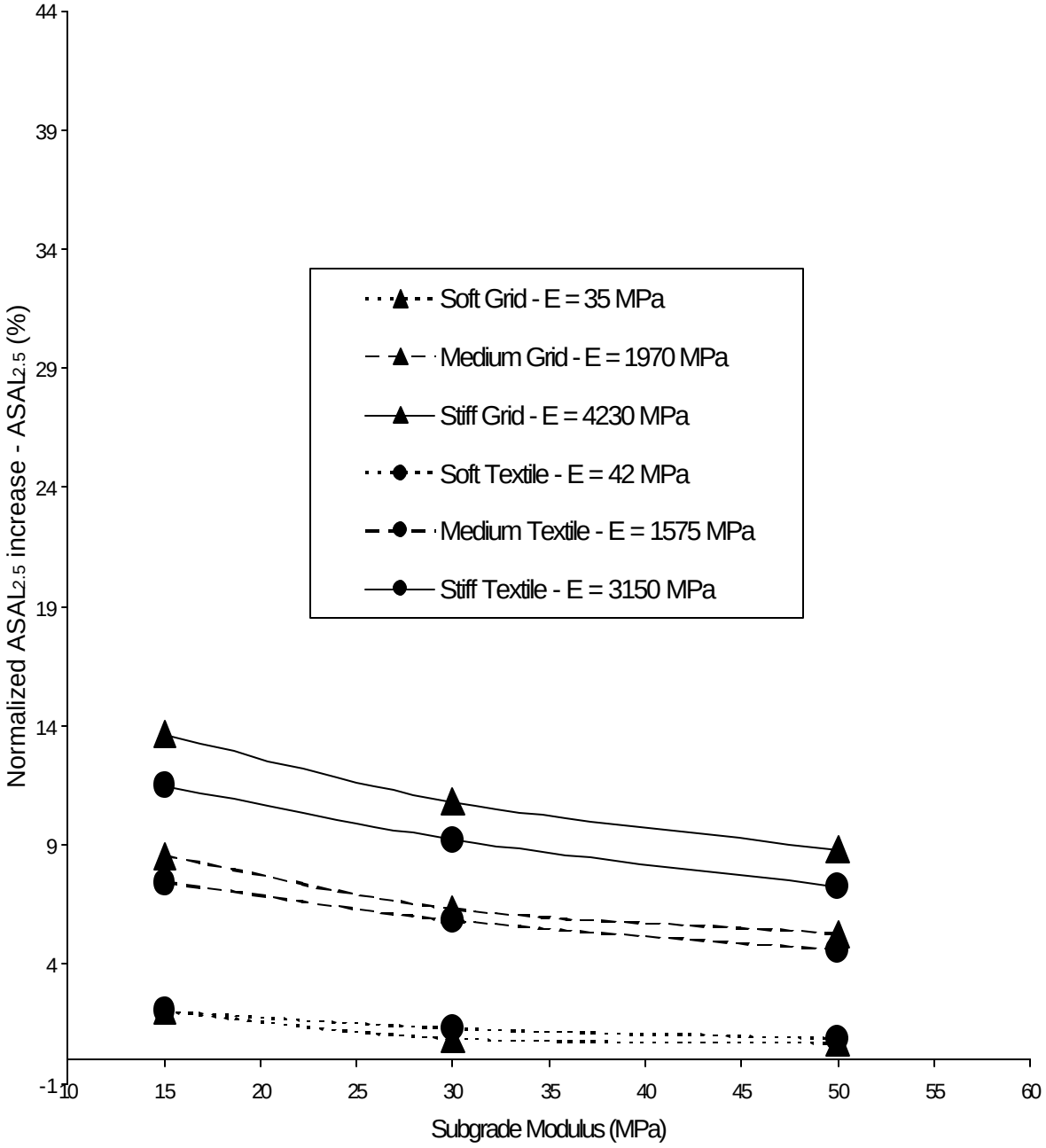

Fig. 22. Normalized $ASAL_{2.5}$ increase vs. subgrade modulus –
(c) 40° C pavement, 300-600 HCADT structure

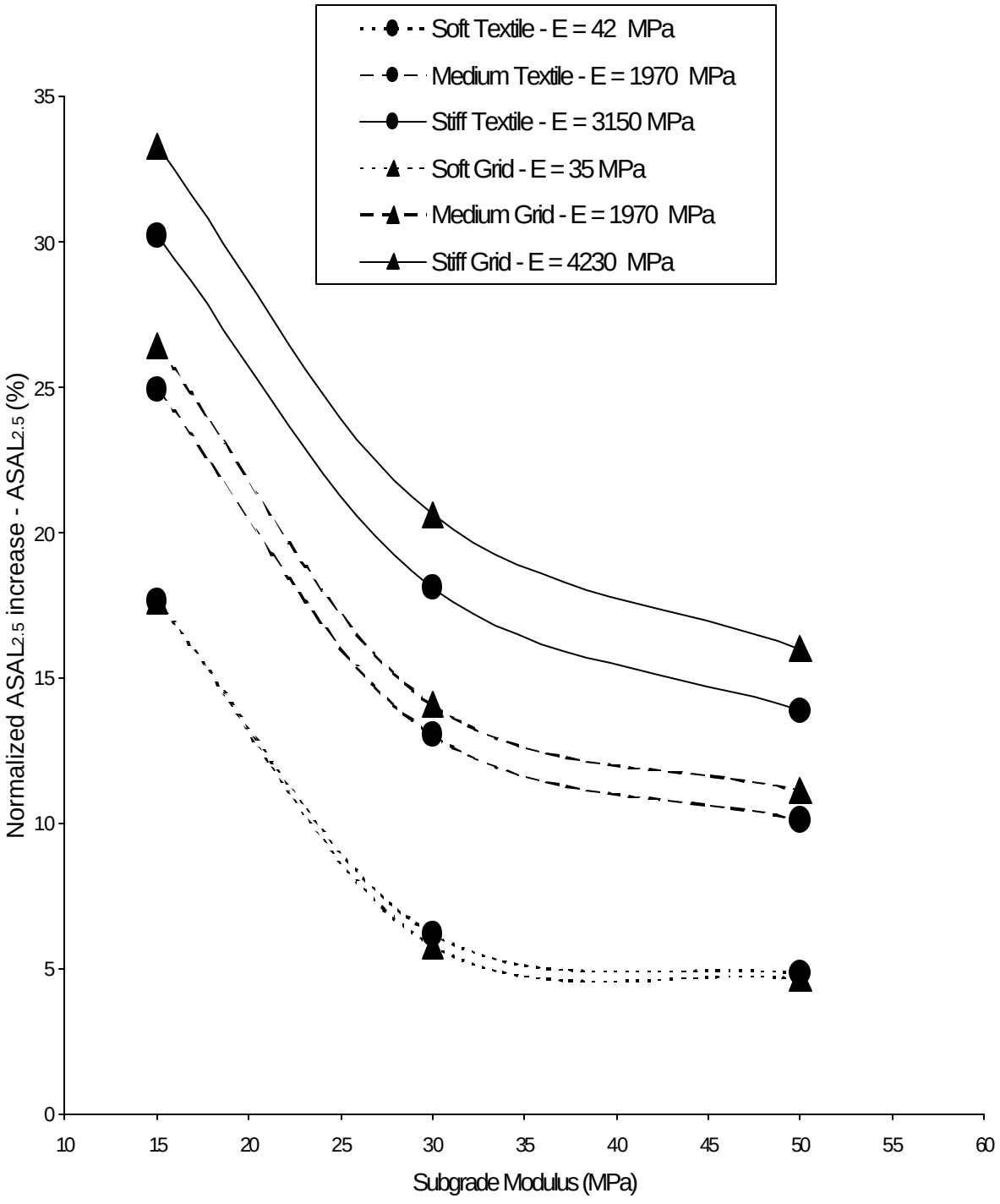

Fig. 23. Normalized $ASAL_{2.5}$ increase vs. subgrade modulus –
(a) -20^{o} C pavement, <150 HCADT structure

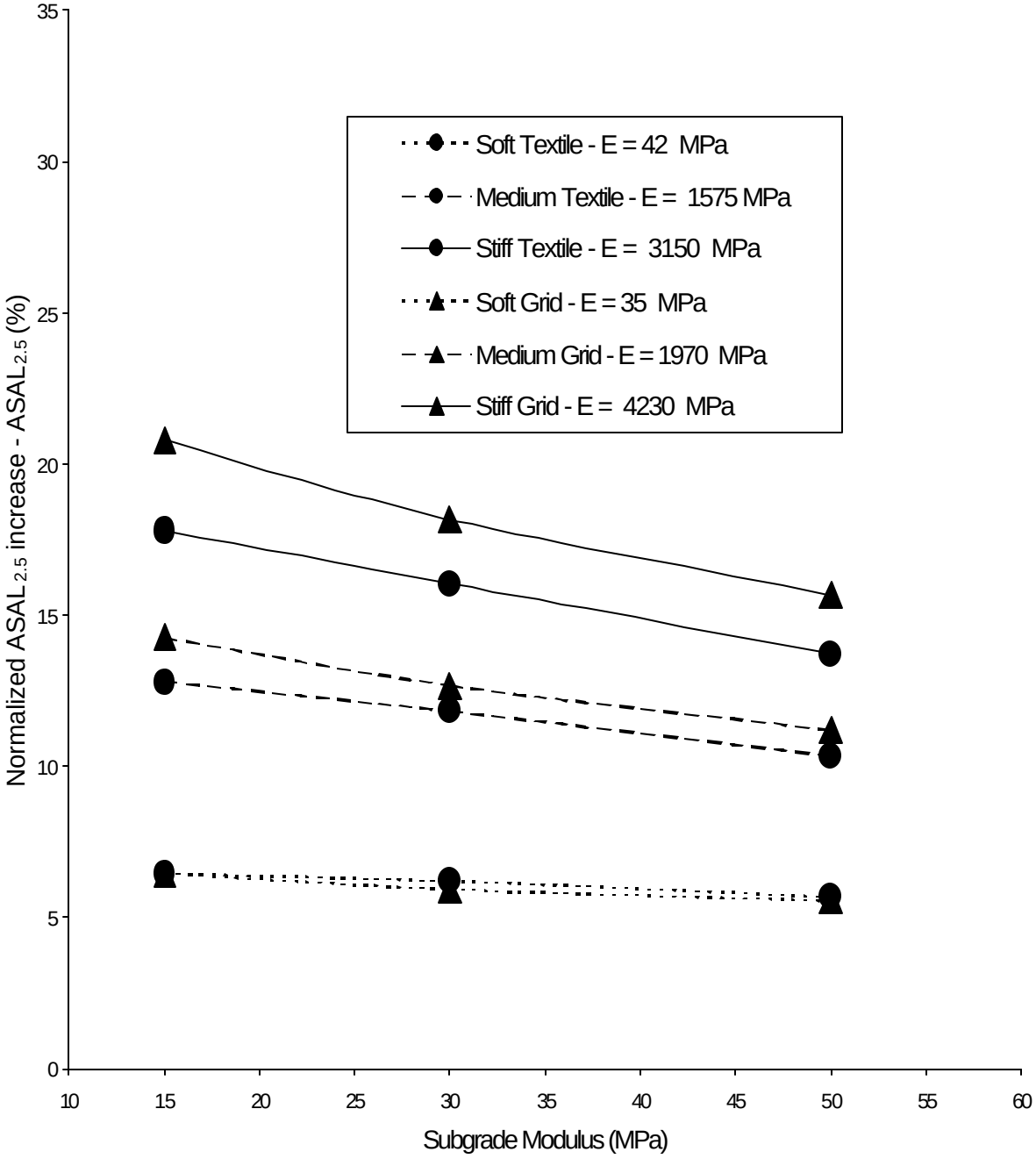

Fig. 23. Normalized $ASAL_{2.5}$ increase vs. subgrade modulus –
(b) -20^{o} C pavement, 150-300 HCADT structure

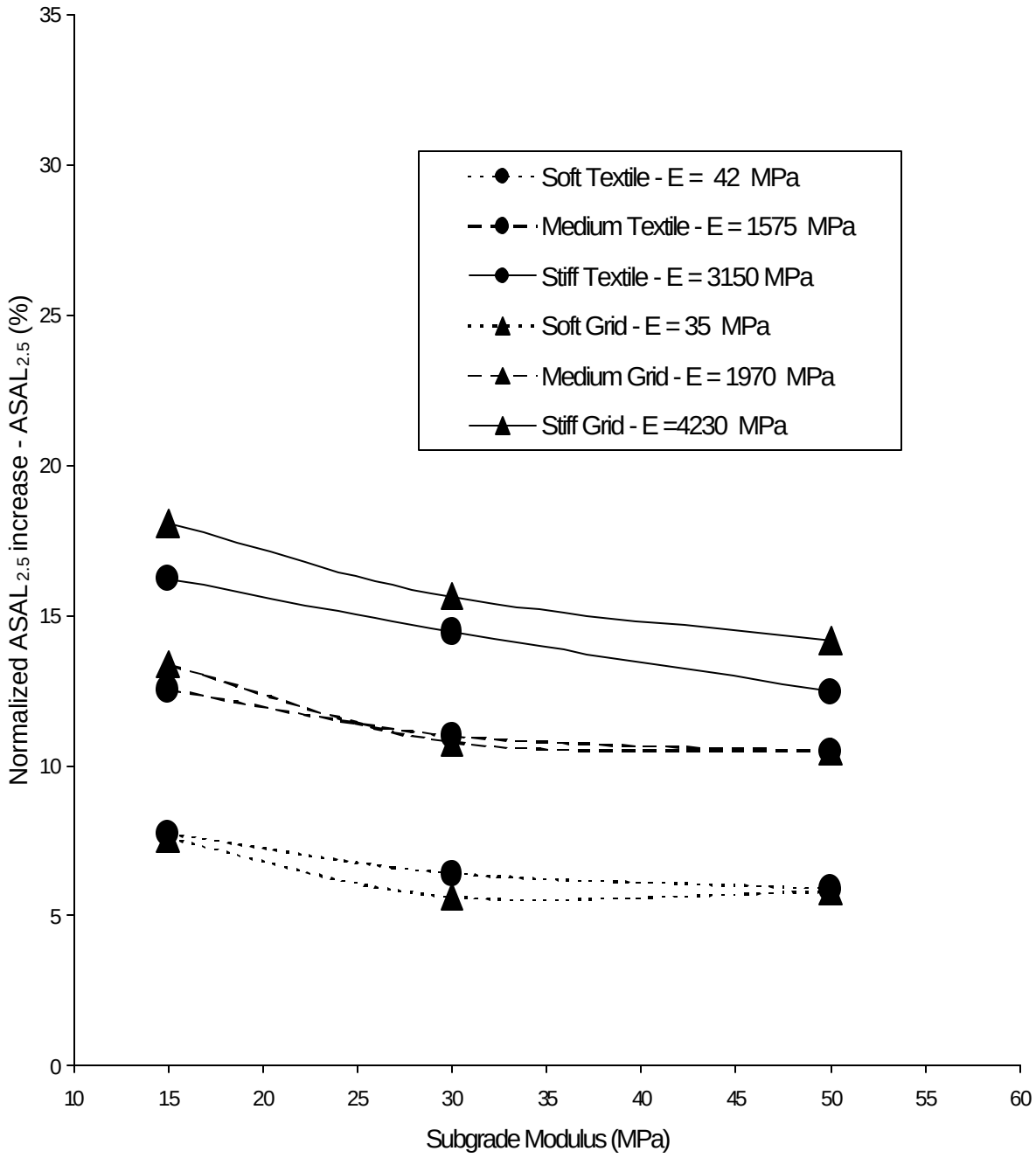

Fig. 23. Normalized $ASAL_{2.5}$ increase vs. subgrade modulus –
(c) -20^{o} C pavement, 300-600 HCADT structure

4.3 Roadway Cross Sections

In addition to the plots of percent normalized deflection reduction and percent normalized $ASAL_{2.5}$ increase, the deflection data from the testing have been summarized to give an idea of the dimensions of each road section. A figure indicating base thickness, pavement thickness, subgrade modulus, and deflection for each stiffness of geosynthetic has been created. Although not drawn to scale, the graphs shown in Fig. 24 – 33 do indicate the relative thickness of each layer and the resulting relative magnitude of the deflection. Also indicated in each figure are the values of the subgrade modulus and the values of deflection for each stiffness of geosynthetic used.

Underdesigned, Unsurfaced - Textile

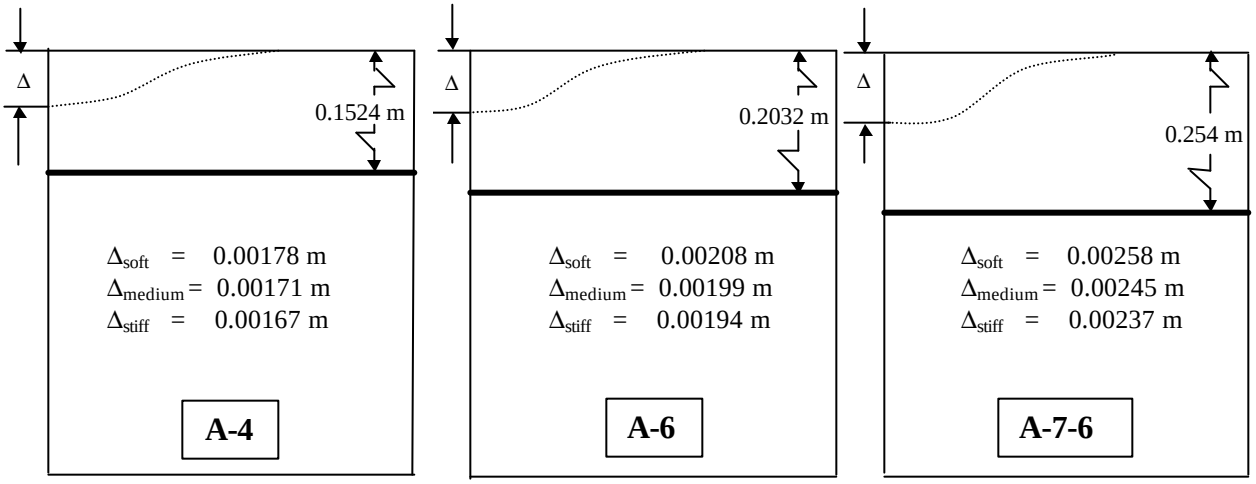

Medium Subgrade
E = 50 MPa

Medium-Soft Subgrade
E = 30 MPa

Soft Subgrade
E = 15 MPa

Underdesigned, Unsurfaced - Grid

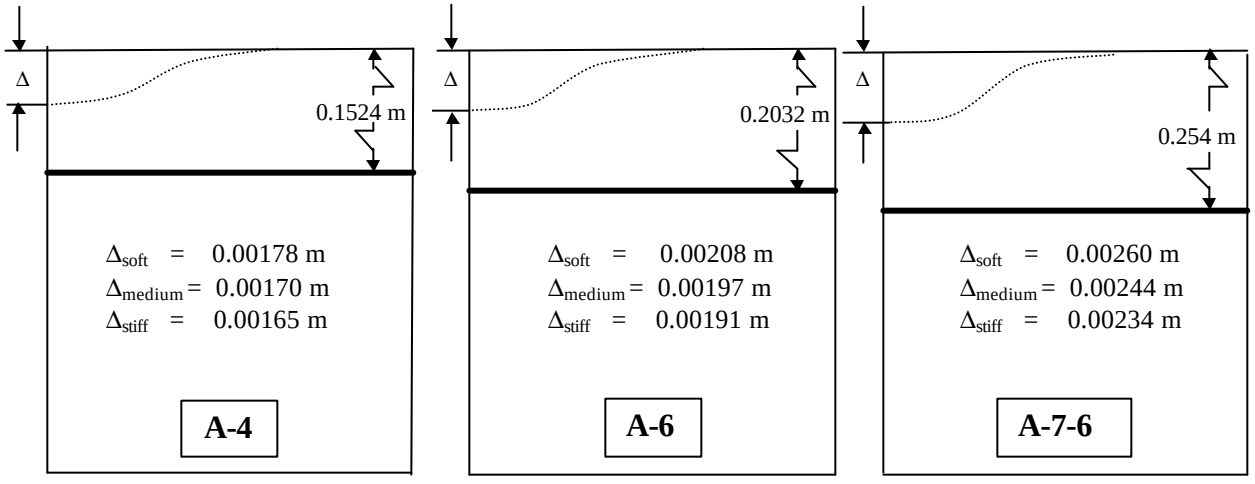

Medium Subgrade
E = 50 MPa

Medium-Soft Subgrade
E = 30 MPa

Soft Subgrade
E = 15 Mpa

Fig. 24. Road cross-sections and deflections for underdesigned, unsurfaced

<150 HCADT, Unsurfaced - Textile

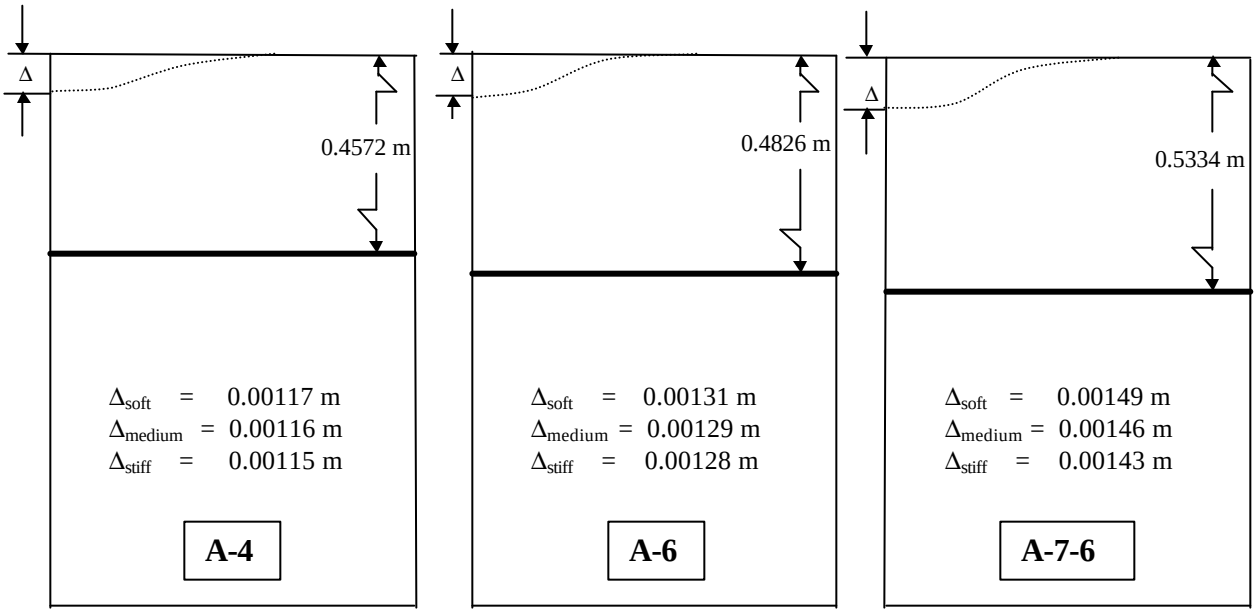

Medium Subgrade
E = 50 MPa

Medium-Soft Subgrade
E = 30 MPa

Soft Subgrade
E = 15 MPa

<150 HCADT, Unsurfaced - Grid

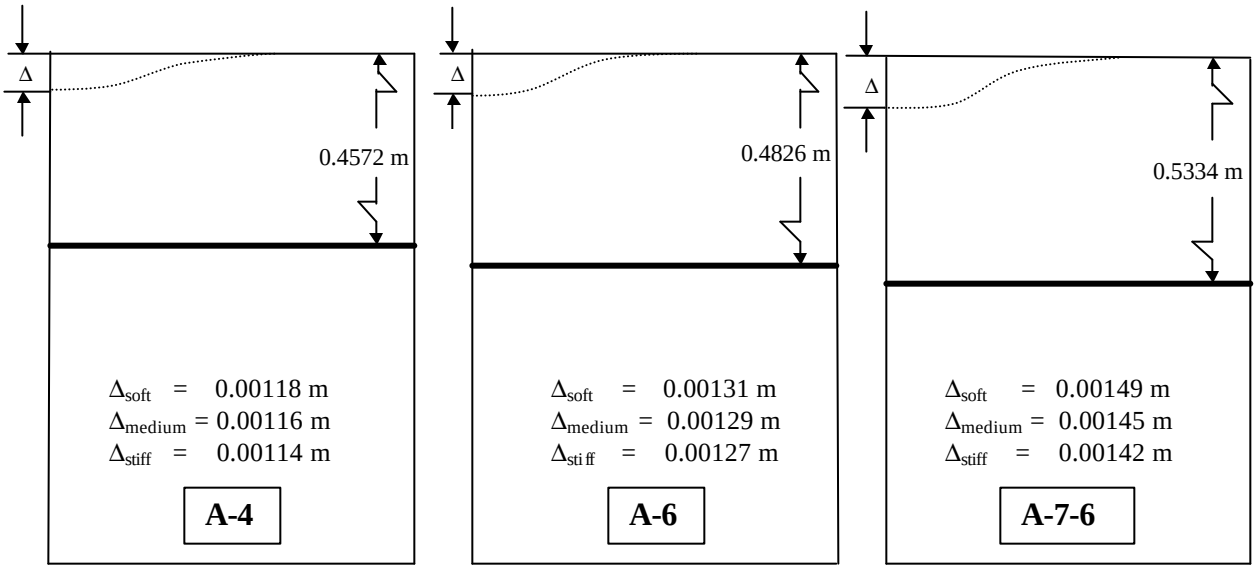

Medium Subgrade
E = 50 MPa

Medium-Soft Subgrade
E = 30 MPa

Soft Subgrade
E = 15 Mpa

Fig. 25. Road cross-sections and deflections for <150 HCADT structure, unsurfaced

150-300 HCADT, Unsurfaced - Textile

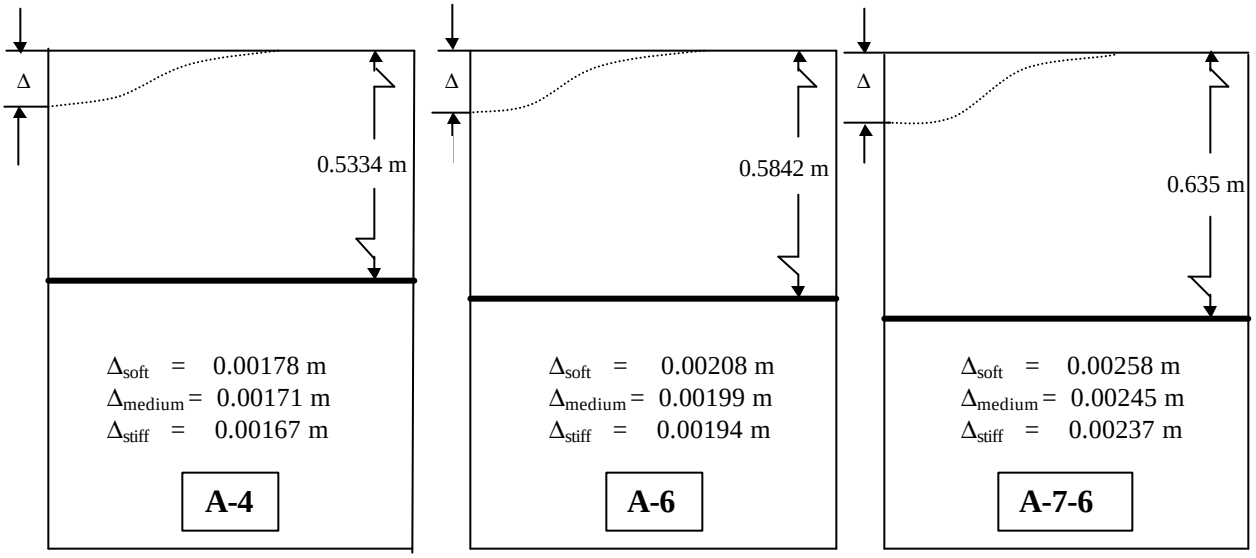

Medium Subgrade
E = 50 MPa

Medium-Soft Subgrade
E = 30 MPa

Soft Subgrade
E = 15 MPa

150-300 HCADT, Unsurfaced - Grid

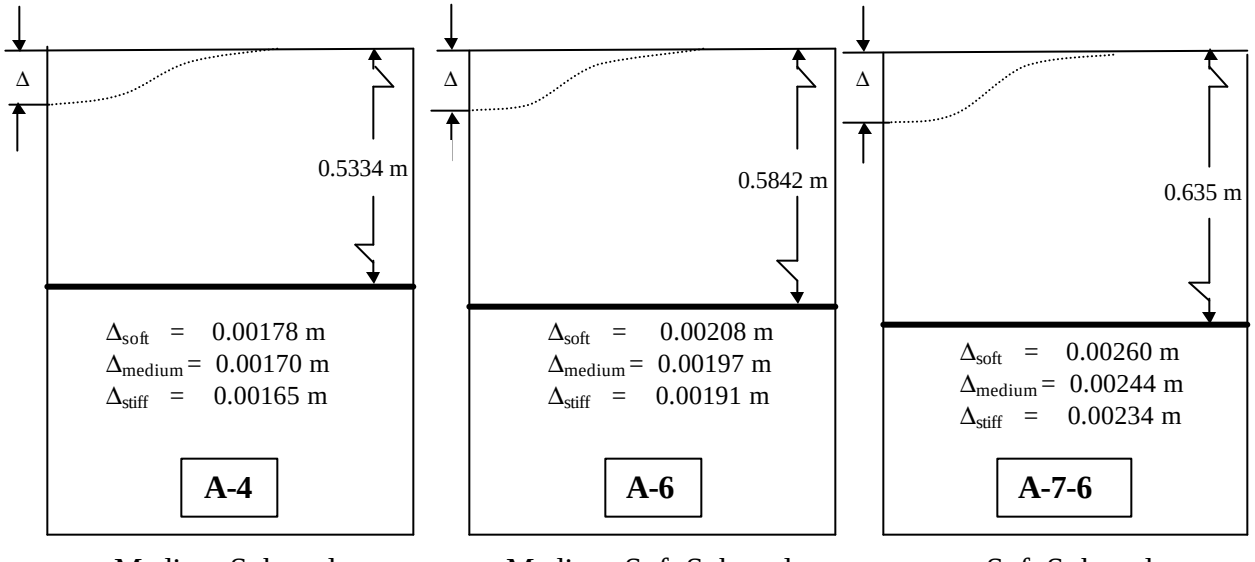

Medium Subgrade
E = 50 MPa

Medium-Soft Subgrade
E = 30 MPa

Soft Subgrade
E = 15 MPa

Fig. 26. Road cross-sections and deflections for 150-300 HCADT structure, unsurfaced

300-600 HCADT, Unsurfaced - Textile

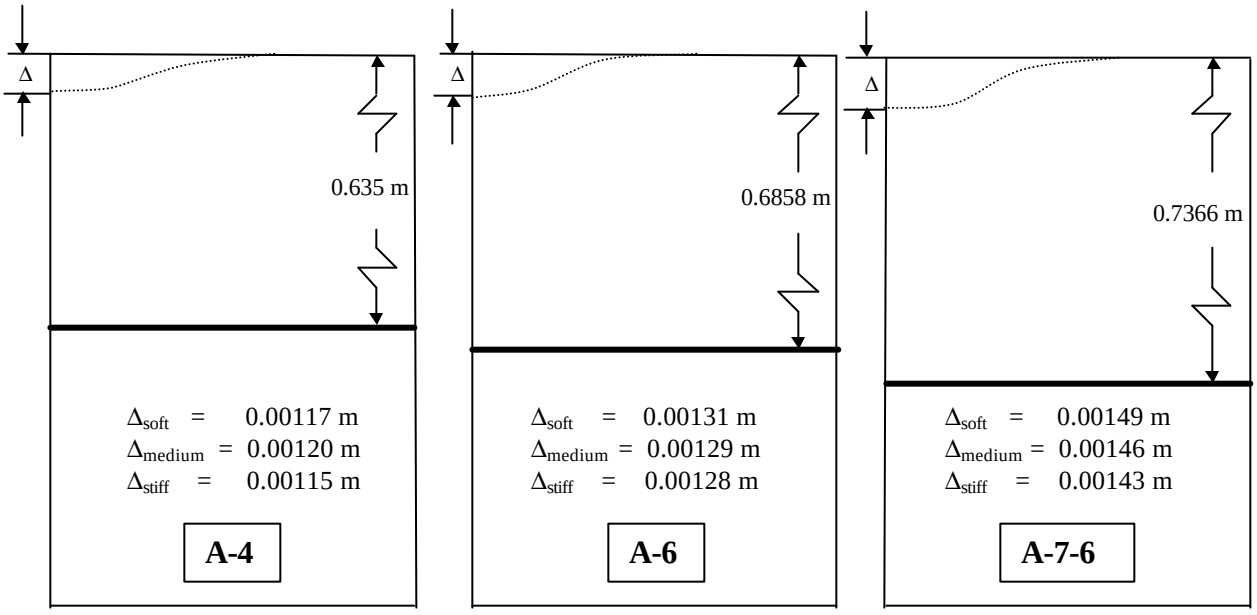

Medium Subgrade
E = 50 MPa

Medium-Soft Subgrade
E = 30 MPa

Soft Subgrade
E = 15 MPa

300-600 HCADT, Unsurfaced - Grid

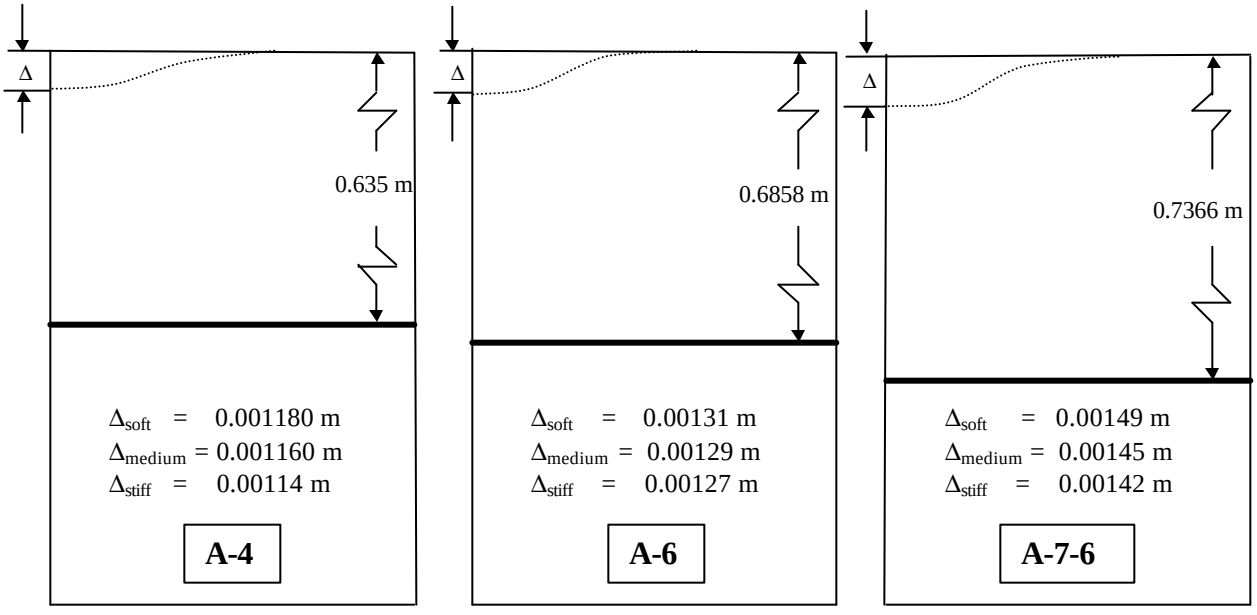

Medium Subgrade
E = 50 MPa

Medium-Soft Subgrade
E = 30 MPa

Soft Subgrade
E = 15 MPa

Fig. 27. Road cross-sections and deflections for 300-600 HCADT structure, unsurfaced

<150 HCADT, Surfaced, -20° C - Textile

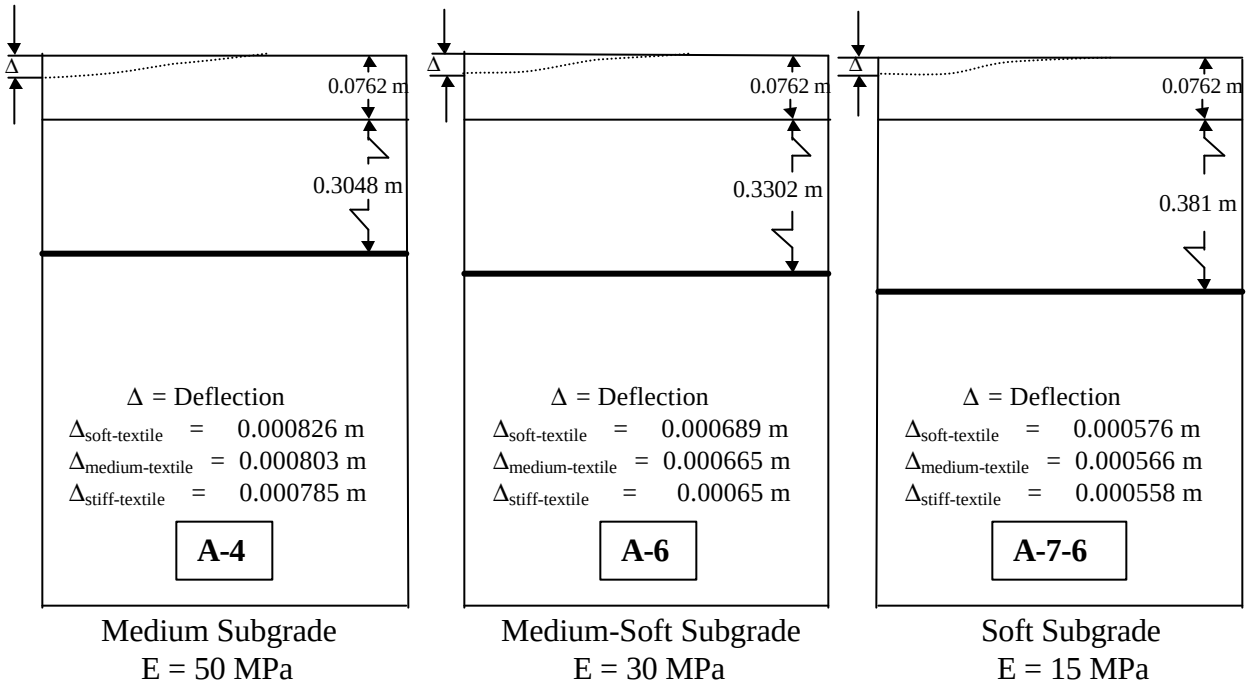

<150 HCADT, Surfaced, -20° C - Grid

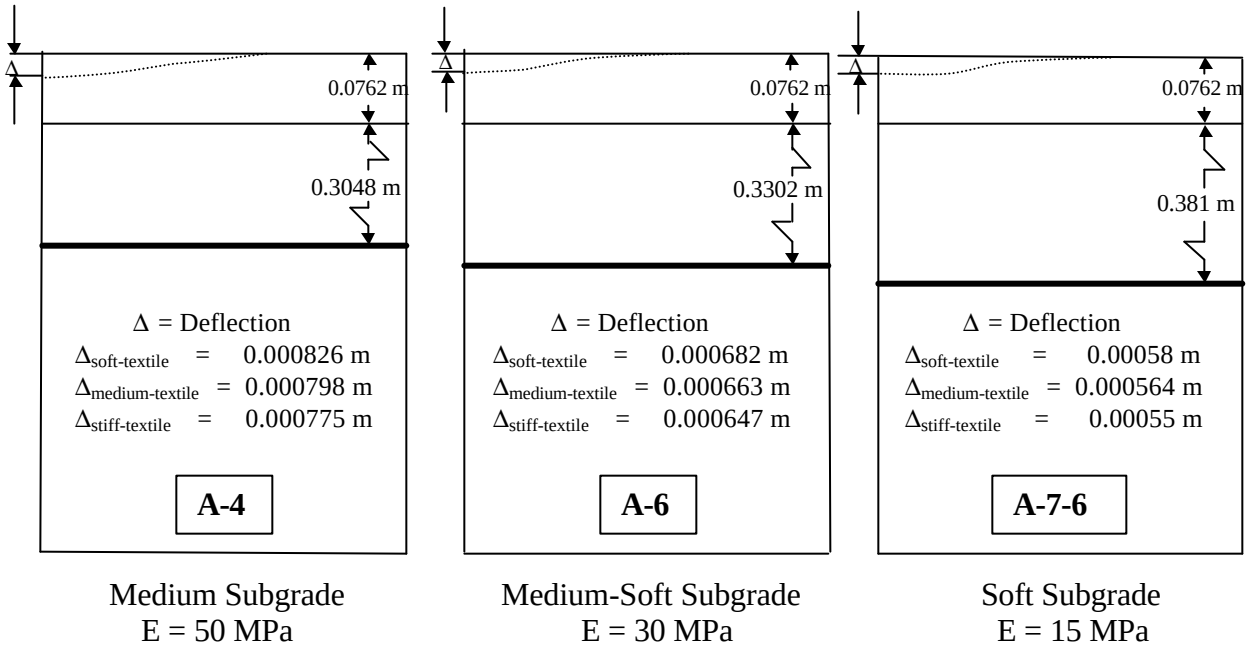

Fig. 28. Road cross-sections and deflections for <150 HCADT structure, surfaced, -20° C

150-300 HCADT, Surfaced, -20° C - Textile

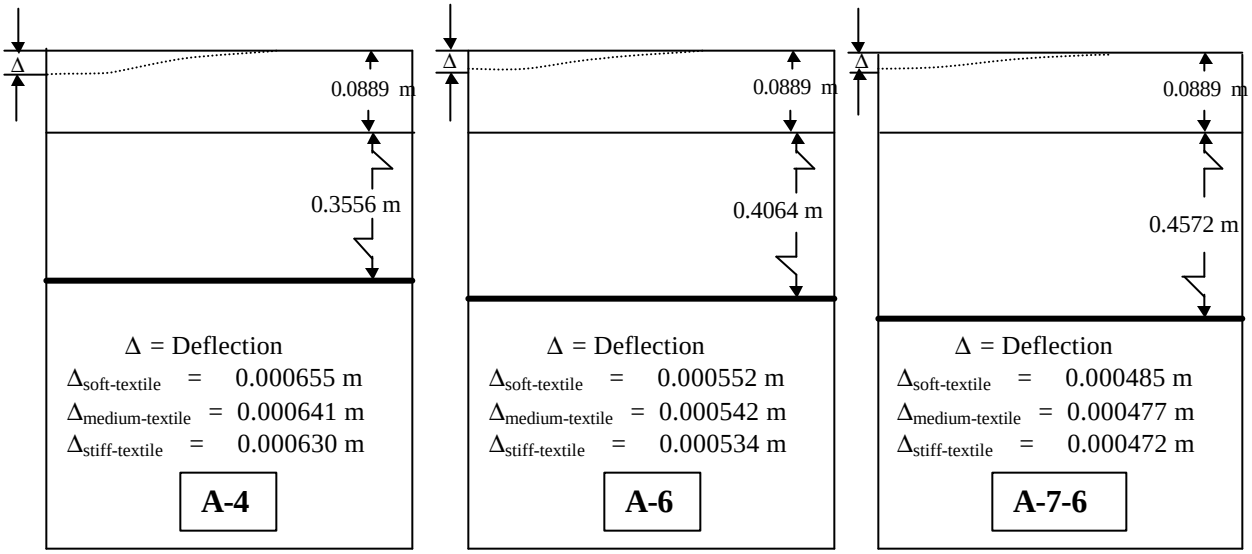

Medium Subgrade
E = 50 MPa

Medium-Soft Subgrade
E = 30 MPa

Soft Subgrade
E = 15 MPa

150-300 HCADT, Surfaced, -20° C - Grid

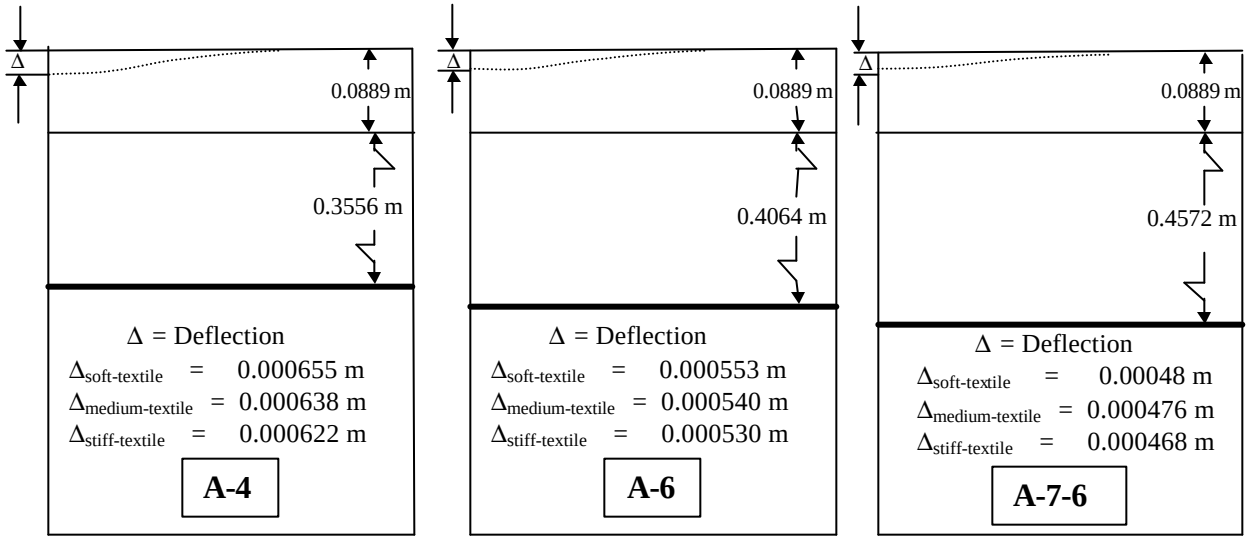

Medium Subgrade
E = 50 MPa

Medium-Soft Subgrade
E = 30 MPa

Soft Subgrade
E = 15 MPa

Fig. 29. Road cross-sections and deflections for 150-300 HCADT structure, surfaced, -20° C

300-600 HCADT, Surfaced, -20° C - Textile

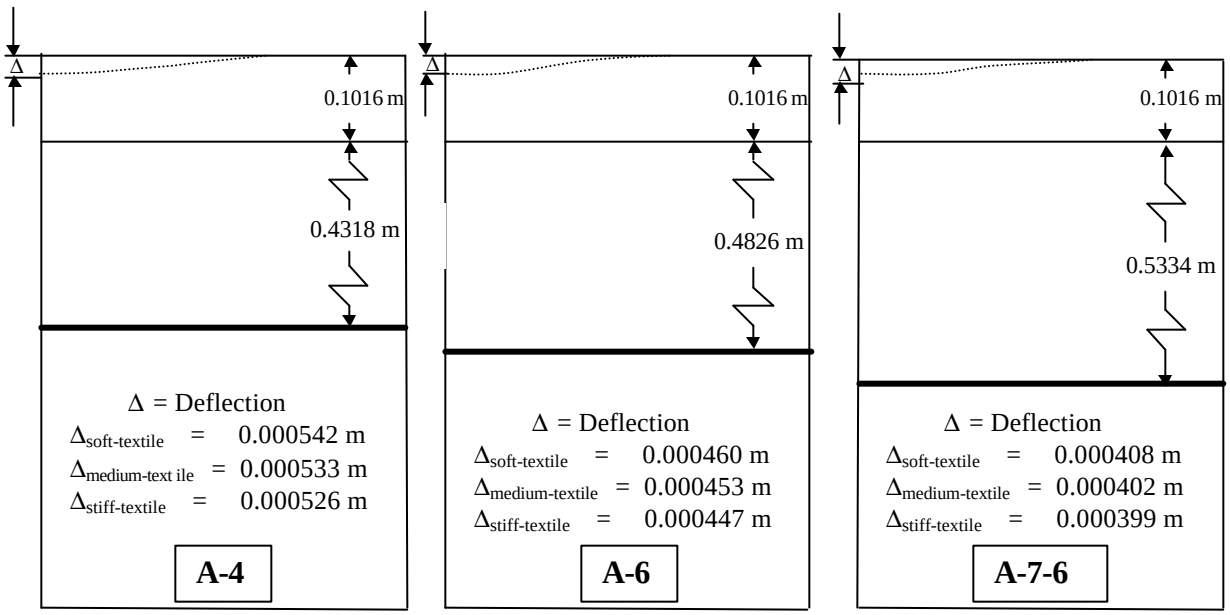

Medium Subgrade
E = 50 MPa

Medium-Soft Subgrade
E = 30 MPa

Soft Subgrade
E = 15 MPa

300-600 HCADT, Surfaced, -20° C - Grid

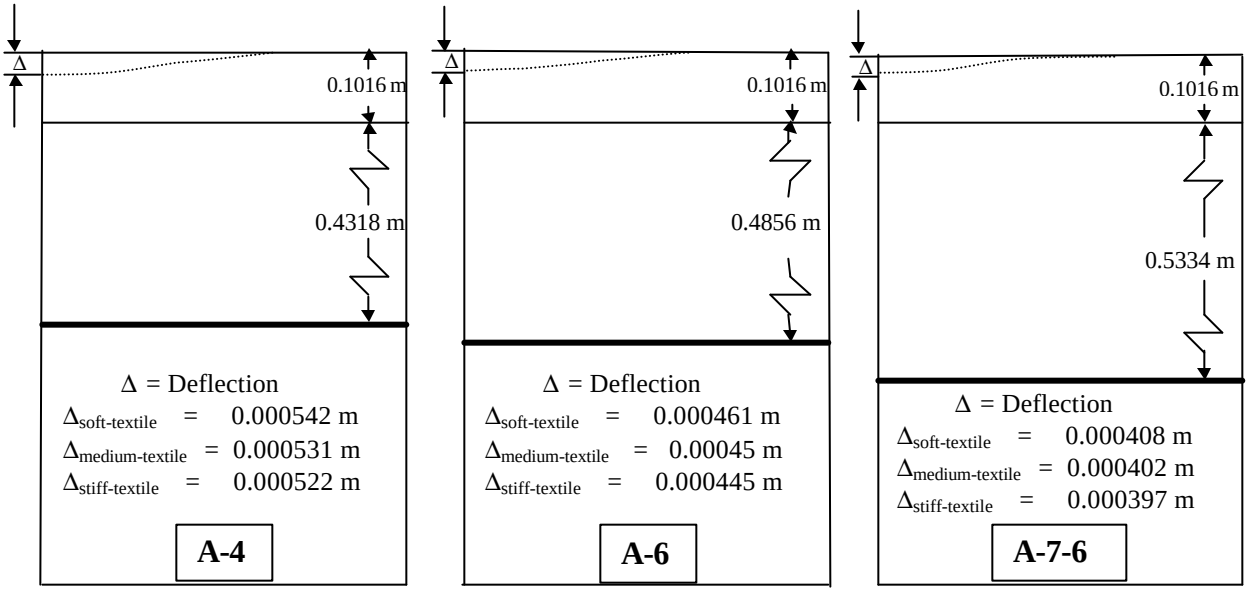

Medium Subgrade
E = 50 MPa

Medium-Soft Subgrade
E = 30 MPa

Soft Subgrade
E = 15 MPa

Fig. 30. Road cross-sections and deflections for 300-600 HCADT structure, surfaced, -20° C

<150 HCADT Structure, Surfaced, 40° C - Textile

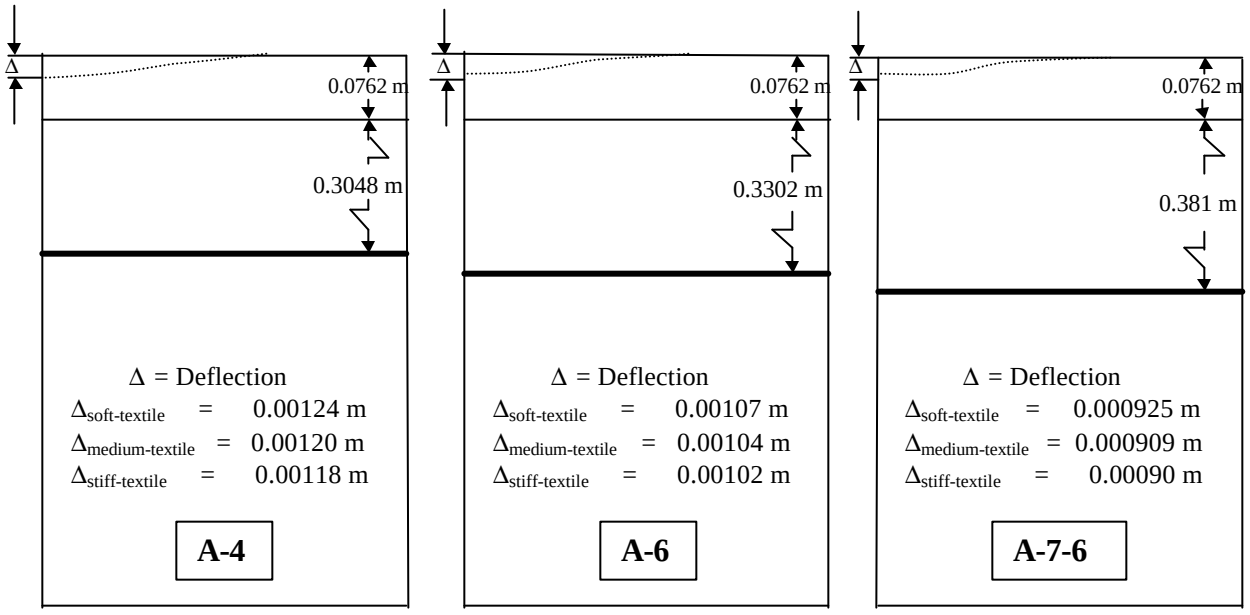

Medium Subgrade
E = 50 MPa

Medium-Soft Subgrade
E = 30 MPa

Soft Subgrade
E = 15 MPa

<150 HCADT Structure, Surfaced, 40° C - Grid

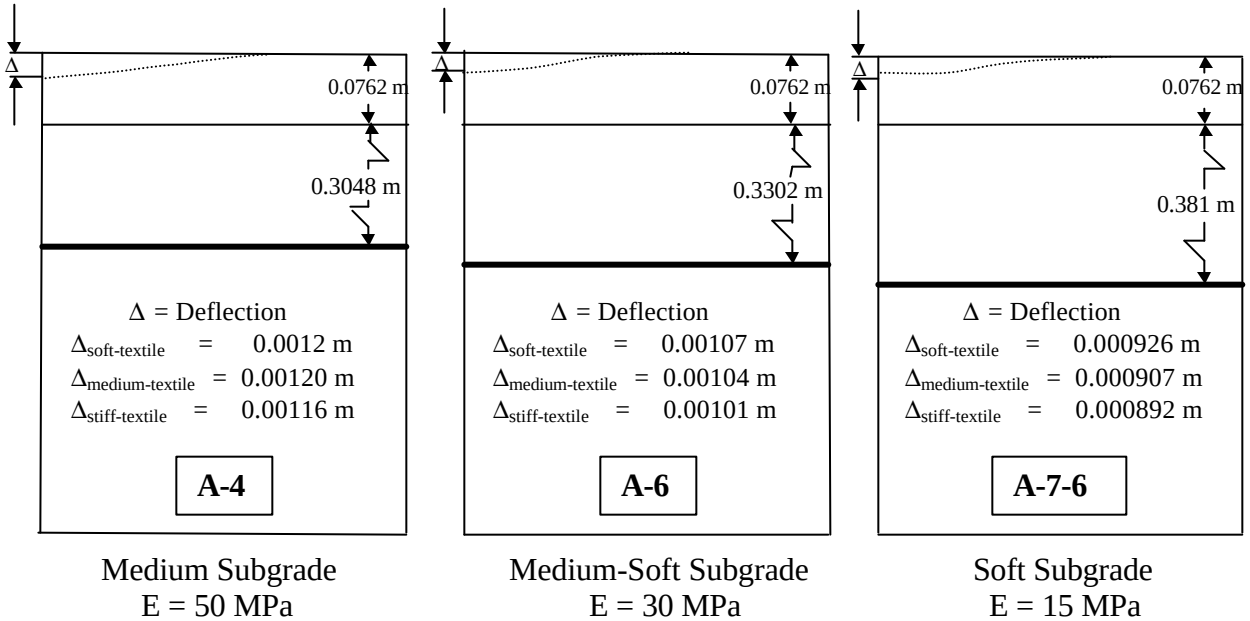

Medium Subgrade
E = 50 MPa

Medium-Soft Subgrade
E = 30 MPa

Soft Subgrade
E = 15 MPa

Fig. 31. Road cross-sections and deflections for <150 HCADT structure, surfaced, 40° C

150-300 HCADT, Surfaced, 40° C - Textile

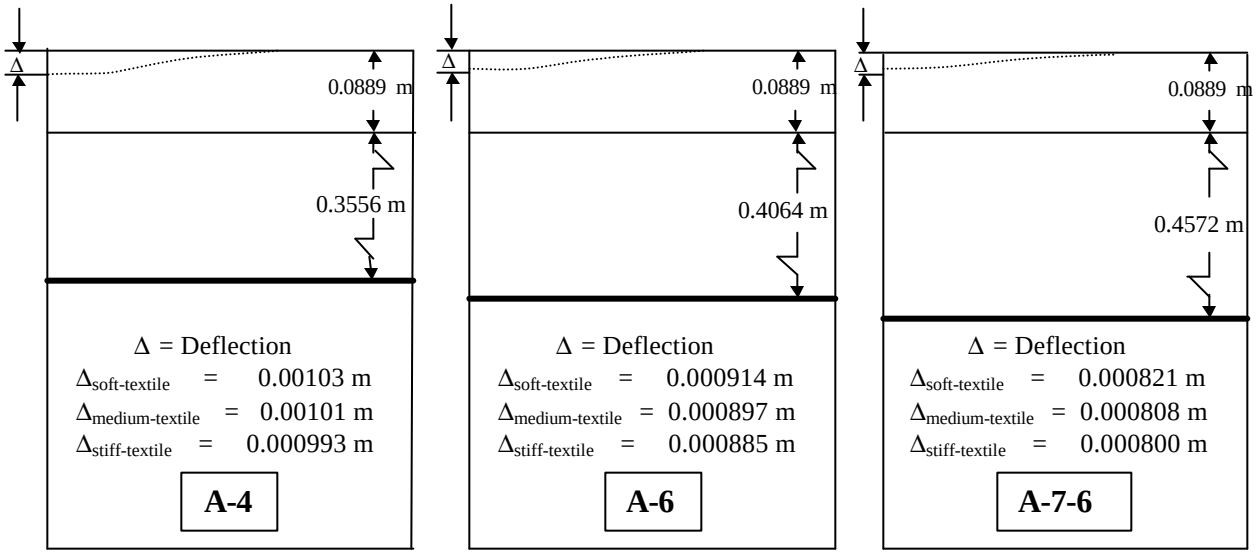

Medium Subgrade
E = 50 MPa

Medium-Soft Subgrade
E = 30 MPa

Soft Subgrade
E = 15 MPa

150-300 HCADT, Surfaced, 40° C - Grid

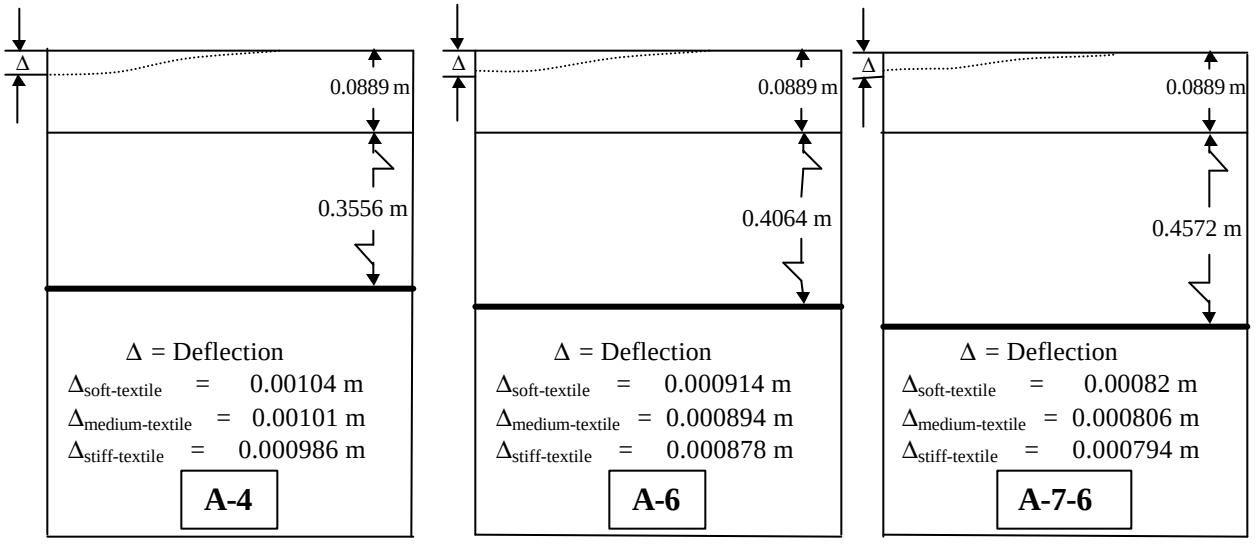

Medium Subgrade
E = 50 MPa

Medium-Soft Subgrade
E = 30 MPa

Soft Subgrade
E = 15 MPa

Fig. 32. Road cross-sections and deflections for 150-300 HCADT structure, surfaced, 40° C

300-600 HCADT, Surfaced, 40° C - Textile

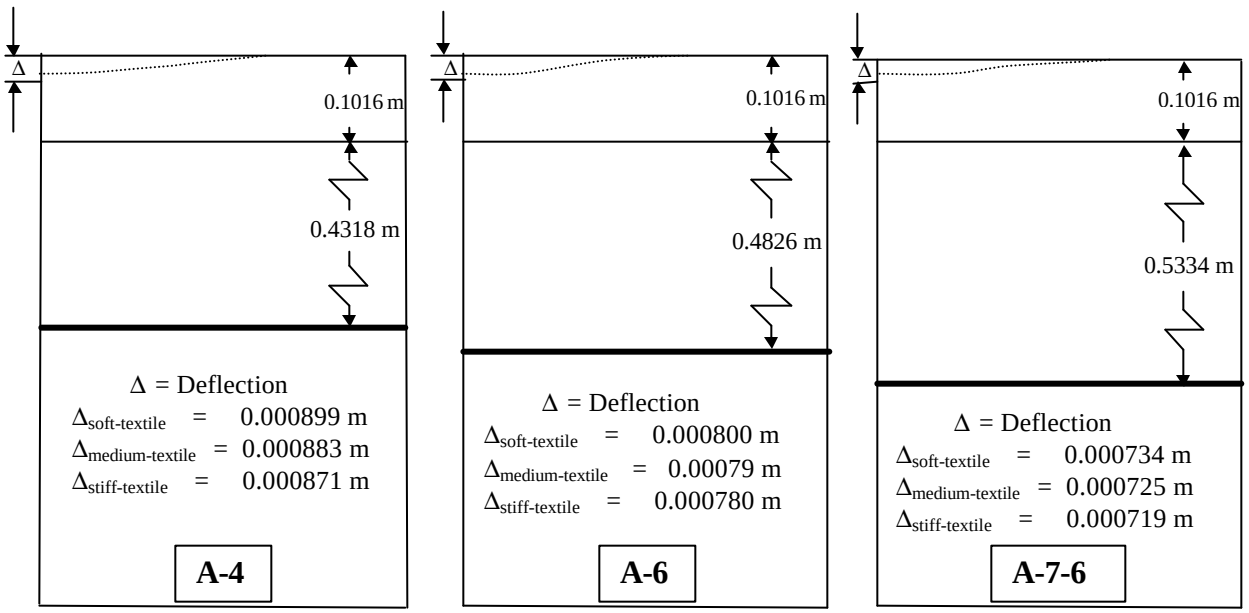

Medium Subgrade
E = 50 MPa

Medium-Soft Subgrade
E = 30 MPa

Soft Subgrade
E = 15 MPa

300-600 HCADT, Surfaced, 40° C - Grid

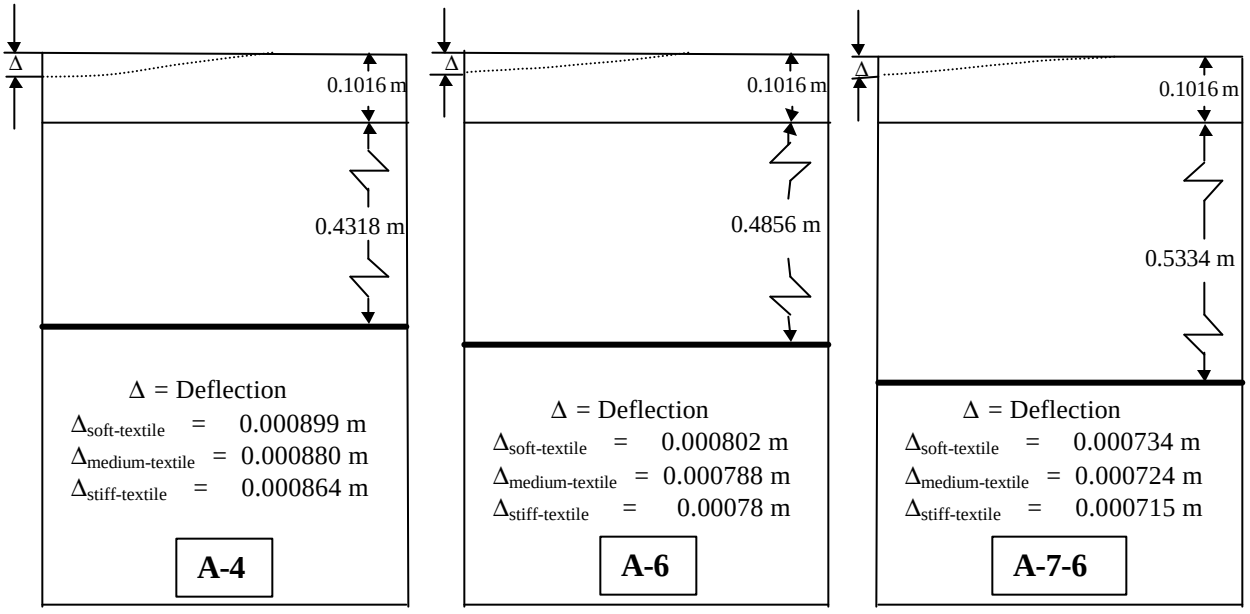

Medium Subgrade
E = 50 MPa

Medium-Soft Subgrade
E = 30 MPa

Soft Subgrade
E = 15 MPa

Fig. 33. Road cross-sections and deflections for 300-600 HCADT structure, surfaced, 40° C

4.4 Stress Distributions

The horizontal stress distributions for two representative cases have been plotted along the three vertical sections shown in Fig. 34. The plots represent the horizontal stresses in the center of the sixth, tenth, and fifteenth column of elements from the axis of symmetry. These columns are located 16 cm (6.3”), 25.3 cm (10”), and 39.7cm (15.6”) from the axis of symmetry. On the plots, the stress distributions are labeled by their distance from the axis of symmetry. For example, the sixth column stress distributions are labeled as 6.3”. For comparison, the horizontal stress distributions for the unreinforced case have also been plotted. Figures 35 (a)-(c) represent the unsurfaced, underdesigned roadway over a soft stiffness subgrades, and Figs. 36 (a)-(c) represent the unsurfaced, underdesigned roadway over a medium stiffness subgrade. Only stress distributions for the geotextile reinforced roadways are shown.

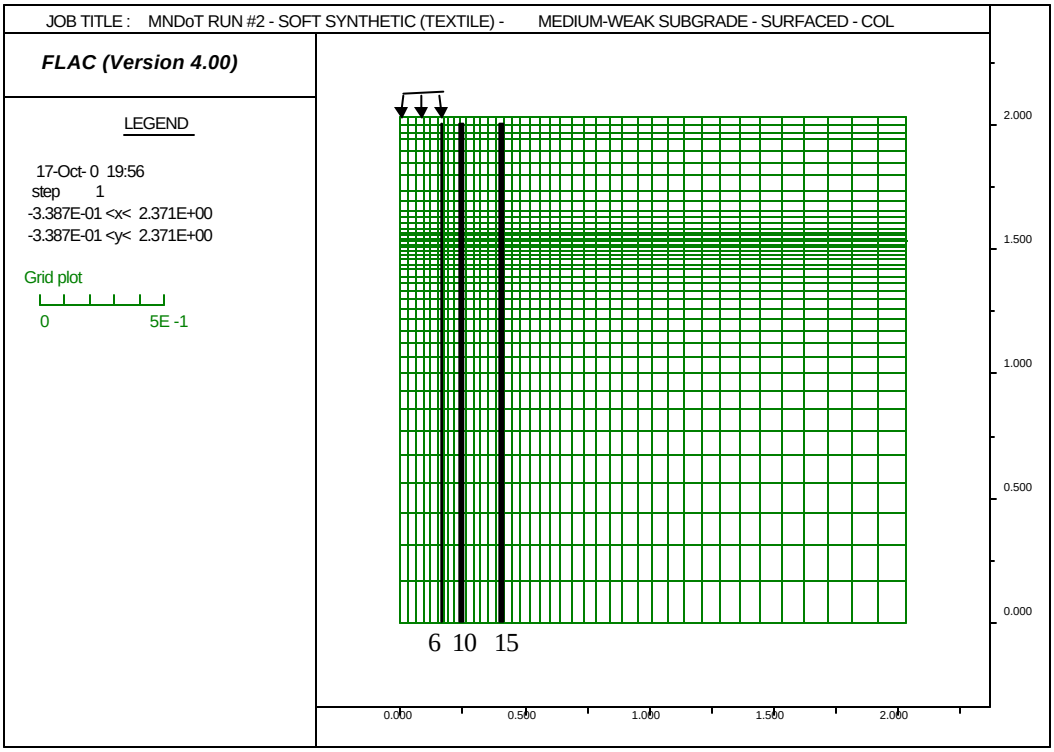

Fig. 34. Position of horizontal stress distributions.

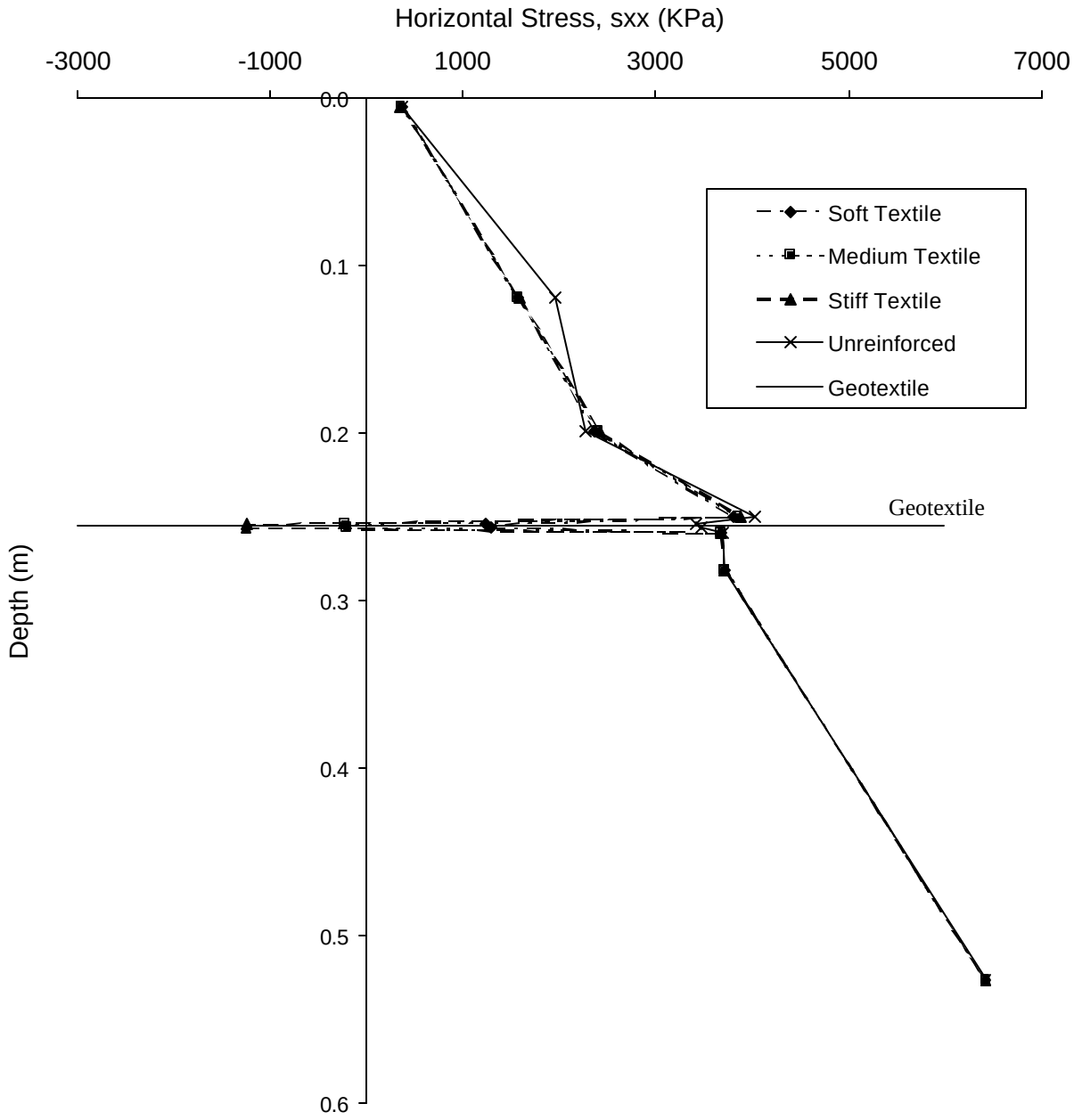

Fig. 35. Horizontal stress vs. depth – (a) Underdesigned, unsurfaced, soft subgrade, 6.3”

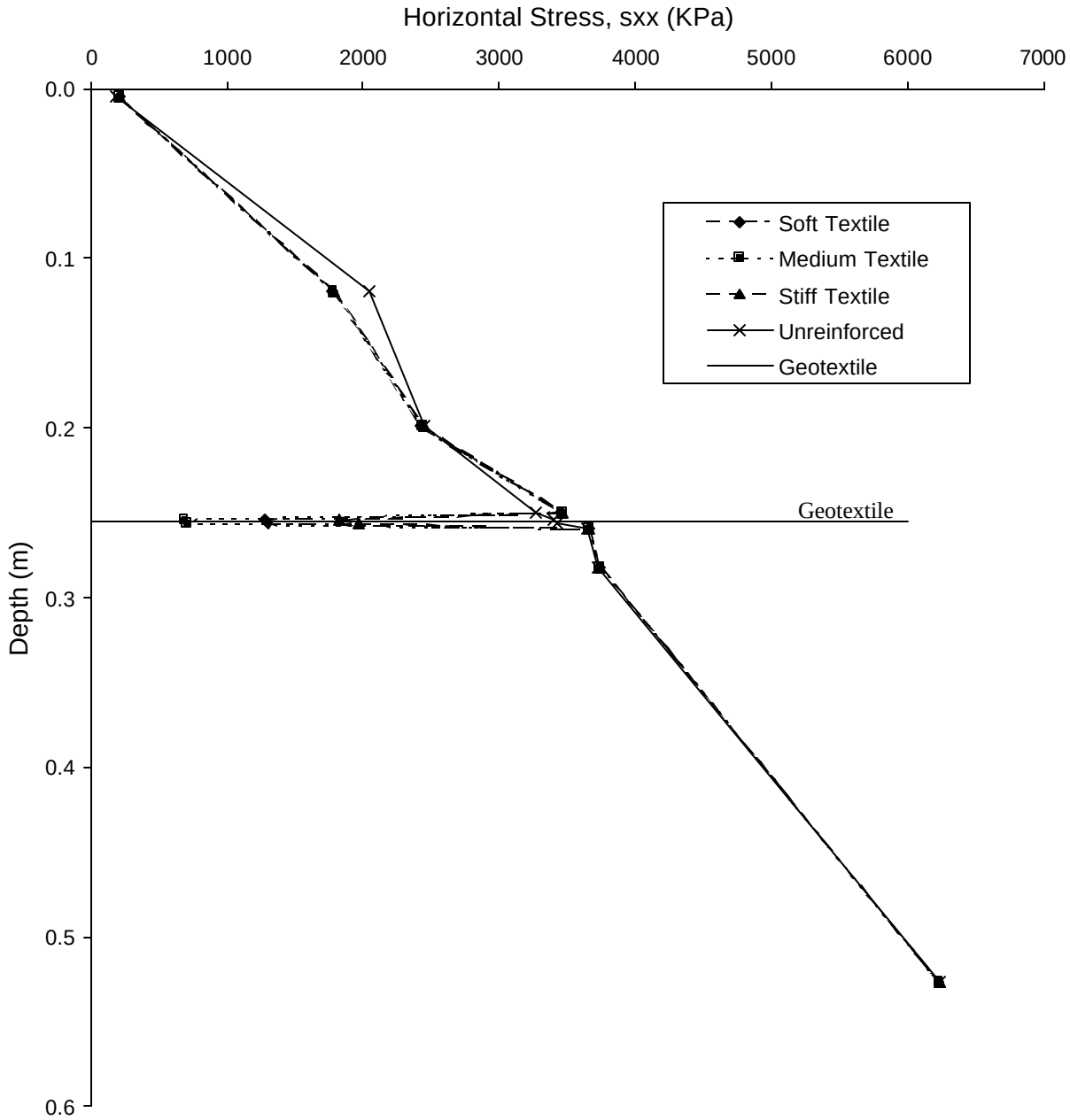

Fig. 35. Horizontal stress vs. depth – (b) Underdesigned, unsurfaced, soft subgrade, 10”

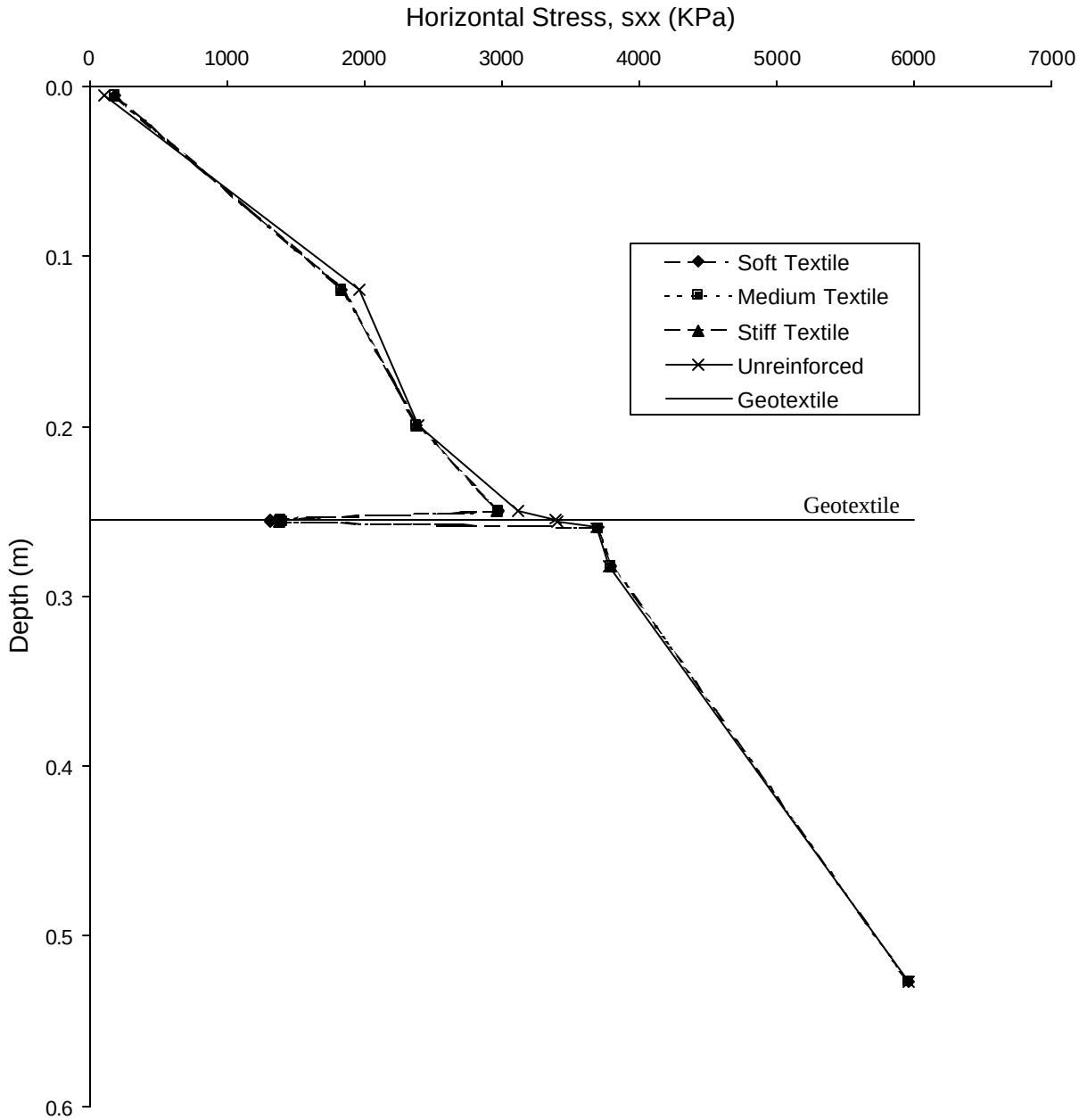

Fig. 35. Horizontal stress vs. depth – (c) Underdesigned, unsurfaced, soft subgrade, 15.6”

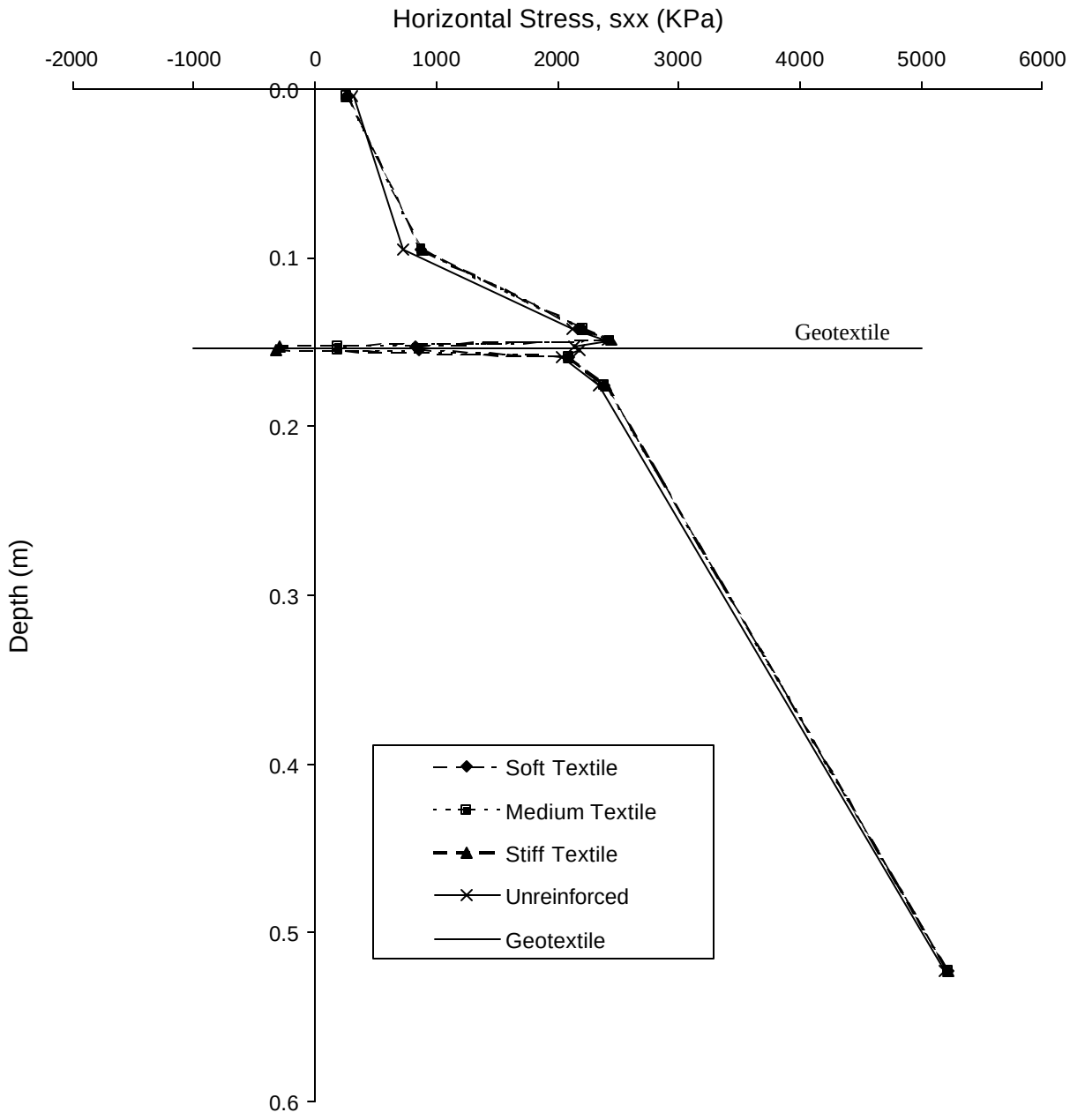

Fig. 36. Horizontal stress vs. depth – (a) Underdesigned, unsurfaced, medium subgrade, 6.3”

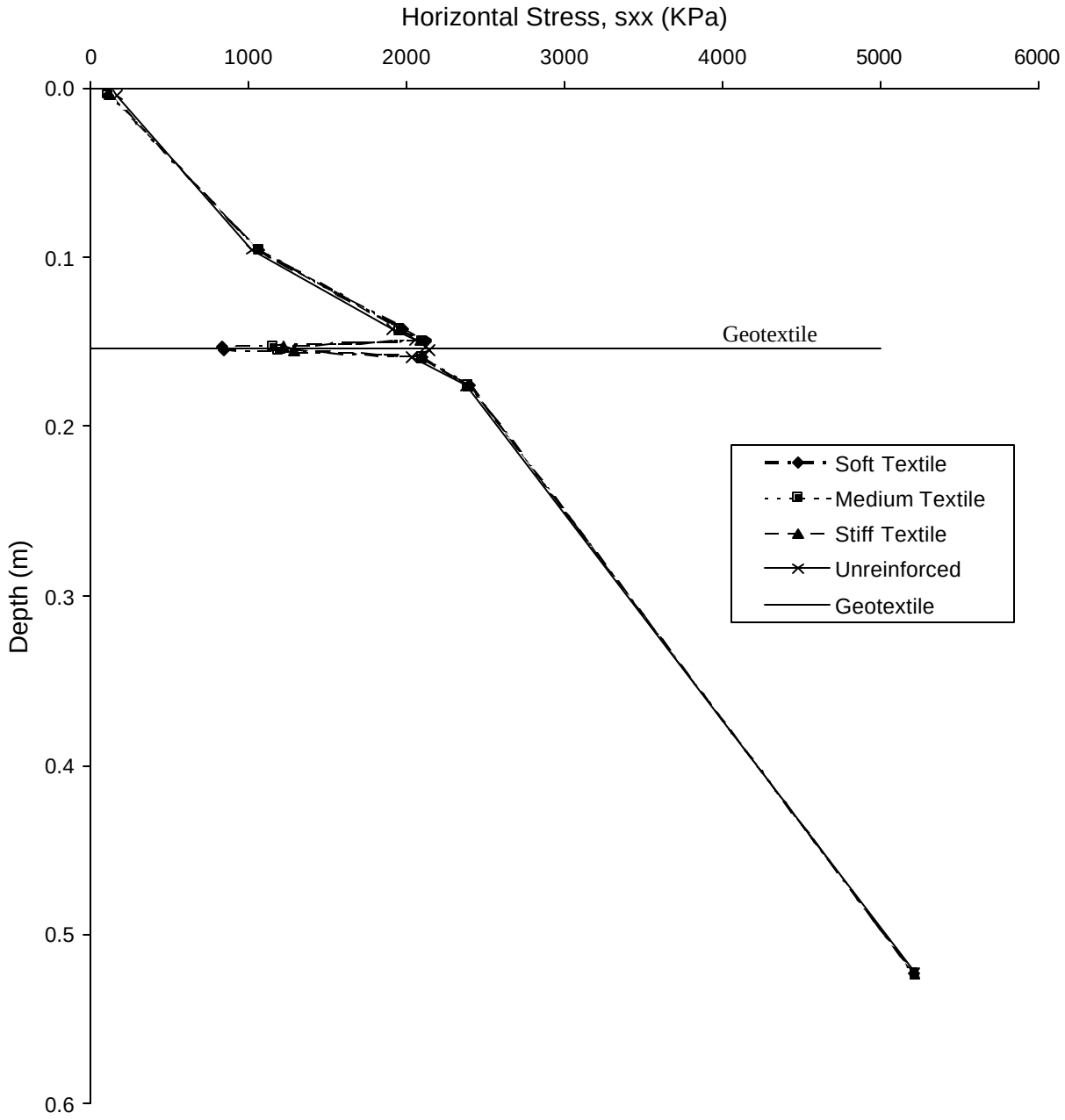

Fig. 36. Horizontal stress vs. depth – (b) Underdesigned, unsurfaced, medium subgrade, 10”

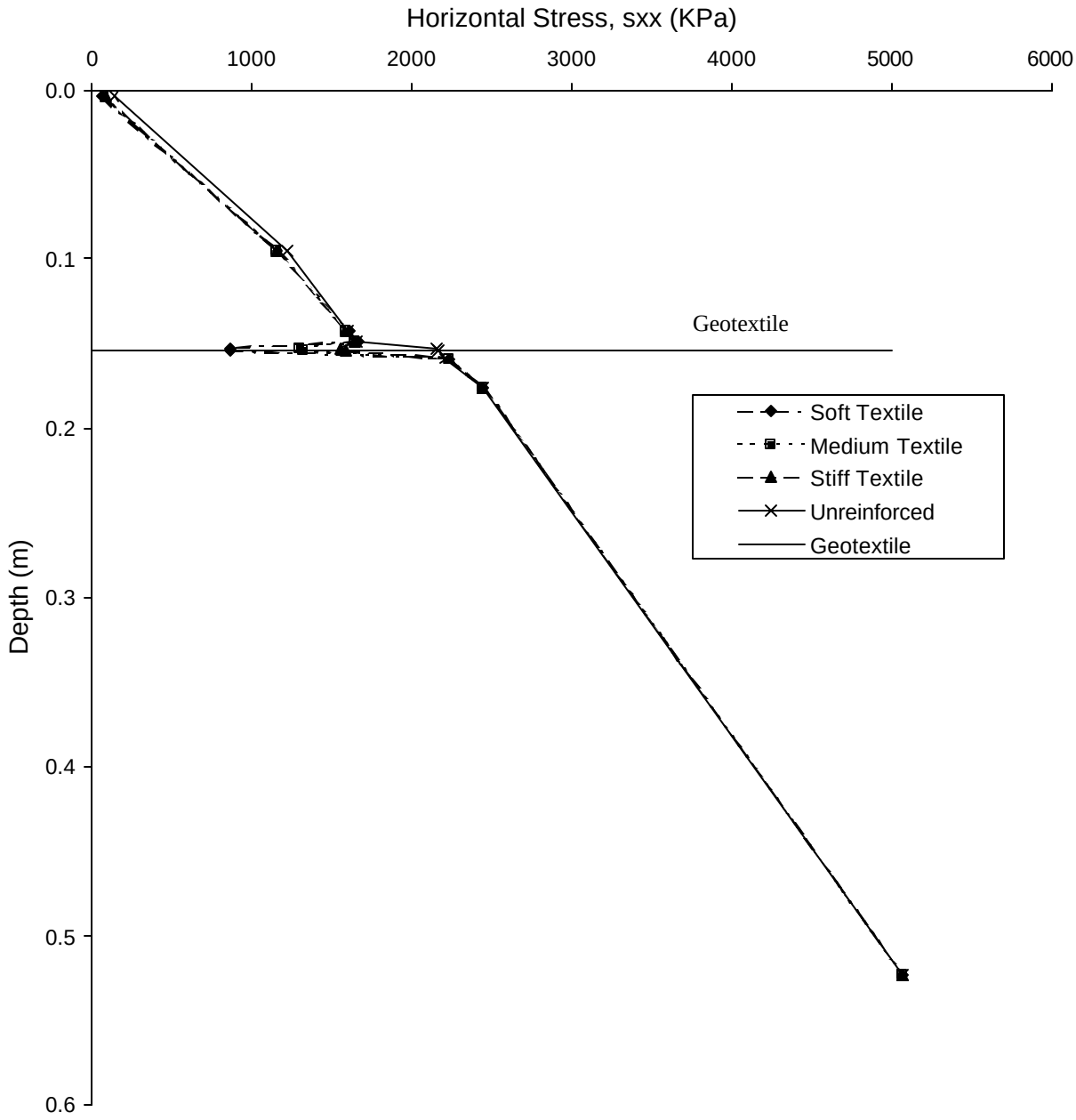

Fig. 36. Horizontal stress vs. depth – (c) Underdesigned, unsurfaced, medium subgrade, 15.6”

CHAPTER 5
ANALYSIS OF RESULTS

By closely examining the plotted results, important information can be obtained regarding the benefits of using geosynthetics to reinforce low-volume roads. It should also be noted that cases involving the stiff subgrade material outlined in the analysis matrix were not included in the results section of the report. For these cases, the results indicate that very little benefit, in terms of deflection, was to be gained, as the subgrade material was already of very high quality. For this reason, no further testing was done using the stiff subgrade, and the results are not included in this report. Again, no attempt was made to include the separation function of geosynthetics in this study. Only benefits derived from the reinforcement function of geosynthetics are considered.

5.1 Percent Normalized Deflection Reduction

The addition of geosynthetic reinforcement improves the performance of the roadway by decreasing deflections. For all cases studied, if the stiffness of the geosynthetic used was greater than that of the subgrade, the resulting deflection was less than that of the unreinforced case. In other words, adding a stiffer material to the road cross section decreased deflection under a given load. The deflection is dependent on the Young's modulus of the geosynthetic, with the largest modulus geosynthetics producing the largest benefits.

In regard to geogrids vs. geotextiles, the results indicated that one type is not superior to the other given the assumptions used in this study and the ability of the model to simulate the in situ properties. To illustrate this result, the maximum normal and shear stress along the interface

were evaluated. For the loading conditions considered, Table 7 indicates that no yielding was observed at the interfaces as the mobilized friction angle is much less than that for the interface.

Table 7. Representative maximum mobilized friction angle at the interface

$\phi_{subgrade/geosynthetic}$	τ (MPa)	σ (MPa)	$\phi_{mobilized}$
19.5	19.65	514.2	2.19
10	19.57	514.3	2.18

Therefore, the resulting behavior of the system in terms of deflections is based solely on the stiffness of the materials. In other words, the frictional interfaces do not play any role in affecting the surface deflection as the loading is not large enough to produce any yielding. Since the loading was small in this study, this difference between geogrids and geotextile was not apparent as the system remained elastic. If, however, the study included a bearing capacity investigation, the difference between similar stiffness geogrids and geotextiles would become apparent as the frictional nature of the interface would influence the results.

The results are shown in Tables 8, 9, and 10.

Table 8. Percent normalized deflection reduction – unsurfaced cases

UNDERDESIGNED - UNSURFACED

Subgrade	**Soft**			**Medium-Soft**			**Medium**		
Syn.	Soft	Medium	Stiff	Soft	Medium	Stiff	Soft	Medium	Stiff
Grid	4.77	10.31	14.02	0.05	5.14	8.03	-0.79	3.85	6.4
Textile	5.36	10.13	13.14	0.05	4.28	6.92	-1.13	3.00	5.33

≤150 HCADT - UNSURFACED

Subgrade	**Soft**			**Medium-Soft**			**Medium**		
Syn.	Soft	Medium	Stiff	Soft	Medium	Stiff	Soft	Medium	Stiff
Grid	1.06	3.45	5.58	0.08	2.05	3.58	-0.34	1.2	2.22
Textile	1.13	3.32	4.85	0.08	1.75	2.97	-0.26	0.94	1.79

150-300 HCADT - UNSURFACED

Subgrade	**Soft**			**Medium-Soft**			**Medium**		
Syn.	Soft	Medium	Stiff	Soft	Medium	Stiff	Soft	Medium	Stiff
Grid	0.15	2.01	2.58	0	1.4	2.64	-0.45	0.71	1.6
Textile	0.17	1.49	2.68	0	1.15	2.06	-0.27	0.80	1.43

300-600 HCADT - UNSURFACED

Subgrade	**Soft**			**Medium-Soft**			**Medium**		
Syn.	Soft	Medium	Stiff	Soft	Medium	Stiff	Soft	Medium	Stiff
Grid	0.08	1.37	2.49	0	1.05	2.01	-0.28	0.56	1.21
Textile	0.10	1.05	1.93	0	0.87	1.57	-0.28	0.46	0.93

Table 9. Percent Normalized Deflection Reduction – 40° C Pavement

<150 HCADT - WARM

Subgrade	Soft			Medium-Soft			Medium		
Syn.	Soft	Medium	Stiff	Soft	Medium	Stiff	Soft	Medium	Stiff
Grid	9.16	12.16	14.73	1.93	4.69	6.80	-0.31	2.17	3.76
Textile	9.23	11.72	13.70	2.02	4.23	5.88	0.14	1.88	3.10

150-300 HCADT - WARM

Subgrade	Soft			Medium-Soft			Medium		
Syn.	Soft	Medium	Stiff	Soft	Medium	Stiff	Soft	Medium	Stiff
Grid	1.14	3.72	6.00	-0.04	2.15	3.95	-0.07	1.74	3.16
Textile	1.53	3.62	5.38	0.00	1.80	3.19	-0.02	1.46	2.54

300-600 HCADT - WARM

Subgrade	Soft			Medium-Soft			Medium		
Syn.	Soft	Medium	Stiff	Soft	Medium	Stiff	Soft	Medium	Stiff
Grid	0.63	2.72	4.42	0.27	1.99	3.46	0.22	1.66	2.80
Textile	0.63	2.36	3.69	0.41	1.84	2.94	0.27	1.44	2.30

Table 10. Percent Normalized Deflection Reduction – -20° C Pavement

<150 HCADT - COLD

Subgrade	Soft			Medium-Soft			Medium		
Syn.	Soft	Medium	Stiff	Soft	Medium	Stiff	Soft	Medium	Stiff
Grid	5.79	8.99	11.71	1.82	4.55	6.86	1.45	3.56	5.22
Textile	5.79	8.44	10.46	1.94	4.21	5.95	1.51	3.22	4.48

150-300 HCADT - COLD

Subgrade	Soft			Medium-Soft			Medium		
Syn.	Soft	Medium	Stiff	Soft	Medium	Stiff	Soft	Medium	Stiff
Grid	2.03	4.62	6.92	1.86	4.08	5.98	1.74	3.59	5.11
Textile	2.03	4.13	5.85	1.95	3.80	5.24	1.78	3.30	4.44

300-600 HCADT - COLD

Subgrade	Soft			Medium-Soft			Medium		
Syn.	Soft	Medium	Stiff	Soft	Medium	Stiff	Soft	Medium	Stiff
Grid	2.40	4.32	5.94	1.77	3.45	5.09	1.83	3.34	4.59
Textile	2.45	4.04	5.30	2.03	3.52	4.69	1.85	3.34	4.02

For all cases in which the geosynthetic added is stiffer than the subgrade, the tables indicate that the deflections are decreased. For geogrid reinforced unsurfaced roads, the range of percent normalized deflection reduction is from 0 to 14%, and for geotextiles the range is from 0 to 13%. For geogrid reinforced 40^{o} C paved roads, the range is from 0 to 15%, and for geotextiles from 0 to 14%. Similarly for geogrid reinforced -20^{o} C paved roads, the range is from 1.5% to 12%, and for geotextiles, from 1.5% to 11%. For all cases studied, the amount of the deflection decrease depends on the road cross-section and geosynthetic used. The largest deflection reductions take place for the highest modulus geosynthetics, while the lowest modulus geosynthetics yield a negligible effect.

5.2 Percent Normalized $ASAL_{2.5}$ Increase

In addition to displaying the benefits of geosynthetic reinforcement in terms of deflections, Figs. 22 (a)-(c) – 23 (a)-(c) were created to display the effect on service life. Since Eq. 4.2 is based on deflection, the serviceability results follow the same trends as the deflection results. In other words, the stiffer the geosynthetic added, the greater the increase in service life. Only the surfaced cases were analyzed as Eq. 4.2 is not applicable to unsurfaced roads. Tables 11 and 12 illustrate the results.

Table 11. Percent normalized $ASAL_{2.5}$ increase – 40^{o} C pavement

<150 HCADT - WARM

Subgrade	**Soft**			**Medium-Soft**			**Medium**		
Syn.	Soft	Medium	Stiff	Soft	Medium	Stiff	Soft	Medium	Stiff
Grid	26.80	34.40	40.40	6.10	14.40	20.50	-1.00	6.90	11.70
Textile	27.00	33.32	38.05	6.42	13.10	17.88	0.46	5.97	9.72

150-300 HCADT - WARM

Subgrade	**Soft**			**Medium-Soft**			**Medium**		
Syn.	Soft	Medium	Stiff	Soft	Medium	Stiff	Soft	Medium	Stiff
Grid	3.70	11.60	18.20	-0.10	6.80	12.30	-0.20	5.60	9.90
Textile	4.87	11.30	16.39	0.00	5.72	9.98	-0.08	4.68	8.01

300-600 HCADT - WARM

Subgrade	**Soft**			**Medium-Soft**			**Medium**		
Syn.	Soft	Medium	Stiff	Soft	Medium	Stiff	Soft	Medium	Stiff
Grid	2.00	8.60	13.70	0.90	6.30	10.80	0.70	5.30	8.80
Textile	2.03	7.45	11.51	1.33	5.86	9.23	0.88	4.61	7.27

Table 12. Percent normalized $ASAL_{2.5}$ increase – -20^{o} C pavement

<150 HCADT - COLD

Subgrade	**Soft**			**Medium-Soft**			**Medium**		
Syn.	Soft	Medium	Stiff	Soft	Medium	Stiff	Soft	Medium	Stiff
Grid	17.62	26.38	33.28	5.78	14.05	20.61	4.65	11.11	15.98
Textile	17.62	24.90	30.18	6.18	13.03	18.07	4.81	10.08	13.85

150-300 HCADT - COLD

Subgrade	**Soft**			**Medium-Soft**			**Medium**		
Syn.	Soft	Medium	Stiff	Soft	Medium	Stiff	Soft	Medium	Stiff
Grid	6.46	14.25	20.80	5.93	12.67	18.17	5.55	11.19	15.66
Textile	6.46	12.80	17.78	6.21	11.83	16.04	5.68	10.34	13.71

300-600 HCADT - COLD

Subgrade	**Soft**			**Medium-Soft**			**Medium**		
Syn.	Soft	Medium	Stiff	Soft	Medium	Stiff	Soft	Medium	Stiff
Grid	7.58	13.38	18.06	5.64	10.79	15.63	5.82	10.46	14.17
Textile	7.74	12.53	16.21	6.43	10.98	14.45	5.89	10.46	12.47

The tables indicate that the addition of geosynthetic reinforcement increases the service life of paved roads for almost all cases. For 40^{o} C paved roads reinforced with geogrids, the range of percent normalized $ASAL_{2.5}$ increase is from 0 to 40%, and for geotextiles from 0 to 38%. For -20^{o} C paved roads reinforced with geogrids, the range of percent normalized $ASAL_{2.5}$ increase is from 4.5% to 33%, and for geotextile from 5% to 30%. For both types of geosynthetic, the benefit depended on the road cross-section, with the softest sections yielding the largest increases in service life.

5.3 Stress Distributions

Figures 35 (a)-(c) and 36 (a)-(c) illustrate the effects geosynthetic reinforcement have on the horizontal stress distribution. Since the effects are difficult to quantify, only the representative cases of the geotextile reinforced, unsurfaced roads over the soft and medium stiffness subgrade were included.

The plots indicate that shear stress in the base material resulting from the applied surface load is transferred to the geosynthetic placing the geosynthetic in tension. To say that the geosynthetic is in tension is not initially apparent from the plots, as the horizontal stress distribution remains in compression. However, the solution procedure used to calculate the gravitational stress field initially places the geosynthetic into compression. Upon application of the load, the magnitude of compression at the depth of the geosynthetic is reduced, in some cases resulting in tension. The magnitude of the tension is increased with the stiffness of the geosynthetic and the proximity to the axis of symmetry. Additionally, the stiffness of the subgrade material also effects the level of tension in the geosynthetic, with the softer subgrade

producing higher levels of tension. The observed tension in the geosynthetic layer illustrates that the reinforcing mechanism of a tensioned membrane.

The changes in the horizontal stress field in the base material and subgrade were not significant enough to be apparent in the plots provided.

CHAPTER 6
CONCLUSIONS AND RECOMMENDATIONS

Conclusions

Based on the work described in the previous chapters, the following conclusions can be drawn.

1. Numerical analysis of geosynthetic roadways can be done using *FLAC*. The analyses completed for this study were able to implement differing constitutive models and material properties for a layered system. The possible slipping nature of the geosynthetic/subgrade and geosynthetic/base interfaces was modeled using interface elements that obeyed the Mohr-Coulomb failure criterion. Static testing was done on typical Minnesota road cross sections.

2. The deflection response of roadway is governed by the Young's modulus of the geosynthetic used. Since the loading considered for this study was light, the roadway remained elastic under application of the load. Therefore, the response of the reinforced system depended on the stiffness of the geosynthetic used. For this study, the stiffest geosynthetic produced a 0% to 15% reduction in normalized deflection relative to the unreinforced roadway depending on the cross section considered.

3. The service life of a roadway may also be increased with the addition of geosynthetic reinforcement. The deflections calculated were used to determine a normalized percent $ASAL_{2.5}$ increase for the surfaced sections considered. Since the deflections were controlled

by the Young's modulus of the geosynthetic, the largest modulus geosynthetic produced the largest increase in service life. For the cases studied, the largest modulus geosynthetic produced a 0% to 40% increase in service life relative to the unreinforced case depending on the amount and type of HMA, amount of aggregate base, and subgrade considered.

4. The addition of geosynthetic reinforcement affects the horizontal stress distribution when loaded. The horizontal stress distributions were calculated at three sections within the loaded soil. The stress distributions showed that the geosynthetics were in a state of tension upon application of the load. This indicates that the tensioned membrane effect was providing additional support to the wheel load. The magnitude of tension in the geosynthetic depended on the stiffness of the geosynthetic, with the stiffest geosynthetics yielding the largest tension values. Additionally, the stiffness of the subgrade affected the geosynthetic tension, with the softer subgrade producing a larger tension. No significant deviations in horizontal stress were seen in the base material or the subgrade.

Recommendations

Based on the work described in previous chapters, the following recommendations are made.

1. In deflection-related design conditions, the use of geosynthetic reinforcement to significantly reduce deflections may be relied upon only when the subgrade material is of very poor quality.

2. Other beneficial effects of geosynthetic reinforcement should be considered when separation and bearing capacity during construction are of concern. However, these effects were not investigated in this project

3. Further study should be conducted regarding the benefit/cost issues regarding the geosynthetic reinforcement of low volume roads.

REFERENCES

Barksdale, R., Robnett, Q., Lai, J., and Zeevaert-Wolff, A., "Experimental and Theoretical Behavior of Geotextile Reinforced Aggregate Soil Systems," *Second International Conference on Geotextiles*, Las Vegas, Nevada, pp. 375-380, 1982.

Bearden, J. and Labuz, J., Fabric for Reinforcement and Separation in Unpaved Roads – Final Report, Minnesota Department of Transportation, St. Paul, Minnesota, p 51, 1998.

Bearden, J. and Labuz, J., Fabric for Reinforcement and Separation in Unpaved Roads – Interim Report, Minnesota Department of Transportation, St. Paul, Minnesota, pp. 52-64, 1998.

Burd, H.J., and Brocklehurst, C.J., "Finite element studies of the mechanics of reinforced unpaved roads," *Proc. Fourth International Conference on Geotextiles, Geomembranes, and Related Products*, Hauge, Netherlands, pp. 217-221, 1990.

CD-ROM: Geosynthetics: Use in Streets and Highways, LRRB, 1998.

Carroll, R.G., Walls, J.C., and Haas, R., "Granular Base Reinforcement of Flexible Pavements Using Geogrids," *Proc. Geosynthetics Conference*, New Orleans, La., pp. 46-57, 1987.

Coetzee, M., Hart, R., Varona, P., and Cundall, P., *FLAC* Basics, Itasca Consulting Group, Inc., Minneapolis, MN, 1995.

Das, B.M., Principles of Foundation Engineering, Fourth Edition, Brooks/Cole Publishing Company, Pacific Grove, Ca, 1999.

Davies, M.C.R., and Bridle, R.J., "Predicting the permanent deformation of reinforced flexible pavements subject to repeated loading," *Proc. Inter.Reinf.Soil Conf.*, British Geotechnical Society, pp. 421-425, 1990.

Dondi, G., "Three-Dimensional Finite Element Analysis of a Reinforced Paved Road," *Proc. Fifth International Conference on Geotextiles, Geomembranes, and Related Topics*, Vol. 1, pp. 95-100, 1994.

FLAC – *Fast Lagrangian analysis of continua*, Itasca Consulting Group, Inc., Minneapolis, MN, 1993.

Geosynthetic Manufacturers' Association, GMA White Paper II, Geosynthetic Reinforcement of the Aggregate Base Course of Flexible Pavement Structures, prepared for the American Association of State Highway and Transportation Officials Committee 4E on Geotextile/Geogrid Specifications.

Geotechnical Fabrics Report Specifier's Guide, 1999.

Giannini, F. and Camomilla, G., "Progetto Strutturale delle Pavimentazioni, Impiegato per le Autostrade Italiane," *Autostrade*, Vol. 2, pp. 4-17, 1978.

Haas, R. Hudson, W.R., and Zaniewski, J., Modern Pavement Management, Krieger Publishing Company, Malabar, FL., 1994.

Martin, J.P., Koerner, R.M., and Whitty, J.E., Experimental Friction Evaluation of Slippage Between Geomembranes, Geotextiles, and Soils, *Proc*. 1st International Conference on Geomembranes, pp.191-196, 1984.

Perkins, S.W. and Ismeik, M., "A Synthesis and Evaluation of Geosynthetic-Reinforced Base Layers in flexible Pavements: Part I," *Geosynthetics International*, Vol. 4, No. 6, pp. 549-605, 1997.

Perkins, S.W. and Ismeik, M., "A Synthesis and Evaluation of Geosynthetic-Reinforced Base Layers in flexible Pavements: Part II," *Geosynthetics International*, Vol. 4, No. 6, pp. 605-621, 1997.

Saxena, S.K., and Budiman, J.S., Interface Response of Geotextiles, *Proc.* 11th International Conference on Soil Mechanics and Foundation Engineering, pp. 1801-1804, 1985.

Wathugala, G.W., Huang, B., and Pal, S., "Numerical Simulation of Geosynthetic Reinforced Flexible Pavements," *Transportation Research Record*, No. 1534, pp. 58-65, 1996.

WESLEA, Van Cauwelaert, F.J., Alexander, D.R., White, T.D., and Barker, W.R., "Multilayer Elastic Program for Backcalculating Layer Moduli in Pavement Evaluation," Nondestructive Testing of Pavements and Backcalculation of Moduli, ASTM STP 1026, A.J. Bush III and G. Y. Baladi, Eds., American Society for Testing and Materials, Philadelphia,pp. 171-188, 1989.

APPENDIX A

FLAC SAMPLE DATA FILE

; SAMPLE DATA FILE
; The following is a sample input file used by the program FLAC to analyze
; the deflection response of a geosynthetic reinforced low volume roads. The
; data file actually contains six test sections, or FLAC simulations. The
; title of each simulation is listed at the beginning of each new run.
; Since the simulations are meant to represent actual road sections, the
; gravity stress distribution must be included. The solution procedure
; employed is to determine the stress distribution once, for the softest
; geosynthetic considered, and save this stress distribution. When stiffer
; geosynthetics are considered, the material properties of the reinforcement
; layer are changed and the calculation allowed to proceed under the
; influence of the wheel load.
; This solution procedure is valid as the horizontal stress field depends
; only on the density of the materials and the value of Poisson's ratio.
; Neither of these change from geosynthetic to geosynthetic. Also, the
; softest geosynthetic is considered first as the displacement field is not
; important at the completion of the graviational stress field calculation.
; Therefore, adding a stiffer material will not require additional calculations as the
; material will not deflect.
;
;
; **********
title
MNDoT RUN #2 - SOFT SYNTHETIC (GRID) - SOFT SUBGRADE - SURFACED - -20 C - 300-600
;

```
; ***************************************************************************
;
; Create grid - axisymmetric
config ax
grid 40 49
;
; ***************************************************************************
;
; Use Mohr-Coulomb material model for entire grid at this point.
; An elastic model will be applied to geosynthetic and HMA layers
; after the different layers have been partitioned.
;
mod mohr
;
; ***************************************************************************
;
; Null zones above and below synthetic layer - to be replaced with
; interface elements.
;
mod null i=1,41 j=22
mod null i=1,41 j=27
;
; ***************************************************************************
;
; Mark edges of synthetic & asphalt layers so that elastic material model may
; be applied to synthetic & asphalt regions.
;
mark i=1,41 j=22
mark i=1,41 j=27
mark i=1,41 j=46
;
```

```
; ***************************************************************************
;
; apply elastic material model to synthetic & asphalt regions
model el reg i=1 j=26
model el reg i=1 j=49
;
; ***************************************************************************
;
; Record history of vertical displacement under center of load.
hi yd i=1 j=50
;
; ***************************************************************************
; Material Properties:
;
; The material properties used are:
; bu = bulk modulus [kPa]
; sh = shear modulus [kPa]
; coh = cohesion [kPa]
; fr = friction angle [degrees]
; d = density [kg/m^3]
;
; sub-grade layer (soft)
pro bu 25000 sh 5357.14 coh 7.47 fr 15  d 1020 reg i=1 j=1
;
; synthetic layer (soft)
pro bu 19444.4 sh 14583.3 d 1020 reg i=1 j=26
;
; base layer
pro bu 166666.67 sh 55555.55 fr 30  d 2040 reg i=1 j=38
pro bu 166666.67 sh 55555.55 fr 30  d 2040 reg i=1 j=45
;
```

```
; - 20 C HMA layer
pro bu 8333333.3 sh 3846153.8 d 2040 reg i=1 j=49
;
; ***************************************************************
;
; Create desired global geometry
;
; Force grid to specific dimensions for given road as determined from
; the Minnesota State Aid Design Guidelines.  A graded mesh is used such
; that the element aspect ratio does not drastically change between layers.
; Dimensions of grid are in meters.
;
gen 0,0 0,1.39446 0.15,1.39446 0.15,0 i=1,6 j=1,22 ratio 1 0.85
gen 0.15,0 0.15,1.39446 2.032,1.39446 2.032,0 i=6,41 j=1,22 ra 1.05 0.85
gen 0,1.39446 0,1.397 0.15,1.397 0.15 1.39446 i=1,6 j=23,27
ge 0.15,1.39446 0.15,1.397 2.032,1.397 2.032,1.39446 i=6,41 j=23,27 ra 1.05 1
gen 0,1.397 0,1.6637 0.15,1.6637 0.15,1.397 i=1,6 j=28,39 rat 1 1.2
gen 0.15,1.397 0.15,1.6637 2.032,1.6637 2.032,1.397 i=6,41 j=28,39 ra 1.05 1.2
gen 0,1.6637 0,1.9304 0.15,1.9304 0.15,1.6637 i=1,6 j=39,46 ratio 1 0.9
ge 0.15,1.6637 0.15,1.9304 2.032,1.9304 2.032,1.6637 i=6,41 j=39,46 ra 1.05 0.9
gen 0,1.9304 0,2.032 0.15,2.032 0.15,1.9304 i=1,6 j=46,50
gen 0.15,1.9304 0.15,2.032 2.032,2.032 2.032,1.9304 i=6,41 j=46,50 ra 1.05 1
;
; ***************************************************************
;
; Fix model boundary conditions
;
; Model boundary is fixed horizontally and vertically along the bottom
; edge of the grid, and constrained laterally along the vertical boundaries.
;
```

```
fix x i=1
fix x y j=1
fix x i=41
;
; ********************************************************************
;
; Create interfaces above and below synthetic layer - Use frictional
; interface elements. Kn & Ks are quite small for gravitational stress
; calcualtion such that materials with different Poisson's ratios can
; deform in a natural state under influence of gravity.
; Interface friction angle taken from experiments outlined in literature.
; Tension bond used to hold two sections of grid together during
; gravity settlements.
;
int 1 Aside from 1,22 to 41,22 Bside from 1,23 to 41,23
int 1 kn=8.48e4 ks=1.48e1 fric=27 tbond 7.4e1
int 2 Aside from 1,27 to 41,27 Bside from 1,28 to 41,28
int 2 kn=8.48e4 ks=1.48e1 fric=30 tbond 7.4e1
;
; ********************************************************************
;
; Display every 50th value of unbalanced force during stepping
set ncw 50
;
; ********************************************************************
;
; Apply gravity stress and step to equilibrium. Save gravitational stress
; distribution as file "grav24.sav" to be used by remaining 5 data files.
set grav 9.81
step 30000
;
```

```
sav grav24.sav
;
; ***************************************************************************
;
; Increase values of interface Kn and Ks as outlined in FLAC manual such
; that elastic deformations at the interface are limited while keeping
; computation times manageable.
;
int 1 kn=7.48e8 ks=7.48e7 fric=27 tbond 7.4e1
int 2 kn=7.48e8 ks=7.48e7 fric=30 tbond 7.4e1
;
step 3000
;
; ***************************************************************************
;
; Set velocities and displacements resulting from gravitational stress
; calculation back to zero.
;
ini xd 0 yd 0
ini xvel 0 yvel 0
;
; ***************************************************************************
;
; Apply 40kN (9000lb) wheel load as a uniform pressure over a 150 mm
; radius and cycle until equilibrium is achieved.
;
apply nstress = -569 i=1,6 j=50
step 50000
;
; ***************************************************************************
```

```
;
; Write output to "sav" file so data may be examined at a later time
; when all calculations have been completed.
;
sav run28a.sav
;
; ********************************************************************
;<><><><><><><><><><><><><><><><><><><><><><><><><><><><><><><><><><><
; ********************************************************************
;
; Reset FLAC to begin calculation with a different geosynthetic.
;
new
title
MNDoT RUN #2 - MEDIUM SYNTHETIC (GRID) - SOFT SUBGRADE - SURFACED - -20
C - 300-600
;
; ********************************************************************
;
; Display every 50th value of unbalanced force during stepping
set ncw 50
;
; ********************************************************************
;
; Restore gravitational stress field determined with a softer geosynthetic.
; This procedure is valid as the gravitational stress field only depends
; on the density of the material and the value of Poisson's ratio.  Since
; niether of theses changes between geosynthetics, and the displacement
; field is not important at this point, the procedure is allowable.
;
rest grav24.sav
```

```
;
; ***************************************************************************
;
; Change material properties of geosynthetic layer.
;
; synthetic layer (medium)
pro bu 1094444 sh 820833.3 d 1020 reg i=1 j=26
;
step 3000
;
; ***************************************************************************
;
; Increase values of interface Kn and Ks as outlined in FLAC manual such
; that elastic deformations at the interface are limited while keeping
; computation times manageable.
;
int 1 kn=7.48e8 ks=7.48e7 fric=27 tbond 7.4e1
int 2 kn=7.48e8 ks=7.48e7 fric=30 tbond 7.4e1
;
step 3000
;
; ***************************************************************************
;
; Set velocities and displacements resulting from gravitational stress
; calculation back to zero.
;
ini xd 0 yd 0
ini xvel 0 yvel 0
;
; ***************************************************************************
;
```

```
; Apply 40kN (9000lb) wheel load as a uniform pressure over a 150 mm
; radius and cycle until equilibrium is achieved.
;
apply nstress = -569 i=1,6 j=50
step 90000
;
; ********************************************************************
;
; Write output to "sav" file so data may be examined at a later time
; when all calculations have been completed.
;
sav run28b.sav
;
; ********************************************************************
;<><><><><><><><><><><><><><><><><><><><><><><><><><><><><><><><><<
; ********************************************************************
;
; Reset FLAC to begin calculation with a different geosynthetic.
;
new
title
MNDoT RUN #2 - STIFF SYNTHETIC (GRID) - SOFT SUBGRADE - SURFACED - -20 C -
300-600
;
; ********************************************************************
;
; Display every 50th value of unbalanced force during stepping
set ncw 50
;
; ********************************************************************
;
```

```
; Restore gravitational stress field determined with a softer geosynthetic.
; This procedure is valid as the gravitational stress field only depends
; on the density of the material and the value of Poisson's ratio.  Since
; niether of theses changes between geosynthetics, and the displacement
; field is not important at this point, the procedure is allowable.
;
rest grav24.sav
;
; ***************************************************************
;
; Change material properties of geosynthetic layer.
;
; synthetic layer (stiff)
pro bu 2350000 sh 1762500 d 1020 reg i=1 j=26
;
step 3000
;
; ***************************************************************
;
; Increase values of interface Kn and Ks as outlined in FLAC manual such
; that elastic deformations at the interface are limited while keeping
; computation times manageable.
;
int 1 kn=7.48e8 ks=7.48e7 fric=27 tbond 7.4e1
int 2 kn=7.48e8 ks=7.48e7 fric=30 tbond 7.4e1
;
step 3000
;
; ***************************************************************
;
```

```
; Set velocities and displacements resulting from gravitational stress
; calculation back to zero.
;
ini xd 0 yd 0
ini xvel 0 yvel 0
;
; *****************************************************************
;
; Apply 40kN (9000lb) wheel load as a uniform pressure over a 150 mm
; radius and cycle until equilibrium is achieved.
;
apply nstress = -569 i=1,6 j=50
step 120000
;
; *****************************************************************
;
; Write output to "sav" file so data may be examined at a later time
; when all calculations have been completed.
;
sav run28c.sav
;
; *****************************************************************
;<><><><><><><><><><><><><><><><><><><><><><><><><><><><><><><><><
; *****************************************************************
;
; Reset FLAC to begin calculation with a different geosynthetic.
;
new
title
MNDoT RUN #2 - SOFT SYNTHETIC (TEXTILE) - SOFT SUBGRADE - SURFACED - -20
C - 300-600
```

```
;
; ****************************************************************
;
; Display every 50th value of unbalanced force during stepping
set ncw 50
;
; ****************************************************************
;
; Restore gravitational stress field determined with a softer geosynthetic.
; This procedure is valid as the gravitational stress field only depends
; on the density of the material and the value of Poisson's ratio.  Since
; niether of theses changes between geosynthetics, and the displacement
; field is not important at this point, the procedure is allowable.
;
rest grav24.sav
;
; ****************************************************************
;
; Change material properties of geosynthetic layer.
;
; synthetic layer (soft)
pro bu 23333.3 sh 17500 d 1020 reg i=1 j=26
;
step 3000
;
; ****************************************************************
;
; Increase values of interface Kn and Ks as outlined in FLAC manual such
; that elastic deformations at the interface are limited while keeping
; computation times manageable.
;
```

```
int 1 kn=7.48e8 ks=7.48e7 fric=27 tbond 7.4e1
int 2 kn=7.48e8 ks=7.48e7 fric=30 tbond 7.4e1
;
step 3000
;
; ***************************************************************************
;
; Set velocities and displacements resulting from gravitational stress
; calculation back to zero.
;
ini xd 0 yd 0
ini xvel 0 yvel 0
;
; ***************************************************************************
;
; Apply 40kN (9000lb) wheel load as a uniform pressure over a 150 mm
; radius and cycle until equilibrium is achieved.
;
apply nstress = -569 i=1,6 j=50
step 50000
;
; ***************************************************************************
;
; Write output to "sav" file so data may be examined at a later time
; when all calculations have been completed.
;
sav run28d.sav
;
; ***************************************************************************
;<><><><><><><><><><><><><><><><><><><><><><><><><><><><><><><><><><><><><><><><
; ***************************************************************************
```

```
;
; Reset FLAC to begin calculation with a different geosynthetic.
;
new
title
MNDoT RUN #2 - MEDIUM SYNTHETIC (TEXTILE) - SOFT SUBGRADE - SURFACED -
-20 C - 300-600
;
; ***************************************************************
;
; Display every 50th value of unbalanced force during stepping
set ncw 50
;
; ***************************************************************
;
; Restore gravitational stress field determined with a softer geosynthetic.
; This procedure is valid as the gravitational stress field only depends
; on the density of the material and the value of Poisson's ratio.  Since
; niether of theses changes between geosynthetics, and the displacement
; field is not important at this point, the procedure is allowable.
;
rest grav24.sav
;
; ***************************************************************
;
; Change material properties of geosynthetic layer.
;
; synthetic layer (medium)
pro bu 875000 sh 656250 d 1020 reg i=1 j=26
;
step 3000
```

```
;
; ****************************************************************
;
; Increase values of interface Kn and Ks as outlined in FLAC manual such
; that elastic deformations at the interface are limited while keeping
; computation times manageable.
;
int 1 kn=7.48e8 ks=7.48e7 fric=27 tbond 7.4e1
int 2 kn=7.48e8 ks=7.48e7 fric=30 tbond 7.4e1
;
step 3000
;
; ****************************************************************
;
; Set velocities and displacements resulting from gravitational stress
; calculation back to zero.
;
ini xd 0 yd 0
ini xvel 0 yvel 0
;
; ****************************************************************
;
; Apply 40kN (9000lb) wheel load as a uniform pressure over a 150 mm
; radius and cycle until equilibrium is achieved.
;
apply nstress = -569 i=1,6 j=50
step 90000
;
; ****************************************************************
;
```

```
; Write output to "sav" file so data may be examined at a later time
; when all calculations have been completed.
;
sav run28e.sav
;
; ********************************************************************
;<><><><><><><><><><><><><><><><><><><><><><><><><><><><><><><><><><<
; ********************************************************************
;
; Reset FLAC to begin calculation with a different geosynthetic.
;
new
title
MNDoT RUN #2 - STIFF SYNTHETIC (TEXTILE) - SOFT SUBGRADE - SURFACED - -20
C - 300-600
;
; ********************************************************************
;
; Display every 50th value of unbalanced force during stepping
set ncw 50
;
; ********************************************************************
;
; Restore gravitational stress field determined with a softer geosynthetic.
; This procedure is valid as the gravitational stress field only depends
; on the density of the material and the value of Poisson's ratio.  Since
; niether of theses changes between geosynthetics, and the displacement
; field is not important at this point, the procedure is allowable.
;
rest grav24.sav
;
```

```
; ***************************************************************************
;
; Change material properties of geosynthetic layer.
;
; synthetic layer (stiff)
pro bu 1750000 sh 1312500 d 1020 reg i=1 j=26
;
step 3000
;
; ***************************************************************************
;
; Increase values of interface Kn and Ks as outlined in FLAC manual such
; that elastic deformations at the interface are limited while keeping
; computation times manageable.
;
int 1 kn=7.48e8 ks=7.48e7 fric=27 tbond 7.4e1
int 2 kn=7.48e8 ks=7.48e7 fric=30 tbond 7.4e1
;
step 3000
;
; ***************************************************************************
;
; Set velocities and displacements resulting from gravitational stress
; calculation back to zero.
;
ini xd 0 yd 0
ini xvel 0 yvel 0
;
; ***************************************************************************
;
```

```
; Apply 40kN (9000lb) wheel load as a uniform pressure over a 150 mm
; radius and cycle until equilibrium is achieved.
;
apply nstress = -569 i=1,6 j=50
step 120000
;
; ***************************************************************************
;
; Write output to "sav" file so data may be examined at a later time
; when all calculations have been completed.
;
sav run28f.sav
;
; ***************************************************************************
;<><><><><><><><><><><><><><><><><><><><><><><><><><><><><><><><><><><><><><><>
; ***************************************************************************
```